Development of trivalent DNA vaccine encapsulated in chitosan TPP nanoparticles against EV-A71 and CV-A16

By YEW JIA SHENG

Dissertation submitted in fulfilment of the requirements for the degree of Masters in Life Science

Centre of virus and vaccine research
Sunway University
Malaysia

2024

Name of Candidate: YEW JIA SHENG

IC /Passport No: 971231-10-5291

Student ID: 16037830

Name of Degree: Masters in Life Sciences

Title of Project Paper/Research Report/Dissertation/Thesis ("this Work"):

Development of trivalent DNA vaccine encapsulated in chitosan TPP nanoparticles against EV-A71 and CV-A16

I do solemnly and sincerely declare that:

- 1. I am the sole author/writer of this Work;
- 2. This Work is original;
- 3. Any use of any work in which copyright exists was done by way of fair dealing and for permitted purposes and any excerpt or extract from, or reference to or reproduction of any copyright work has been disclosed expressly and sufficiently and the title of the Work and its authorship have been acknowledged in this Work;
- 4. I do not have any actual knowledge nor do I ought reasonably to know that the making of this work constitutes an infringement of any copyright work;
- 5. I hereby assign all and every right in the copyright to this Work to the Sunway University (SunU), who henceforth shall be owner of the copyright in this Work and that any reproduction or use in any form or by any means whatsoever is prohibited without the written consent of Sunway University having been first had and obtained;
- 6. I am fully aware that if in the course of making this Work I have infringed any copyright whether intentionally or otherwise, I may be subject to legal action or any other action as may be determined by Sunway University.

Date: 15/5/2024

Date: 15/5/2024

Candidate's Signature

U

Subscribed and solemnly declared before,

Witness's Signature

Name : **Dr. Ong Seng Kai**

Designation : Senior lecturer

Trivalent DNA vaccine Encapsulated in Chitosan TPP Nanoparticles enhanced

immunogenicity against EV-A71 and CV-A16

Hand foot and mouth disease (HFMD) is a prevalent global disease commonly occurring in young children under 6 years of age. Enterovirus 71 (EV-A71) and Coxsackievirus 16 (CV-A16) have been isolated as the major causative agents for most HFMD outbreaks in the Asia Pacific region. Severe HFMD could lead to cardiopulmonary and neurological failure or death. Currently, there are no US-FDA approved HFMD vaccines or antiviral treatments available in the market. The current China FDA approved vaccine for HFMD is a monovalent inactivated vaccine targeting EV-A71 without providing protection against CV-A16. In this study, we attempt to design a trivalent DNA vaccine candidate that could be administered to confer cross protection against EV-A71 and CV-A16. Chitosan-TPP Nanoparticles encapsulation of plasmid vaccine candidate was carried out to enhance immune response and prevent degradation. The VP1, VP2 genes of EV-A71 and VP1 gene of CV-A16 were cloned into the pIRES2-AcGFP1vector to form the recombinant plasmid pIRES-VP121. Chitosan TPP nanoparticles (NPs) encapsulating the trivalent pDNA were synthesized through ionic gelation followed by in vitro characterization. In vivo immunization of 4 weeks old ICR mice was carried out to evaluate the immunologic enhancement of Chitosan Nanoparticles. The formulated chitosan TPP (CS-TPP-NPs (pIRES-VP121)) were highly monodispersed with an average size of ~200nm. Chitosan TPP NPs encapsulating the pDNA showed >70% encapsulation efficiency and good cellular uptake in mice macrophage cells were observed. The plasmid DNA vaccine was protected from DNase I digestion by chitosan TPP NPs. In vivo immunization studies demonstrated enhanced immunogenic responses by CS-TPP-NPs (pIRES-VP121) due to self adjuvanting properties of chitosan nanoparticles. Mice administered with CS-TPP NPs (pIRES-VP121) intramuscularly were observed to have the highest IFN-y response (~15-fold increment). Sera from mice immunized with the naked pDNA and CS-TPP-NPs (pIRES-VP121) demonstrated good viral clearance against wild-type EV-A71 and CV-A16 in RD cells. Unfortunately, murine sera administered with naked pDNA and CS-TPP-NPs (pIRES-VP121) showed reduced ability to neutralize mouse adapted virus (MAV) strains of EV-A71 and CV-A16. CS-TPP-NPs (pIRES-VP121) could serve as a prototype for future development of multivalent HFMD DNA vaccine candidates.

ACKNOWLEDGEMENTS

I would like to acknowledge and give my thanks to my previous supervisor **Prof. Poh**Chit Laa for giving me an opportunity to develop my writing skills through review paper

and practical skills in the lab. Her constant constructive criticism was what made the completion of the project possible.

My sincere gratitude to **Dr. Ong Seng Kai** for taking over the supervisory role during the thesis completion stage of my project when Prof. Poh retired.

In addition, a thank you to **Dr. Lim Hui Xuan** and **Dr. Malihe Masomian** who served as my co-supervisors during my MsC project. Dr. Malihe has given me guidance in most of my in-vitro experiments whereas Dr. Lim's expertise in animal study has been of enormous help in the final stage of the project.

I would like to extend my appreciation to my lab mates **Wen** and **Ivy** as their companionship was what supported me in staying through the end of my project.

Special thanks to **Dr. Tan Soon Hao**, associate **Prof. Ong Kien Chai** and **Prof. Wong Kum Thong** of **University Malaya** for providing the wild-type and mouse adapted strains of EV-A71 and CV-A16, as well as the EV-A71 monoclonal antibody. Special thanks to **Dr. Cha Yee Kuen (UPM)** for providing detailed explanation regarding the methodology of chitosan TPP nanoparticles formulation through ionic gelation in person. Finally, I wish to acknowledge the financial assistance provided by the **Research Scholarship of Sunway University master's degree** throughout my postgraduate research.

TABLE OF CONTENTS

| TITLE PAGE | i |
|------------------------------------|-----|
| ORIGINAL LITERARY WORK DECLARATION | ii |
| ABSTRACT | iii |

| ACKNOWLEDGEMENTSiv |
|--|
| TABLE OF CONTENTSv |
| LIST OF FIGURESx |
| LIST OF TABLESxv |
| LIST OF SYMBOLS AND ABBREIVATIONSxvi |
| LIST OF APPENDICESxxii |
| CHAPTER 1 INTRODUCTION |
| 1.1 Etiology and background of HFMD |
| 1.2 Challenges faced by HFMD vaccines |
| CHAPTER 2 LITERATURE REVIEW5 |
| 2.1 EV-A71 and CV-A16 as HFMD causative agents5 |
| 2.2 Structure of HFMD etiological agents |
| 2.3 Cyclical occurrence of HFMD |
| 2.4 Status of HFMD vaccine development9 |
| 2.4.1 China FDA approved inactivated HFMD vaccines and aftermath of IV |
| implementation10 |
| 2.5 Experimental HFMD vaccines |
| 2.5.1 Inactivated vaccine (IV) |
| 2.5.2 Virus like particle (VLP) vaccine14 |
| 2.5.3 Live attenuated vaccine (LAV)15 |

| 2.5.4 Epitope mapping and recombinant peptide/protein vaccines against HFMD17 |
|---|
| 2.5.4.1 Immunogenic epitopes and recombinant vaccines of EV-A7117 |
| 2.5.4.2 Neutralizing epitopes identified in CV-A1620 |
| 2.5.5 Plasmid DNA vaccine |
| 2.6 Background of plasmid vaccine. 22 |
| 2.7 Mechanism of plasmid antigen presentation in vivo |
| 2.8 IRES sequences and translation of plasmid DNA |
| 2.9 Advantages of DNA vaccine |
| 2.10 Vaccination strategies |
| 2.10.1 Limitations of DNA vaccine |
| 2.10.2 Nanoparticles as delivery platform for plasmid DNA |
| 2.10.3 Chitosan as nanocarrier for plasmid vaccine30 |
| Chapter 3 Materials and method34 |
| 3.1 Mammalian and murine cell lines34 |
| 3.1.1 Revival and culture of cells |
| 3.1.2 Subculture and maintenance of cell lines |
| 3.1.2.1 293T cells34 |
| 3.1.2.2 J774A.1 cells |
| 3.1.3 Storage of 293T and J774A.135 |
| 3.2 Construction of recombinant plasmid DNA |

| 3.3 Transformation of trivalent plasmid into <i>E. coli</i> |
|---|
| 3.4 Plasmid isolation and purification |
| 3.5 Transfection of 293T cells with the recombinant DNA plasmid |
| 3.6 Confirmation of plasmid and protein expression <i>in vitro</i> |
| 3.7 Preparation of chitosan solutions and plasmid DNA-TPP solutions39 |
| 3.8 Synthesis of chitosan TPP nanoparticles (chitosan NPs) through ionic gelation39 |
| 3.9 Characterization of the chitosan encapsulating plasmid DNA40 |
| 3.9.1 Encapsulation efficacy of the nanospheres40 |
| 3.9.2 Morphology, size, polydispersity index, and zeta potential of the chitosan |
| NPs |
| 2 IN Transfortion of chitogen encongulated nIDES V/DIDI |
| 3.10 Transfection of chitosan encapsulated pIRES-VP12141 |
| 3.11 Hemolysis assay |
| |
| 3.11 Hemolysis assay |

| 3.19 Ethics statement |
|---|
| CHAPTER 4 RESULTS |
| 4.1 Design and construction of the trivalent plasmid vaccine candidate |
| 4.2 Sequencing of the VP121 genes inserted |
| 4.3 Expression of the recombinant plasmid pIRES VP121 in 293T cells55 |
| 4.4 Viral protein expressions of pIRES VP121 in 293T mammalian cells |
| 4.5 Characterization of the chitosan TPP nanoparticles |
| 4.5.1 Encapsulation efficiency of chitosan nanoparticles correlate to the concentration |
| of plasmid encapsulated60 |
| 4.5.2 Morphology, size, polydispersity index, and zeta potential of the chitosan TPP |
| NPs62 |
| 4.6 Chitosan TPP NPs were able to protect encapsulated pDNA from digestion by |
| DNase I |
| 4.7 Chitosan TPP NPs were suitable nanocarriers for cellular uptake of pDNA into murine |
| macrophage cells69 |
| 4.8 Chitosan TPP NPs and chitosan polymer did not have hemolytic effects on RBCs of |
| ICR mice even at high concentrations71 |
| 4.9 Chitosan TPP nanoparticles and chitosan polymer were not cytotoxic in murine |
| macrophage cells |
| 4.10 Chitosan TPP NPs encapsulation of the trivalent pDNA vaccine candidate enhanced |
| cellular immune response |

| 4.11 Chitosan encapsulation of pIRES-VP121 enhanced the levels of IFN-γ |
|--|
| secretion84 |
| 4.12 Chitosan encapsulation of pIRES-VP121 enhanced neutralization against the wild- |
| type EV-A71 and CV-A1686 |
| 4.13 Molecular analysis of wild type and mouse adapted EV-A71, CV-A1690 |
| CHAPTER 5 DISCUSSION92 |
| CHAPTER 6 CONCLUSION |
| CHAPTER 7 BIBLIOGRAPHICAL REFERENCES |
| APPENDICES |

LIST OF FIGURES

Figure 1.1 Distribution of HFMD cases in Asia-pacific region, referenced from the 4 surveillance summary of HFMD by World Health Organization (WHO) in 2018 (World Health Organization. Regional Office for the Western, 2018).

| Figure 2.1 | Schematic representation of enterovirus genome (image generated through biorender software), generated image referenced from Mandary and Poh (2018). | 7 |
|------------|--|----|
| Figure 2.2 | DNA vaccine was able to induce humoral immune response by transfection of somatic cells followed with B cells activation leading to antibody production, CD4+ T cells were also able to stimulate B cells division. APCs could be activated by direct transfection or indirectly by cross-priming, followed by activation of CD8+ T cells through MHC class I molecules thereby inducing cellular immune response. Image was generated with biorender.com. | 25 |
| Figure 2.3 | Schematic representation of i) Chitosan encapsulating inactivated whole influenza virus and ii) Chitosan encapsulating plasmid DNA vaccine. Image was generated with biorender.com. | 33 |
| Figure 4.1 | Recombinant pIRES VP121 trivalent plasmid construct harbouring the pIRES2-AcGFP1 plasmid vector carrying VP1, VP2 genes of EV-A71 and VP1 gene of CV-A16. | 50 |
| Figure 4.2 | Gene sequences inserted into the multiple cloning site of the pIRES2-AcGFP1 plasmid vector. | 51 |
| Figure 4.3 | Complete sequence of the genes inserted into the multiple cloning site. | 53 |
| Figure 4.4 | Fluorescent microscopy images of 293T cells transfected with 1µg (b, f, j), 2µg (c, g, k) and 3µg (d, h, l) of pIRES-VP121 recombinant plasmid with non-transfected cells (a, e, i) serving as the negative control. From top to bottom, Images were captured under 20x magnification (500 µm scale bar) in (I) brightfield, (II) FITC and (III) merged channels respectively. | 56 |
| Figure 4.5 | SDS PAGE gels loaded with 293T cell lysates harvested at 24h (a) and 48h (b) after transfection with 1µg,2 µg and 10 µg of recombinant pIRES-VP121, with non-transfected 293T cell lysates that served as negative controls. *Protein ladder: Precision Plus Protein TM unstained protein standards (Bio-Rad, California, USA) | 58 |

| Figure 4.6 | Western blots of recombinant protein expression by 293T cells transfected with pIRES-VP121 trivalent pDNA. Western blot analysis was carried out using primary A) EV-A71 VP1 monoclonal antibody, B) EV-A71 VP2 polyclonal antibody and C) His tag antibody. *Protein ladder: PM2610 (Smobio, Taiwan). | 59 |
|------------|--|----|
| | (Smobio, Taiwan). | |

- Figure 4.7 Morphology of the CS-TPP-NPs (pIRES-VP121) were visualized from 63 SEM imaging: CS-TPP-NPs(pIRES-VP121) (100μg) at magnification of 12kx (1μm scale bar).
- Figure 4.8 Average diameter and polydispersity index of A) blank CS-TPP-NPs, B) 64 CS-TPP-NPs (pIRES-VP121) (50μg pDNA) and C) CS-TPP-NPs (pIRES-VP121) (100μg pDNA).
- Figure 4.9 Zeta potential of A) blank CS-TPP-NPs, B) CS-TPP-NPs (pIRES-VP121) 65 (50µg pDNA) and C) CS-TPP-NPs (pIRES-VP121) (100µg pDNA)
- Figure 4.10 Agarose gel electrophoresis image of plasmid DNA and CS-TPP-NPs 68 (pIRES-VP121) complex: Lane 1: untreated pDNA (control); lane 2: untreated CS-TPP-NPs (pIRES-VP121); lane 3: DNA marker TrackIt™ 1 Kb Plus DNA Ladder (Thermofisher, USA); lane 4: CS-TPP-NPs (pIRES-VP121) treated with DNase I followed by chitosanase; lane 5: pDNA treated with DNase I followed by chitosanase; lane 6: CS-TPP-NPs (pIRES-VP121) treated with DNase I; lane 7: pDNA treated with DNase I
- Figure 4.11 Fluorescent microscopy images of J774A.1 macrophage transfected with 70 naked pDNA (a, e, i), CS-TPP-NPs (pIRES-VP121) (5μg/ml, 48h) (b, f, j), CS-TPP-NPs (pIRES-VP121) (5μg/ml, 72h) (c, g, k) and XfectTM reagent (5μg/ml, 48h) (d, h, l) were captured under 10x magnification (scale bar 500μm); I. images from BF channel, II. images from FITC channel and III. images merged from the FITC and BF channel.
- Figure 4.12 Murine RBCs were incubated with (a) blank Chitosan TPP NPs, (b) CS- 72 TPP-NPs (pIRES-VP121) and (c) chitosan polymer at a concentration of 400μg/ml. (d) Triton-X and (e) PBS solution mixed with RBCs served as the positive and negative control, respectively. Hemolysis images of samples were taken after OD reading. Experiments were performed in quadruplicates for each sample.
- Figure 4.13 Hemolysis rate of ICR mice red blood cells (RBCs) following incubations 73 with blank Chitosan NPs, CS-TPP-NPs (pIRES-VP121), and chitosan polymer at a concentration of 400μg/ml. Experiment was performed in quadruplicates for each sample, data were presented as mean ± SD with error bar indicating the standard deviation. Triton-x represents 100% hemolysis (positive control) and PBS represents the absence of hemolysis (negative control).

- Figure 4.14 J774A.1 mice macrophages evaluated by MTS assay after 48h incubation 75 with blank Chitosan NPs, CS-TPP-NPs (pIRES-VP121) and chitosan polymer at different concentrations (400μg/ml, 200μg/ml, 100μg/ml). Experiments were performed three times independently with similar results, media alone served as the control. Data was presented as mean ± SD, error bar indicates the standard deviation.
- Figure 4.15 Timeline of A) groups of mice receiving a single booster dose post-immunization B) groups of mice receiving two booster doses post-immunization. Image was generated using Biorender.com.
- **Figure 4.16** Gating strategy performed in Kaluza software to identify the live 79 CD3⁺CD4⁺ and live CD3⁺CD8⁺ T cells populations.
- Figure 4.17 Dot plots from flow cytometry analysis (A) showing the subsets of IFN-γ 80 expressing CD4⁺ T cells from splenocytes of naïve mice and mice immunized with 50μg or 100μg of naked pDNA, followed by 1 booster dose. IFN-γ expressing CD4⁺ from each group of mice (population %) were presented on bar chart (B) indicating mean ± SD with error bar representing the standard deviation. Statistical significance was analysed with unpaired t-test: *P≤0.05 against naïve splenocytes, **P≤0.01 against naïve splenocytes, ***P≤0.0001 against naïve splenocytes and *****P≤0.0001 against naïve splenocytes. Experiment was performed in quadruplicates for each sample.
- Figure 4.18 Dot plots from flow cytometry analysis (A) showing the subsets of IFN-γ expressing CD8+ T cells from splenocytes of naïve mice and mice immunized with 50μg or 100μg of naked pDNA, followed by 1 booster dose. IFN-γ expressing CD8+ from each group of mice (population %) were presented on bar chart (B) indicating mean ± SD with error bar representing the standard deviation. Statistical significance was analysed with unpaired t-test: *P≤0.05 against naïve splenocytes, **P≤0.01 against naïve splenocytes and ****P≤0.0001 against naïve splenocytes. Experiment was performed in quadruplicates for each sample.
- Figure 4.19 Dot plots from flow cytometry analysis (A) showing the subsets of IFN-γ 82 expressing CD4+ T cells from splenocytes of naïve mice, mice immunized with naked pDNA (100μg, 2 booster) and CHI-pDNA-NPs (100μg, 2 booster). IFN-γ expressing CD4+ from each group of mice (population %) were presented on bar chart (B) indicating mean ± SD with error bar representing the standard deviation. Statistical significance was analysed with unpaired t-test: *P≤0.05 against naïve splenocytes, **P≤0.01 against naïve splenocytes and ****P≤0.0001 against naïve splenocytes. Experiment was performed in quadruplicates for each sample.

- Figure 4.20 Dot plots from flow cytometry analysis (A) showing the subsets of IFN-γ 83 expressing CD8+ T cells from splenocytes of naïve mice, mice immunized with naked pDNA (100μg, 2 booster) and CHI-pDNA-NPs (100μg, 2 booster). IFN-γ expressing CD8+ from each group of mice (population %) were presented on bar chart (B) indicating mean ± SD with error bar representing the standard deviation. Statistical significance was analysed with unpaired t-test: *P≤0.05 against naïve splenocytes, ***P≤0.01 against naïve splenocytes, ***P≤0.0001 against naïve splenocytes. Experiment was performed in quadruplicates for each sample.
- Figure 4.21 The amount of IFN- γ (pg/ml) secreted by splenocytes from mice immunized 85 with 50 μ g pDNA, 100 μ g pDNA at one booster dose, 100 μ g pDNA or CS-TPP-NPs (pIRES-VP121) at two booster doses in comparison with the naïve mice from ELISA assay. Experiment was carried out in triplicates and repeated 3 times independently using the same settings. Data were presented as mean \pm SD and error bar indicates standard deviation. Significance value was analysed with unpaired T test: *P \leq 0.05, **P \leq 0.01, ***P \leq 0.001 and ****P \leq 0.0001 against naïve splenocytes.
- Figure 4.22 Representative micrographs showing the CPE condition of RD cells at 96h post infection with (I.) wild type EV-A71 B4, (II.) wild type CV-A16/N132, (III.) EV-A71 B3 (MAV) and (IV.) CV-A16/N132 (MAV), respectively. RD cells were also incubated with 1:16 dilution of naïve mice sera (a,d,g,j), sera of mice immunized with naked pIRES-VP121 (b,e,h,k), and antisera of mice immunized with CS-TPP-NPs (pIRES-VP121) (c,f,i,l), respectively prior to enterovirus infection. RD cells incubated with monoclonal EV-A71 antibodies (m,n) followed by incubation with wild-type or mouse adapted EV-A71 would serve as the positive controls. Images were taken at 5x magnification with 100μm scale bar.
- Figure 4.23 CPE present in RD cells post incubation with murine sera (1:16) derived from mice immunized with 3 doses of naked pIRES-VP121, CS-TPP-NPs (pIRES-VP121) and infected with an equal amount of wild-type EV-A71, CV-A16 and mouse adapted EV-A71, CV-A16 enteroviruses. Naïve murine sera and EV-A71 monoclonal antibodies incubated with an equal volume of wild-type and mouse adapted EV-A71, CV-A16 enteroviruses served as the positive and negative controls, respectively. Neutralizing assay was carried out in triplicates for each sample, data was presented as mean ± SD and error bar indicates the standard deviation. * NA= not tested.
- Figure 4.24 A) VP1 protein alignment between EV-A71 B4 (wild-type) and EV-A71 91 B3 (MAV) revealed a total of 3 amino acid differences at position 145 (Q-E), 147 (F-E) and 292 (T-K), respectively. B) VP2 protein alignment between EV-A71 B4 (wild-type) and EV-A71 B3 (MAV) revealed single amino acid difference at position 149 (K-I). C) VP1 genome alignment

between CV-A16 N132 (wild-type) and CV-A16 N132 (MAV) revealed single nucleotide change at position 33 (C-T).

LIST OF TABLES

| Table 2.1 | China FDA approved formalin inactivated vaccines. Table adapted from X. He et al. (2021). | 11 |
|-----------|--|----|
| Table 4.1 | Encapsulation efficiency of chitosan TPP nanoparticles encapsulating different concentration of plasmid DNA. | 61 |
| Table 4.2 | Characteristics of Chitosan TPP nanoparticle formulations encapsulating different concentrations of recombinant plasmid DNA pIRES-VP121. | 66 |

LIST OF SYMBOLS AND ABBREIVATIONS

3D^{Pol} 3D polymerase

aa Amino acid

APC Antigen presenting cell

ATCC American Type Culture Collection

BB515 BrilliantTM Blue 515

BSC Biosafety cabinet

BSL Biosafety level

BV786 BrilliantTM Violet 786 fluorophore

CAMS Chinese Academy of Medical Sciences

CD3 cluster of differentiation 3

CD4 cluster of differentiation 4

CD8 cluster of differentiation 8

CFA Complete Freund's adjuvant

cmPALS Continuously Monitored Phase-Analysis Light Scattering

CNS Central nervous system

COVID-19 coronavirus disease- 2019

CPE Cytopathic effects

CS-TPP-NPs Chitosan TPP nanoparticles

CS-TPP-NPs Chitosan TPP nanoparticles encapsulating plasmid

(pIRES-VP121) pIRES-VP121

CTL Cytotoxic T lymphocytes

CV-A10 Coxsackievirus A10

CV-A16 Coxsackievirus A16

CV-A6 Coxsackievirus A6

DMEM Dulbecco's Modified Eagle's Medium

DMSO Dimethyl sulfoxide

DNA Deoxyribonucleic acid

DNAse I Deoxyribonuclease I

ECL Enhanced Chemiluminescence

EDTA ethylenediaminetetraacetic acid

ELISA enzyme-linked immunosorbent assay

ELISpot enzyme-linked immunospot

EMCV Encephalomyocarditis virus

EV-A71 Enterovirus A71

FACS Flow Cytometry Staining

FBS Fetal bovine serum

FDA Food and Drug Administration

FITC Fluorescein isothiocyanate

FVS-780 LIVE/DEAD Fixable Viability Stain 780

HBc Hepatitis B Virus Core Protein

HCL Hydrochloric acid

HFMD Hand foot and mouth disease

HRP Horseradish Peroxidase

IM Intramuscular

ICS intracellular cytokine staining

IFA Incomplete Freund's adjuvant

IFN-γ interferon gamma

IgG immunoglobulin G

IgM immunoglobulin M

IL-12 interleukin 12

IL-2 interleukin 2

IL-4 interleukin 4

IN Intranasal

IRES Internal ribosome entry site

IV Inactivated vaccine

LAV Live-attenuated vaccine

LD50 Lethal dosage (50%)

mAB mouse antibodies

MAV Mouse-adapted virus

MHC major histocompatibility complex

mRNA messenger ribonucleic acid

mTLNE multiple tandem linear neutralizing epitopes

NaCL Sodium Chloride

NaOH Sodium Hydroxide

NDV Newcastle disease virus

OD Optical density

ODN oligodeoxynucleotides

ORF Open reading frame

OVA Ovalbumin

PAMP Pathogen associated molecular pattern

PBS Phosphate buffer saline

PCR phosphate buffered saline

PD Partial deletion

PDI Polydispersity index

pDNA Plasmid DNA

PerCP Peridinin-Chlorophyll-protein

PLGA poly (D, L-lactide-co-glycolide)

PSGL-1 P-selectin glycoprotein ligand-1

PV Poliovirus vaccine

RBC Red blood cells

RD cells Rhabdomyosarcoma cells

RNA ribonucleic acid

ROS Reactive oxygen species

RPMI Roswell Park Memorial Institute medium

RT Room temperature

S protein Spike protein

SARS-CoV-2 severe acute respiratory syndrome coronavirus 2

SCARB2 Scavenger Receptor Class B Member 2

SD Standard deviation

SEM Scanning electron microscopy

TE buffer Tris-EDTA buffer

Th1 T helper 1 cells

TLS tertiary lymphoid structures

UTR Untranslated region

UV-Vis Ultraviolet-visible

VLP Virus like particles

VP (VP1, VP2, Viral envelope protein 1,2, 3, 4

VP3 and VP4)

WHO World health organization

X g gravitational force in centrifugation

LIST OF APPENDICES

APPENDIX I- PUBLICATION

CHAPTER 1 INTRODUCTION

1.1 Background of HFMD

Human hand foot and mouth disease (HFMD) is a global pandemic generally caused by viruses which belong to the *Picornaviridae* family in the genus *Enterovirus* including Enterovirus A71 (EV-A71), Coxsackievirus A6 (CV-A6), CV-A10 and CV-A16 (Pozzetto & Gaudin, 1999; Osterback et al., 2009). Picornaviruses are non-enveloped, icosahedral single-stranded RNA viruses composed of 4 virus capsid proteins (VP1-VP4) and possess the same fundamental architecture across all family members (Smyth & Martin, 2002). Patients with HFMD are usually characterized with fever, rashes and vesicles manifestations in the mouth, hands and feet. Severe complications such as acute encephalomyelitis, cardiopulmonary failure, acute flaccid paralysis leading to fatal outcomes could occur when virulent EV-A71 strains were involved (Fang & Liu, 2018). At recent years, reports of HFMD outbreaks in Asia-pacific region have been more and more frequent especially in Malaysia, Thailand, Vietnam, Japan, China, and India (Nhan et al., 2018; Laor et al., 2020; Xie et al., 2020; Fong et al., 2021; Farahat et al., 2022; Niu et al., 2022). This was supported by surveillance reports of HFMD cases in Asia-pacific countries by WHO up until august of 2018 (Fig. 1.1); Hong Kong reported 212 cases; Macau reported 2323 cases; Singapore reported 26,252 cases; Vietnam reported 32,956 cases where 50% of patients were hospitalized; Japan reported 69,041 cases and China reported 1,381,685 cases including 26 deaths (World Health Organization. Regional Office for the Western, 2018). Health director of Malaysia have reported weekly HFMD cases to exceeded the national alert level of 1,150/week, as of week 19 (May 7-13) of 2023 (malaymail, 2023). This highlights the fact that HFMD is still a threat in Asia and development of an effective HFMD vaccine would be beneficial.

1.2 Challenges faced by HFMD vaccines

In 1975, The first experimental formalin inactivated vaccine (IV) against EV-A71 was developed in Moscow during a "Polio-Like Disease" epidemic in Bulgaria. Unfortunately, the clinical efficacy of whole virus EV-A71 IV was not assessed further due to the lack of subsequent outbreaks (Chumakov et al., 1979; Chong & Klein, 2018).

Currently, there are no US-FDA approved HFMD vaccines or antiviral treatments available on the market (Lalani et al., 2021). There are however 3 formalin inactivated EV-A71 vaccines commercially available and approved by the China FDA with an estimated average of 94.8 % efficacy assuming there is 85% vaccination coverage across the country (Van Boeckel et al., 2016). However, these IV failed to provide cross immunization against HFMD infections caused by CV-A16, CV-A10 and CV-A6. Aside from the use of highly toxic formaldehyde, IV generally require multiple purification in the vaccine manufacturing process and periodical boosters after the initial administration (Aswathyraj et al., 2016). Recent research activities have developed a wide range of experimental vaccines against HFMD pathogens including the virus like particle-based vaccines (VLP), live attenuated vaccine (LAV), recombinant protein-based vaccine, viral vectored vaccine and DNA vaccine, each with their advantages and disadvantages. The only DNA vaccine candidate against EV-A71 designed by Tung et.al was able to induce strong IgG levels but the antibody levels declined upon administration of second booster (Tung et al., 2007). LAV vaccine was reported to induce neurological symptoms in monkey, thus suggesting the possible reversion of vaccine to wild type genotype (Arita et al., 2007). Recombinant peptide vaccine candidates were generally administered together with complete and incomplete Freund's adjuvants (CFA/IFA) and previous studies were mostly conducted in murine models (Wu et al., 2001; Y. X. Li et al., 2014). The use of IFA was discontinued in clinical trials of humans due to safety concerns (Alving, 2002; Chong, Hsieh, et al., 2012). Same site vaccination using IFA have been reported to create tertiary lymphoid structures (TLS), cancer and infections were commonly associated with the presence of TLS (Slingluff et al., 2021; Sato et al., 2023).

Tetravalent VLP vaccine was able to provide long lasting antibody response against all 4 serotypes (EV-A71, CV-A16, CV-A10, CV-A6), the purification and expression of recombinant proteins and VLP were however costly and laborious (Lin et al., 2012; Zhang et al., 2018). Viral vectored EV-A71 vaccine was able to protect mice from lethal challenges but less efficient in comparison to EV-A71 IV (Tian et al., 2012). The protective efficacy provided by current licensed vaccines will eventually decline due to the constant mutations and evolution of EV-A71 (Wang et al., 2021). Enteroviruses that were quiescent for a long period could also reemerge as the predominant strain or subgenotype again (Liu et al., 2014). Therefore, development of new multivalent vaccines is important to match the antigenic evolution of HFMD enteroviruses and to prepare for emergence of new dominant strains or sub-genotypes.

In this study, the concept of constructing a trivalent DNA vaccine would lay down the foundation to develop multivalent HFMD DNA vaccine in future by incorporation of more genes encoding for the relevant enterovirus antigens.

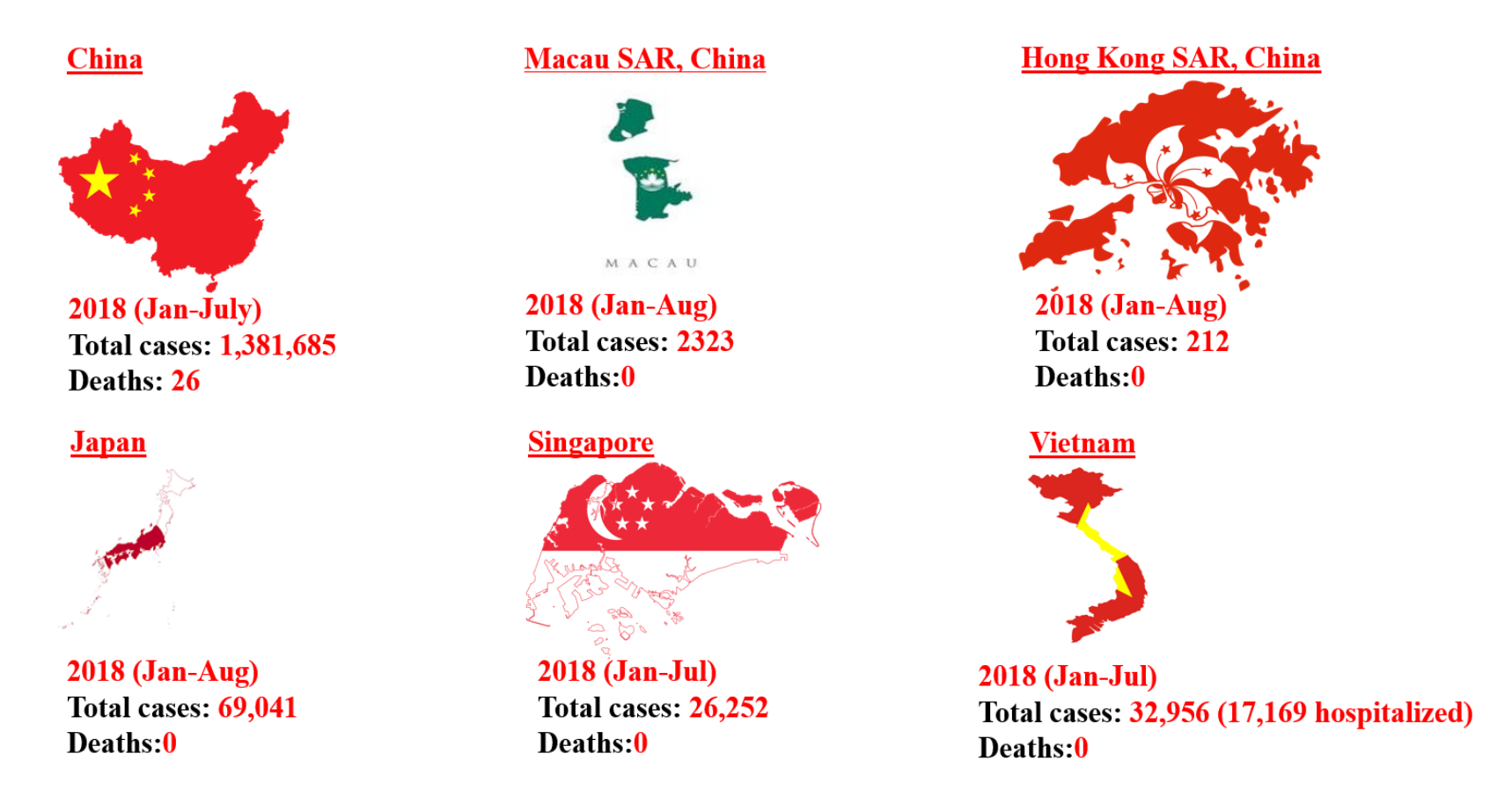


Figure 1.1: Distribution of HFMD cases in Asia-pacific region, referenced from the surveillance summary of HFMD by World Health organization (WHO) in 2018 (World Health Organization. Regional Office for the Western, 2018).

CHAPTER 2 LITERATURE REVIEW

2.1 EV-A71 and CV-A16 as HFMD causative agents

Hand, foot, and mouth disease (HFMD) is a highly contagious viral disease worldwide that is prevalent in the Asia-Pacific region (Ang et al., 2009; Repass et al., 2014). This disease generally affects infants and young children (<6 years of age), but it can also occur in older kids and adults. HFMD is generally characterized with symptoms such as fever, mouth ulcers, rashes or vesicle manifestations on palms and feet. In severe cases, some patients might develop serious cardiopulmonary and neurological complications which could result in fatal outcomes (Wong et al., 2010; Zhang et al., 2010). Fatal EV-A71 HFMD infections could also lead to social economic burdens due to premature death of patients at a young age, losses are estimated at \$80,000 - \$150,000 for each fatal case (Xing et al., 2014). Enterovirus 71 (EV71) and coxsackievirus A16 (CVA16) have always been known as the common causative agents of HFMD (Fujimoto, 2018). In 1951, CV-A16 prototype strain G10 was first isolated in South Africa and only sequenced in 1994 (Sickles et al., 1955; Hagiwara et al., 1978; Pöyry et al., 1994). Since the first study of EV-A71 isolation was recorded in 1969 in the United States, EV-A71 was subsequently accounted as the major causative agent of HFMD outbreaks in the Asia Pacific region starting from the 1990s (Schmidt et al., 1974; Puenpa et al., 2019).

However, vaccine design and in vivo studies of HFMD were more prioritized on EV-A71 due to its association with more severe or fatal CNS complications. HFMD cases caused by CV-A16 infection were generally characterized as self-limiting with mild symptoms (Mao et al., 2014; Hooi et al., 2020). Despite being less common in comparison with EV-A71, CV-A16 have been previously reported to be causing severe CNS complications including rhombencephalitis, pneumonitis and aseptic meningitis (Eyckmans et al., 2014; Chen et al., 2015; Zhang et al., 2015). In 2018, a major HFMD outbreak have infected over 76,000 children in Malaysia. PCR genotyping of 89 samples originating mostly from

children <3 years of age revealed CV-A16 (40%) and CV-A6 (44%) as the predominant serotypes in comparison with EV-A71 (10%) (Lee et al., 2021). Therefore, we have included CV-A16 in the design of our trivalent vaccine candidate as protection against EV-A71 alone would be insufficient.

2.2 Structure of HFMD etiological agents

Enteroviruses and coxsackieviruses including EV-A71, CVA16, CV-A10 and CV-A6 all belong under the *Picornaviridae* family, classified under Enterovirus species A. Picornaviruses are non-enveloped, icosahedral single-stranded RNA viruses composed of 4 virus capsid proteins (VP1-VP4) and possess the same fundamental architecture across all family members (Brown & Pallansch, 1995; Smyth & Martin, 2002).

The positive-sense RNA genome encompasses a single open reading frame (ORF) which was flanked by a 5'- untranslated region (UTR) on the front and 3'-UTR with poly-A tail at the terminus (Lu et al., 2011). The ORF encodes a large polyprotein that would be subsequently cleaved into P1, P2 and P3 precursor proteins which would be processed into 4 structural proteins and 7 non-structural proteins. P1 was cleaved to further form VP1, VP2, VP3 and VP4 structural proteins, VP4 was hidden inside the capsid whereas VP1, VP2 and VP3 were exposed on the external surface. Cleavage of P2 and P3 would form 2A-2C and 3A-3D non-structural proteins, respectively. During the Enterovirus lifecycle, structural proteins VP0, VP1 and VP3 would assemble into a protomer in the cytoplasm. VP0 served as the precursor protein of VP2 and VP4. A pentamer was assembled by 5 protomers and 12 pentamers would form the icosahedral pro-virion upon acquiring the viral genome. VP0 was subsequently cleaved through an autocatalytic mechanism into VP2 and VP4, mature virus particles were completely formed and would be released from infected cells (Anasir & Poh, 2019; Wang et al., 2021; Swain et al., 2022).

The human neutralizing antibodies mainly targets the VP1, VP2 and VP3 capsid proteins with VP1 being extremely valuable to assess vaccine potency as the majority of neutralizing epitopes were mapped to VP1. Despite the architectural similarity, VP2 and VP3 proteins contribute to less neutralizing epitopes in comparison to VP1 (Anasir & Poh, 2019). EV-A71 was classified into genogroups A-G based on their VP1 protein, genogroup A was the designation for prototype strain BrCr-CA-70. Genogroups B and C were further classified as B0-B7 and C1-C6 respectively (Chang et al., 2016; Si et al., 2022). Based on genetic diversity of VP1, CV-A16 could be classified into 3 genogroups A, B and D, genogroup A was denoted for the prototype strain G10. CV-A16 genogroup B could be divided further into sub-genotype B1 (B1a-B1c), B2 and B3 (Wang et al., 2018; Hu et al., 2021). Studies have shown both EV-A71 and CV-A16 consists of 80% sequence identity with largely overlapping neutralizing epitopes, indicating both enteroviruses to be highly conserved (Anasir & Poh, 2019).

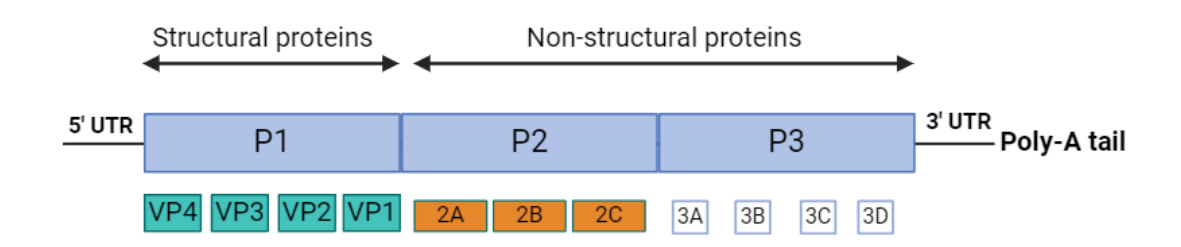


Figure 2.1: Schematic representation of enterovirus genome (image generated through biorender software), generated image referenced from Mandary and Poh (2018).

2.3 Cyclical occurrence of HFMD

HFMD caused by EV-A71 had an epidemiological pattern of outbreaks occurring every 2-4 years which varies between country (Yip et al., 2013; Chong et al., 2015). HFMD outbreaks in Malaysia occur in a 3-year cyclical pattern since the first documented EV-A71 emergence in 1997, followed by late 2000, 2003, 2006, 2009 and 2012 (Chan et al., 2012; Sham et al., 2014; NikNadia et al., 2016). The recent 2018 outbreak of HFMD in

Sarawak also occurred after 3 years of non-outbreak period in 2015, 2016 and 2017. There was a 2.7-fold increase of HFMD cases and incidence rate (per 100,1000) when comparing between year 2017 and 2018 (Fong et al., 2021). A previous study has showed the epidemic years of HFMD in Singapore to also occur in a cyclical pattern (Ang et al., 2015). Since 2011, large scale epidemics of HFMD were predicted to be in a 2-year recurrent cycle in Japan instead (Yoshida et al., 2022). EV-A71 outbreaks in Taiwan were associated with genotype change at a recurring rate of every 3-5 years (Huang et al., 2009).

This cyclical occurrence of HFMD could be attributed to the unpredictable switching of genotypes/sub-genotypes and recombination events between serotypes thereby producing new variants (Chong & Klein, 2018). HFMD enteroviruses are RNA virus which are more prone to mutation, resulting in high genetic diversity (Sanjuán et al., 2010; Duffy, 2018). Most HFMD outbreaks were also associated with peaks of EV-A71 genetic diversity (NikNadia et al., 2016; Chong & Klein, 2018). Intergenotypic shifts were observed in Taiwan where the predominant strain shifted from C2 to B4, later C5 to B5 over the years (1998-2009); Intra-genotypic shifts have been reported in Korea as sub-genotype C3 shifted to C4 (2000-2003/2009) (Yip et al., 2013). EV-A71 C4 was reported to have constantly evolved and persisted through accumulation of amino acid substitutions throughout the outbreak (2008–2012) and non-outbreak (2004–2007) periods in China (Zhang et al., 2013).

EV-A71, CV-A16, CV-A10 and CV-A6 were able to co-circulate which could lead to viral co-infection and possible genetic recombination, thus making HFMD outbreaks even harder to control (Lin et al., 2012; He et al., 2013). Previous studies have reported the emergence of new recombinant variants during outbreaks due to intertypic or intratypic genetic recombination resulting from co-circulation between multiple EV-A71 and CV-A16 genotypes (Yip et al., 2013; Huang et al., 2014; Liu et al., 2014; Mizuta et al., 2014; Chong et al., 2015). Liu et al. (2014) have also reported the reemergence of EV-

A71 C4b and CV-A16 B1b that was previously quiescent for a long period due to possible co-circulation during a large epidemic in China (Liu et al., 2014). Population immunity or seroprevalence was also reported to be higher in older children and during HFMD epidemics. However, susceptible young children would accumulate again over the 2-3 years of non-outbreak period, therefore HFMD outbreak could recur when population seroprevalence reached a lower point (NikNadia et al., 2016). It is therefore important to develop new HFMD vaccines periodically to prepare against new variants which escaped or adapted to the herd immunity.

2.4 Status of HFMD vaccine development

2.4.1 China FDA approved inactivated HFMD vaccines and aftermath of IV implementation

Inactivated whole virus vaccines (IV) would be the first choice among various vaccine candidates since the inactivated poliovirus (PV) vaccine was successfully commercialized and nearly eradicated polio outbreaks. This suggests that IV can be developed as an effective vaccine against enteroviruses (Heinsbroek & Ruitenberg, 2010; Shen et al., 2016). There are currently 3 different vaccine manufacturers for the monovalent EV-A71 vaccine [Sinovac Biotech Co., Ltd., Beijing Vigoo Biological Co., Ltd., and the Chinese Academy of Medical Sciences (CAMS, Kunming Institute)] (**Table. 2.1**). Phase III clinical trials of these formalin inactivated, whole virus alum-adjuvanted EV-A71 vaccines have been successfully completed (Zhu et al., 2013; R. Li et al., 2014; Zhu et al., 2014). These clinical trials involved more than 30,000 children ranging from 6 to 59 months and two doses were administered 4 weeks apart. The efficacy against EV-A71 associated HFMD infections were reported to be more than 90% (Yi et al., 2017). The IV manufactured by these three companies were approved by the China Food and Drug Administration (CFDA) for human use and licensed by the China Medical Products Authority to be sold in China (Wang et al., 2019; Yee et al., 2019). However, monovalent

EV-A71 inactivated vaccines could not provide cross protection against the other 3 enterovirus serotypes (CV-A16, CV-A10, CV-A6) and patients require multiple boosters every 6-12 months due to reliance on humoral immunity for protection (Aswathyraj et al., 2016; Fang & Liu, 2018). Additionally, all three EV-A71 IVs were designed against the C4 subgenotype as it was the most common genotype in China. Failure of EV-A71 IV by CAMS and Sinovac to confer protection against CV-A16 suggest that the vaccines could be genotype specific (X. He et al., 2021). Besides China, Taiwan had been evaluating an EV-A71 IV targeting the B3 sub-genotype in phase II clinical trials. Long lasting seroprotection efficacy were observed in 365 patients between the age of 2 months~11 years, cross reaction was also observed against the other genotypes of EV-A71 (B5, C4a, C4b, and C5) (L. M. Huang et al., 2019).

Since the implementation of EV-A71 IV in China, a surveillance study focusing on the capital Nanchang have observed a gradual decrease of HFMD cases from EV-A71 infection. EV-A71 was only identified in 22.5% of HFMD cases in 2017, followed by 0.5% in 2018 and was absent in 2019; there have also been less than 1% of severe cases commonly associated with EV-A71 reported since 2018. CV-A6 have replaced EV-A71 as the most prevalent HFMD serotype as of 2019 in China (R. Li et al., 2014; F. He et al., 2021).

However, herd immunity that was gained through mass vaccination may wane over time and act as evolutionary pressure which provokes the mutation of pathogen (Rodpothong & Auewarakul, 2012; Dassarma et al., 2022). EV-A71 could continue to persist and give rise to novel strain through the cooperation of inter- or intra-typic recombination, antigenic changes, and genotype shifts (S. W. Huang et al., 2019). New variants of EV-A71 that escape population immunity could reemerge as the dominant strain during future HFMD outbreaks (NikNadia et al., 2016). Previously, EV-A71 C4b that was inactive for six years was identified to be one of the main causative agents responsible for a large outbreak in China (2011-2012) (Liu et al., 2014).

Table 2.1: China FDA approved formalin inactivated vaccines. Table adapted from X. He et al. (2021).

| Manufacturers | EV-A71 subgenotype | Vaccine type | Patient population size | Patient population age | References |
|--|-----------------------|-------------------------|-------------------------|---------------------------|-------------|
| Beijing Vigoo Biological | FY (C4) | | 10,245 | 6-35 months | NCT01508247 |
| Sinovac Biotech | H07 (C4) | Formalin inactivated | 10,077 | 6-35 months | NCT01507857 |
| Chinese academy of medical sciences (CAMS) | M01 (C4) | | 12,000 | 6-71 months | NCT01569581 |

2.5 Experimental HFMD vaccines

2.5.1 Inactivated vaccine (IV)

Recent research activities have developed a wide range of experimental vaccines against multiple HFMD pathogens in the vaccine formulation including studies of the tetravalent inactivated vaccine (IV) and tetravalent Virus like particle-based vaccines (VLP). (Liu et al., 2016; Zhang et al., 2018). The tetravalent IV vaccine candidate was formulated through mixing of formalin inactivated EV-A71, CV-A16, CV-A10 and CV-A6 virus particles. Both mice and rabbit immunized with the combination of EV-A71, CV-A16, CV-A10 and CV-A6 IV particles exhibited cross neutralizing capabilities against all four enteroviruses. However, the neutralizing antibody titer induced by the tetravalent IV against EV-A71 were reported to be significantly higher in comparison to the neutralizing titers against CV-A16, CV-A10 and CV-A6 enteroviruses (Liu et al., 2016).

There was also an experimental trivalent IV study targeting the EV-A71, CV-A16 and CV-A6 enteroviruses (Caine et al., 2015). Murine models that received the trivalent vaccine were protected from lethal challenges of both mouse-adapted EV-A71 and CV-A16 whereas their monovalent vaccine counterparts were unable to provide cross immunization. Protection against CV-A6 was also observed in passive immunization study where murine models were injected with mouse antisera raised against the trivalent vaccine. However, lower neutralizing antibody levels were detected in the trivalent vaccine group in comparison to their monovalent vaccine counterpart. The explanation given was immunologic interference due to immune system needing to build response against 3 viruses instead of one. Immunologic interference is a common issue often found during formulation of multivalent/combined vaccines and was reported previously from trivalent poliovirus and tetravalent dengue vaccine studies (Coller & Clements, 2011; Chokephaibulkit & Perng, 2013).

2.5.2 Virus like particle (VLP) vaccine

Due to their high safety and immunogenicity, recombinant virus-like particles (VLP) vaccines are also considered as an attractive alternative besides IV. The human papillomavirus and hepatitis B virus vaccines are both good examples of successfully commercialized VLP-based vaccines (Roldão et al., 2010; Kushnir et al., 2012). A recent study employed Baculovirus-insect cell expression system to produce monovalent EV-A71-VLP, CV-A16-VLP, CV-A6-VLP and CV-A10-VLP, all 4 monovalent VLP were then combined to construct a tetravalent VLP vaccine (Zhang et al., 2018). Immunization studies of mice showed that the tetravalent VLP vaccine formulation was able to provide broad neutralization against both single and mixed infections of EV-A71, CV-A16, CV-A10 and CV-A6 virus while monovalent VLP did not provide protection against heterotypic challenges. Moreover, neutralizing antibody titers induced by the tetravalent VLP was comparable with their corresponding monovalent counterparts, indicating all 4 VLP components had good compatibility. However, immunologic interference was again observed as CV-A10 and CV-A6 monovalent vaccines demonstrated lower neutralization titers in comparison with both EV-A71 and CV-A16 monovalent vaccine. This immune interference phenomenon correlated with the findings by Liu et al. (2016) but the exact underlying mechanism remained unknown. The author theorized that EV-A71 antigens might consist of strong T cell epitopes not found in other enteroviruses.

2.5.3 Live attenuated vaccine (LAV)

Live attenuated vaccines (LAVs) are the weakened version of virus with reduced virulence while maintaining its antigenic properties (O'Connell & Douam, 2020). LAVs were successfully implemented in vaccination against poliovirus, influenza, rabies, mumps, and measles previously, LAVs administration could also be carried out locally without the need for multiple boosters or aid of adjuvants (Lim & Poh, 2019; Yee et al., 2019; Lin et al., 2020; Nouailles et al., 2023) LAV is capable of mimicking the natural course of infection to elicit lifelong protection thus being more effective in comparison with other vaccine platforms (Lim & Poh, 2019; Nouailles et al., 2023).

Firstly, Arita et al. (2005) constructed an attenuated strain EV71(S1-3') by introduction of mutations in the 3D polymerase, 3'- and 5'- untranslated regions (UTR) of the EV-A71 prototype strain BrCr (genotype A) (Arita et al., 2005). In vitro neutralization assay of a subsequent study showed that monkey sera immunized with EV71(S1-3') was able to cross-neutralize against multiple EV-A71 sub-genotypes (A, B1, B4, C2 and C4), exhibiting highest and lowest neutralizing titers against the parental strain BrCr and genotype C2, respectively. Inoculation of monkeys with the EV71(S1-3') LAV candidate was able to protect them from lethal challenges of virulent EV-A71 BrCr. However, 3 out of 5 monkeys inoculated with the attenuated EV71(S1-3') through intravenous route exhibited tremors and weakness in the leg suggesting possible reversion of the LAV to neurovirulence (Arita et al., 2007).

Subsequently, Yee et al. (2019) designed two LAV vaccine candidates that were named as MMS and pIY. The multiply mutated strain (MMS) was constructed by introduction of nucleotide substitution at 5'-non translated region (NTR), amino acid replacements at VP1, single mutation (G64R) at 3D Polymerase (3D^{Pol}) of a previously identified EV-A71 mutant (Yee et al., 2016). The EV-A71 mutant (sub-genotype B4) carried partial deletion (PD) at the 5'-NTR (11bp). pIY was constructed by introduction of two micro-RNA genes into the same EV-A71 mutated (PD) strain with a G64R mutation. MMS or

pIY administration in mice were able to confer 100% protection against a mouse-adapted EV-A71 virus with no weight loss or hind limb paralysis observed. ELISpot results of both MMS and pIY showed higher amounts of *ex vivo* IFN-γ in murine splenocyctes when compared with an inactivated EV-A71 vaccine, indicating good cellular immunity (Yee et al., 2019).

A study by Yang et al. (2020) evaluated the immune response of a CV-A16 attenuated strain (K168-8Ac) at different passages including P35, P50, P60 and P70 in monkey models via intramuscular (IM.), oral or intranasal route. The K168-8Ac strain of CV-A16 started exhibiting attenuated virulence in mice models at the 17th passage (P17) in a previous study (Yang, 2015). Monkeys immunized by different passages of K168-8Ac did not exhibit any neurological symptoms classified under HFMD. Mild fever was observed in monkeys immunized via oral and IM route (P35, P50). However, immunization through nasal route or with higher passages (P60 and P70) did not induce any fever in monkeys. IM administration of K168-8Ac at all passages were able to induce significantly higher levels of neutralizing antibody in comparison to oral and intranasal route. Immunized monkeys had reduced faecal viral shedding and reduced pulmonary injury in comparison with mock monkeys upon challenged with infection of CV-A16 strain K154. However, vaccination was associated with symptoms of viremia and histopathological damages were not eliminated completely (Yang et al., 2020).

Therefore, inactivated virus, recombinant peptides/proteins, virus-like particles, and genetic based vaccines were more preferred in HFMD vaccine development due to the risk of potential wild-type reversion in LAVs (Chong & Klein, 2018). Administration of LAV in pregnant patients or immunocompromised individual could also lead to increased virulence of the attenuated strain thereby causing severe disease manifestations (Torresi & Kollaritsch, 2019).

2.5.4 Epitope mapping and recombinant peptide/protein vaccines against HFMD

2.5.4.1 Immunogenic epitopes and recombinant vaccines of EV-A71

Most of the crucial epitopes contributing to neutralization of EV-A71 enterovirus was first discovered on the VP1 capsid protein comprised of 297 amino acids, VP1 was located at the most external part of viral capsid (Anasir & Poh, 2019). Previous study reported VP1 to bind with host receptors such as PSGL-1 and SCARB2 upon EV-A71 infection, thereby causing EV-A71 destabilization as a prelude for the release of genome (Plevka et al., 2012; Tan et al., 2013). VP1-145 was reported to act as a molecular switch during receptor binding by modulation of VP1-244K exposure which affects binding to PSGL-1 (Nishimura et al., 2013). Mutations located at VP1-242 and VP1-244 were also discovered to greatly reduce or completely removed binding capabilities to PSGL-1 receptor, respectively (Nishimura et al., 2013). Early studies have also focused on development of recombinant VP1 as a vaccine candidate due to less safety concern and their cost-effective production (Lim & Poh, 2019).

Wu et al. (2001) experimented with a recombinant VP1 protein vaccine expressed through an E.coli host system in comparison with a heat inactivated EV-A71 vaccine (IV). Immunization of newborn mice with inactivated EV-A71 was able to confer 80% protective efficacy against virus challenge at higher lethal dosage (LD50) (2.3×10^3) whereas 100% mortality was observed at 6 days post infection in mice group that received recombinant VP1 protein. However, recombinant protein vaccine immunization was able to protect the mice at a lower LD50 (2.2×10^3) with 95% survival rate at 10 days post infection. Murine immunization with the IV was also generated significantly greater magnitude of IgG levels in comparison with group that received recombinant VP1 protein; Higher IgG titres of >32-fold and >256-fold was reported at 3 weeks and 7 weeks post immunization, respectively (Wu et al., 2001).

A study by Foo et al. (2007) had identified two linear cross sub-genotype neutralizing epitopes at the VP1 region of EV-A71 B4 strain 41 and they were designated as SP55 (163-177 aa) and SP70 (208-222 aa), respectively. Both synthetic peptides SP55 and SP70 demonstrated good neutralizing effects against heterologous strains of EV-A71 subgenotype B2, B5, C2 and C4 with 1:16 and 1:32 dilutions as the neutralizing titers by SP70 whereas 1:8 dilution was reported for SP55 for viral clearance. Additionally, antisera isolated from mice immunized with SP70 were able to provide protection against lethal challenge of clinical strain EV-A71 in neonatal mice models through passive immunization (Foo et al., 2007).

Subsequently, a study by Yong et al. (2016) synthesized 63 immunogenic peptides based on *in silico* prediction of potential EV-A71 B-cell epitopes. A total of 4 IgG-specific and 22 IgM-specific immune-dominant epitopes were identified through screening of sera from children infected with EV-A71. Overall, PEP27 was reported with the highest mean OD value (IgM titers) when screened against serum samples of patients infected with EV-A71 and thus the best IgM dominant epitope. PEP27 mapped to the 142-156 of VP1 was also EV-A71 specific as there were no cross-reactivity to serum samples of patients infected with other non-EV-A71 enteroviruses. The most dominant linear epitope recognized by EV-A71 reactive IgG antibodies denoted as PEP23 was located within VP1 protein, corresponding to amino acid residues 141-155 and highly specific to EV-A71 (Aw-Yong et al., 2016).

Liu et. al (2011) identified another linear cross sub-genotype neutralizing epitope in the VP2 region of EV-A71 which was named as VP2-28 (136-150 aa). VP2-28 was able to bind with an antibody (MAB979) capable of cross-neutralizing multiple EV-A71 sub-genotypes, thereby inhibiting the binding of MAB979 to live EV-A71 virion. The author reported that their formalin inactivated EV-A71 vaccine (IV) had a dose dependent relationship between the neutralizing magnitude of immunized rabbit and mice sera with

the number of VP2-28 epitope units found in the IV. VP2-28 synthetic peptide immunization alone in this study failed to elicit virus neutralizing antibody response in murine models (unpublished data). The author suggested that VP2-28 epitope could be immunodominant in rabbits but cryptic in mice (C. C. Liu et al., 2011).

However, a multiple tandem linear neutralizing epitope (mTLNE) vaccine candidate was constructed through the linking of 3 synthetic peptide epitopes including VP1-SP55, VP1-SP70 and VP2-SP28 of EV-A71(Y. X. Li et al., 2014). Antisera from the immunized BALB/c mice were reported to show cross reactivity with 3 capsid proteins of EV-A71 (VP0, VP1 and VP2) in western blot analysis. Cross sub-genotype neutralizing effects were observed as strong neutralizing antibody titers were elicited by mice immunized with 3 doses of the mTLNE vaccine against EV-A71 genotype C4 and EV-A71 genotype A.

In addition, subsequent study by Xu et al. (2014) identified a linear VP2 cross neutralizing epitope that was mapped to a region (141-155 aa) overlapping with the findings of Liu et al. (2011) (Xu et al., 2014). Gene sequence encoding amino acid residues 141-155 was inserted into the genome of an immune enhancing carrier derived from truncated Hepatitis B virus core protein (HBc-VP2) to generate a chimeric protein HBc-VP2(aa141-155). Antisera of mice immunized with HBc-VP2 (aa141-155) was able to protect newborn BALB/c mice from lethal challenge of mouse-adapted EV-A71 virus (pSVA-MP4) with 100% survival rate at 20 days post infection. The fusion epitope HBc-VP2 (aa141-155) was also proposed to be immunodominant in human as VP2(aa141-155) antibodies were able to inhibit 60% of human sera (EV-A71-infected) from binding with EV-A71 virus sub-genotype C4. Therefore, both the VP1 and VP2 DNA sequences were included in the design of our plasmid vaccine in attempt to improve the T cell and B cell immune response against EV-A71.

2.5.4.2 Neutralizing epitopes identified in CV-A16

The neutralizing linear epitopes of CV-A16 were not as commonly studied in comparison with EV-A71 (Anasir & Poh, 2019). Chong et al. (2012) have screened the antisera of mice or rabbit that were immunized with formalin-inactivated P- or R- viral particles of CV-A16 against a series of overlapping peptides spanning the 4 structural proteins VP1, VP2, VP3 and VP4. P- and R- particles were defined as pseudo-defective and infectious viral particles, respectively by the author based on their viral, immunological, and biochemical properties. A single linear epitope was identified in the VP3 region (176-190 aa) of CV-A16. However, only the murine antisera raised against inactivated CV-A16 R-particle weakly cross-reacted with the corresponding peptide epitope VP3-41 in peptide-ELISA assay. Antisera of rabbits raised against P- or R- particles of CV-A16 failed to recognize any of the 153 synthetic peptides (Chong, Guo, et al., 2012).

Subsequently, Shi et al. (2013) tested a series of overlapping synthetic peptides with full coverage over the CV-A16 VP1 protein amino acid sequence. Among the 95 peptides, a total of six non-overlapping peptides including PEP32, PEP37, PEP55, PEP63, PEP71 and PEP91 were identified as neutralizing epitopes. Antisera derived from mice immunization with these six peptides were all able to cross react with inactivated CV-A16 and VP1 bands were detected in western blot. Neutralization assays have shown that mice antisera harvested post-immunization by these six peptides to be able to neutralize both the homologous (CA16-SZ05) and heterologous strain of CV-A16 (CA16-G08). Furthermore, the author had screened all six peptide epitopes against 11 CV-A16 representative strains including the genotype A (prototype strain G10), genotype B1 (B1a and B1b), and genotype B2 for homology comparison of the VP1 sequences. Three peptide epitopes (PEP55, PEP63 and PEP91) were found to be identical, whereas peptides PEP32 and PEP37 were highly conserved (93.3%) among all eleven strains of CV-A16. However, alignment of peptide epitope PEP71 resulted in low homology among the

eleven strains which was due to the CV-A16 prototype strain G10. The corresponding PEP71 epitope sequences when aligned were found to be identical in the other 10 nongenotype-A CV-A16 strains. PEP71 epitope was located at amino acid residues 211-225 which overlapped with several known EV-A71 VP1 neutralizing epitopes including the VP1 epitope SP70 (208-222 aa) and VP1-43 (211-220 aa) (Shi et al., 2013). SP70 was established as a cross genotype neutralizing epitope whereas VP1-43 was recognized as an EV-A71 strain-specific epitope (Foo et al., 2007; C. C. Liu et al., 2011). Therefore, the VP1 gene of CV-A16 was included in the design of our trivalent plasmid vaccine to confer immune response against CV-A16.

2.5.5 Plasmid DNA vaccine

Tung et al. (2007) constructed a monovalent DNA vaccine by cloning the EV-A71 VP1 gene into a eukaryotic expression vector pVAX1. The viral VP1 protein was successfully expressed in vitro in a mammalian cell line (Vero), VP1 expression was confirmed through western blot and indirect immunofluorescence assay (IFA). The recombinant DNA construct was subsequently used to immunize mice models, virus neutralization assay results of the pVAX1-VP1 immunized mice sera demonstrated broad neutralizing abilities as only 50% of cytopathic effect (CPE) was observed in Vero cells infected with EV-A71. ELISA results of the immunized mice sera showed significant increase of anti-VP1 IgG levels after the first booster but declined following the second booster. The author provided a possible explanation which was due to the shifting of humoral immunity to cellular immune response, this was usually accompanied with an increase of cytolytic T cells (Tung et al., 2007). A similar observation was made by Tanghe et al. (2000) as mice immunized with tuberculosis vaccine have decreased antibody levels after the second booster which was accompanied with increased IFN-y and IL-2 levels (Tanghe et al., 2000). Therefore, this calls for a novel multivalent DNA vaccine that targets more than one HFMD pathogens.

2.6 Background of plasmid vaccine

In 1990, the ability of plasmid DNA (pDNA) to transfect cells was first reported from a simple experiment of pDNA vectors carrying foreign genes which were injected into murine skeletal muscle resulting in the expression of foreign proteins (Wolff et al., 1990). The potential immunogenicity of pDNA expressed proteins gave rise to the technology of DNA vaccination involving the delivery of pDNA either through intranasal, dermal, intramuscular, rectal, or oral route (Hobson et al., 2003). Upon internalization, DNA vaccines would be transcripted into mRNA in the nucleus and later transferred to the cytoplasm for translation into protein (Bai et al., 2017).

2.7 Mechanism of plasmid antigen presentation in vivo

Antigenic peptides originating from extracellular source (exogenous) were almost exclusively loaded onto MHC class II molecules and presented to CD4⁺ helper T cells; This in turn stimulate B cells leading to neutralizing antibody response and complete activation of CD8⁺ T cells (den Haan et al., 2014). MHC class II molecules were commonly found on the surface of professional antigen presenting cells (APCs) such as B cells, dendritic cells, thymic epithelial cells and macrophages (Roche & Furuta, 2015). Endogenous antigens derived from intracellular proteins originating from the cytosol or nucleus were instead loaded on MHC class I molecules that were present on the surface of all nucleated cells (Leung, 2015). Viral specific cytotoxic T lymphocytes (CTL) differentiated by CD8⁺ T cells were able to recognize peptide-MHC class I complexes (pMHCI) expressed by the infected cells and eradicate them to prevent the spread of virus (Hewitt, 2003; Wieczorek et al., 2017). However, cross-presentation could also occur as exogenous antigens were presented by MHC class I molecules of specific subpopulations of dendritic cells to initiate CD8⁺ T cell immunity (Joffre et al., 2012).

There are three antigen presentation mechanism of administered plasmid DNA compiled by Qin et al. (2021) (**Fig. 2.1**): 1) Internalized plasmid DNA could be taken up by resident

somatic cells including muscle or epithelial cells depending on the administration route. The somatic cells would subsequently secrete the expressed antigens leading to B cells activation. 2) DNA vaccines can directly transfect professional antigen presenting cells (APC) such as macrophages and dendritic cells (DC), leading to direct antigen presentation to the respective CD4+ and/or CD8+ T cells through both MHC class I and II complexes. 3) Professional APCs take up the antigens expressed by transfected somatic cells; pDNA transfected somatic cells that underwent apoptosis could also be phagocytosed by APCs. Antigens were subsequently presented to CD4⁺ and CD8⁺ T cells upon migration of APCs into the draining lymph nodes, triggering both humoral and cellular immunity. This is also the pathway where cross-presentation occurs as exogenous antigens were processed and presented on MHC class I molecules (Donnelly et al., 2000; Joffre et al., 2009; Coban et al., 2013; Langer et al., 2013). Dendritic cells were the most efficient in carrying out this process despite other APCs such as monocytes were also reported with cross priming capabilities (Leirião et al., 2012). CD4⁺ T cells were involved in B cells activation along with differentiation into plasma cells responsible for antibody secretion and formation of memory B cells (Tay et al., 2019). On the other hand, cytotoxic CD8⁺ T cells serve as an effector of host cellular immunity which kills off infected cells (Zhang & Bevan, 2011). Aside from binding with the same antigen carrying APC, interactions between CD4⁺ and CD8⁺ T lymphocytes were also crucial in establishing protective immunity against infection. DNA vaccination studies in early 1997 and 1998 have shown that CD8+ cytotoxic T cells activation were highly dependent on CD4+ helper T cells and dendritic cells derived from bone marrow instead of tissue-specific cells (Iwasaki et al., 1997; Maecker et al., 1998). This was further supported by studies showing the inability of CD8⁺ T cells to develop into CD8⁺ memory cells at the absence of CD4⁺ signalling (CD40 deficiency) despite repeated priming (Bourgeois et al., 2002; Rapetti et al., 2008). A study by Barinov et al. (2017) has also shown that presence of CD8⁺ would modulate and accelerate the activation as well as division of CD4⁺ T cells in vivo. Upon contact with Dendritic cells carrying antigenic peptide, CD8⁺ T cells were able to physically extract a small fragment of the DC membrane carrying MHC class II molecules, this process is known as trogocytosis. The CD8⁺ T cell was capable of directly presenting the immunogenic peptide to naïve CD4⁺ T cells thereby stimulating their differentiation in vitro (Barinov et al., 2017). Therefore, DNA vaccination is capable of inducing a strong protective immune response by activating both the cellular and humoral branch of adaptive immunity (Nguyen et al., 2009).

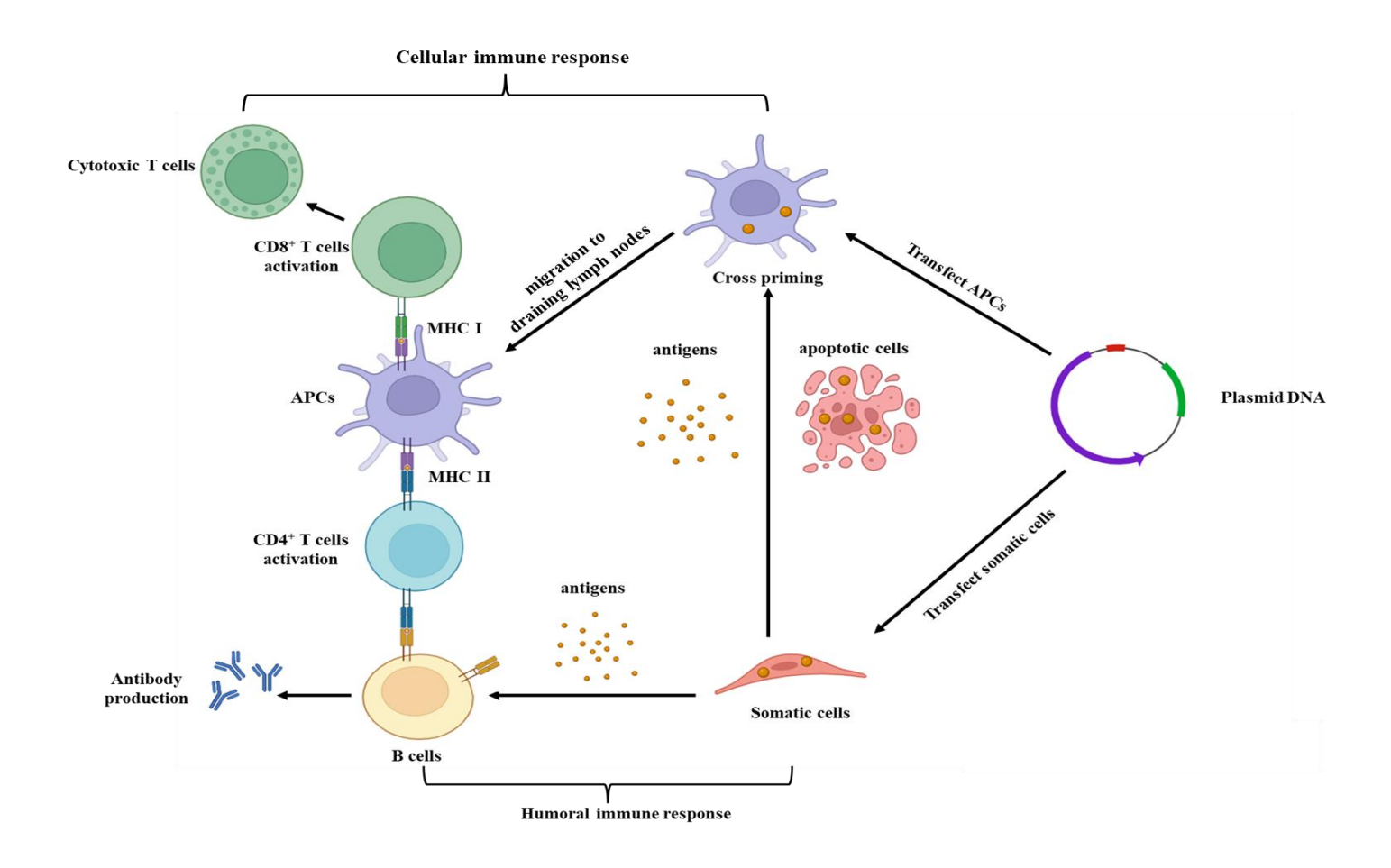


Figure 2.2: DNA vaccine was able to induce humoral immune response by transfection of somatic cells followed with B cells activation leading to antibody production, CD4⁺ T cells were also able to stimulate B cells division. APCs could be activated by direct transfection or indirectly by cross-priming, followed by activation of CD8⁺ T cells through MHC class I molecules thereby inducing cellular immune response. Image was generated with biorender.com.

2.8 IRES sequences and translation of plasmid DNA

The process of eukaryotic mRNAs translation to protein were mainly initiated through a cap-dependent manner. Ribosomes would first bind to the 7-methylguanosine cap located at the 5' end of mRNA and scan for the initiation codon (AUG) to begin the translation process (Cooper & Hausman, 2000). However, specific internal ribosome entry site (IRES) sequences were discovered to be able to direct the internal binding of 40s ribosomal subunits to downstream AUG start codon thereby initiating the translation process in a cap-independent manner (Ambrosini et al., 2021). IRES sequence was first discovered in the noncoding region (5' UTR) of poliovirus followed by (picornavirus) encephalomyocarditis virus (EMCV) mRNA (Pelletier & Sonenberg, 1988; Jang & Wimmer, 1990). Aside from viral mRNA, some cellular mRNAs were also found to consists of IRES sequence which was first identified in an immunoglobulin heavy chain binding protein (BiP) (Yang & Sarnow, 1997). To date, poliovirus and EMCV derived IRES elements were commonly used in commercial and experimental construction of polycistronic vectors for expression of heterologous proteins, gene transfer or gene therapy (Hennecke et al., 2001; Bochkov & Palmenberg, 2006). Expression of protein was also reported to be higher when the cytokine gene was positioned as the first cistron in the bicistronic plasmid (Hennecke et al., 2001). IRES elements derived from EMCV were reported to be of similar or stronger translation strength when compared to IRES sequences of other origin including rhinovirus, poliovirus and foot and mouth disease (Borman et al., 1997). However, the expression of EMCV IRES dependent second gene were also documented at range of 20% to 50% in relative of the first cistron (Mizuguchi et al., 2000; Wang et al., 2005). Prior to the discovery of IRES sequences, co-expression of two heterologous genes were mainly achieved through insertion of two separate promoters in a single vector. However, transcriptional interference and/or suppression of gene expression could occur as the activation of first promoter could supress or inactivate the second promoter which have been observed in studies (Cullen et al., 1984; Emerman & Temin, 1984, 1986). This phenomenon of promoter interference leads to a subset of transfected cells actively expressing only one of the target gene instead of both genes. Aside from the use of multiple promoters, two or more genes could be linked or fused together into a chimeric gene sequence and target genes were co-expressed in the form of fusion protein (Huang et al., 2018; Jeong et al., 2021). However, there is still concerns on misfolding of the proteins which leads to expression of largely inactive chimeric proteins (Randall, 2010). Therefore, IRES sequence is favourable for simultaneous expression of multiple genes as translation of the first cistron would be initiated by cap-dependent translation whereas the second or following cistron would be translated independently through an IRES mediated mechanism (Kozak, 1995; Al-Allaf et al., 2019). We have implemented two IRES sequences derived from poliovirus for expression of the second and third enterovirus genes in the design of our trivalent HFMD plasmid vaccine candidate.

2.9 Advantages of DNA vaccine

Recently, there have been a rise of interest in studies of DNA vaccine candidates since the SARS-CoV-2 infection outbreaks and COVID-19 cases that have been terrorizing the globe. A study in Thailand constructed 3 DNA vaccines each encoding the 1) full length SARS-CoV-2 spike (S) protein, 2) S1 and 3) S2 regions of S protein. These recombinant plasmids were administered via TriGrid delivery system into mice models through intramuscular route. This study provided insight where SARS-COV-2 full length S protein induced cellular and humoral immunity were much more potent than that of truncated S1 or S2 immunogen (Prompetchara et al., 2021).

In contrary to conventional vaccines such as inactivated and live attenuated vaccines, DNA vaccination is an attractive alternative due to its advantages including: (1) a safer platform by directly working with the transgene, without the need to handle virulent pathogen during vaccine synthesis (Liu, 2011), (2) induction of antibody and cell-

mediated immunity through closely mimicking live pathogens without the risk of reversion to wild type (Nguyen et al., 2009; Jazayeri & Poh, 2019), (3) fairly stable at room temperature thereby saving the costs for cold storage and transportation (Quaak et al., 2010; Liu, 2011), (4) relatively fast and low manufacturing cost for large inventory doses in a scalable manner (Cai et al., 2009; Khan et al., 2014), (5) no further purification of recombinant protein is required as protein antigens of interest will be directly expressed in host cells (Liu, 2011) and (6) transgene sequence can be easily manipulated to adapt to fast emerging new disease variants, optimize antigen specificity and improve immunogenicity (Coban et al., 2011; Deering et al., 2014; Iurescia et al., 2014).

2.10 Vaccination strategies

2.10.1 Limitations of DNA vaccine

Currently, there were three DNA vaccines licensed for veterinary applications in fish, horse and dogs with a fourth vaccine that was approved for hormonal therapy in pigs. All four DNA vaccines were administered through injection of naked plasmid by the intramuscular (IM) route (Liu, 2011). IM or intradermal delivery of DNA vaccines through parental route were able to provide protection and induce systemic immunity in multiple studies involving murine models (Hobson et al., 2003). However, most cases of standard IM injection only conferred weak immune responses and rarely provide mucosal immunity (Hobson et al., 2003; Nguyen et al., 2009). Additionally, rodent models had limited amount of muscle mass and the transfections were therefore aided by physical pressure during IM injection. Higher order mammals would instead require adjuvants or transfection aids such as intramuscular electroporation (Khan et al., 2014).

There are still limitations of DNA vaccine as high immunogenicity results observed in small animal models may not be replicated in large animal models (Jazayeri & Poh, 2019). Additionally, pDNA delivery needs to occur in appropriate tissues or cell types for effective innate and adaptive immune response coordination (Nguyen et al., 2009).

Therefore, it is important to choose a suitable route for DNA vaccine administration using a potent delivery platform.

2.10.2 Nanoparticles as delivery platform for plasmid DNA

The formulation of pDNA vaccine into micro or nanoscale particles could provide controlled, target cell and site-specific release (Farris et al., 2016). Vaccine efficacy is greatly affected by characteristics of particles including the surface charge, hydrophobicity, surface modification and particle size. Microparticles would allow sustained exposure of pDNA to cells due to its bulky size (>0.5 µm) and they were mainly taken up by macrophages through phagocytosis (O'Hagan et al., 2004; Hajizade et al., 2014). In comparison, nanoparticles (20~200 nm) were mainly taken up by DCs through endocytosis and could directly enter lymph nodes to achieve higher transfection efficacy (Prabha et al., 2002; Nguyen et al., 2009). Nanoparticles were also shown to be more cytotoxic when compared with microparticles due to its relatively larger surface area while having a smaller size (Sahu et al., 2016). Cationic particles were preferentially taken up by non-phagocytic cells while anionic particles were mainly ingested by phagocytic cells. Additionally, cationic nanoparticles such as chitosan are highly cytotoxic in comparison with anionic particles such as PLGA (Fröhlich, 2012). Nanoparticles surface can also be engineered with immunostimulatory ligands that mimics pathogen associated molecular patterns (PAMPs) to promote immunity and inflammatory response (Hajizade et al., 2014). There are three methods for attachment of nanoparticles with pDNA which includes adsorption, conjugation and encapsulation (Hajizade et al., 2014).

2.10.3 Chitosan as nanocarrier for plasmid vaccine

Chitosan is one of the most important derivatives of chitin found on the shells of crustaceans like prawns and crabs. It is a naturally occurring polysaccharide, cationic and highly basic and it has been approved by the U.S. FDA for tissue engineering and wound

healing functions (Elieh-Ali-Komi & Hamblin, 2016; Kumar et al., 2017). Chitosan is well-known for their mucoadhesive properties that prevent nasal clearance as it interacts with the negatively charged mucus by forming a complex through ionic bonding or ionic interactions, therefore increasing the antigen retention time in the nasal mucosa (Aderibigbe & Naki, 2019). Chitosan can be an ideal nanomaterial used for DNA vaccine delivery due to its cationic nature as it causes electrostatic binding to the anionic structure of DNA leading to the formation of polymer-DNA complexes that will protect the DNA from enzyme degradation (Cao et al., 2019). Chitosan-based nanoparticles have been widely investigated in vaccine development against several infectious diseases such as influenza and Newcastle disease.

Bande et al. (2020) constructed a bivalent plasmid DNA vaccine against an economically important poultry disease known as infectious bronchitis (IB). The plasmid DNA was encapsulated in chitosan-saponin nanoparticles. Chitosan encapsulation of the bivalent IB vaccine candidate was shown to improved protection efficacy against two strains of IB virus challenges. Additionally, chickens immunized with the chitosan-saponin encapsulated pDNA vaccine displayed comparable amount of antibody titer and virus shedding reduction despite receiving a single booster in comparison with chickens immunized with naked pDNA which received two booster doses.

Chitosan nanoparticle encapsulated inactivated whole influenza virus with CpG oligonucleotide (CpG ODN) or with the Quillaja saponin (QS) adjuvant have been shown to induce Th1 type responses in immunized rabbits (**Fig. 2.2i**). The dry powder nanosphere vaccine was administered intranasally to the rabbit on days 0, 45, 60, followed by intramuscular (IM) injection as the final booster on day 75. Both chitosan encapsulated whole inactivated virus with CpG (CH+ WV+ CpG) and chitosan encapsulated whole inactivated virus with QS (CH+WV+QS) stimulated significantly higher levels of IgG than the mock group, with the CH+WV+CpG group induced the highest IgG antibody

level amongst all the group. This finding is in line with the detection of the IgG result where the CH+WV+CpG group induced the highest IgG antibody in the group immunized with this vaccine formulation. Similarly, the CH+WV+ CpG group elicited the highest sIgA titers in the nasal swab of the immunized rabbits. For the cellular mediated responses, a Th-1 biased response was observed in the group immunized with CH+WV+CpG as indicated by an increase of IL-2 and IFN-γ secretions than the mock group. This could be attributed to the mucoadhesive effect of the chitosan and the adjuvant effect of the CpG. Thus, the vaccine formulation of chitosan encapsulated inactivated influenza whole virus and CpG (CH+WV+CpG) elicited the best humoral and cellular mediated responses against influenza virus (Dehghan et al., 2014).

The enhanced protective efficacy of a Newcastle disease virus (NDV) DNA vaccine encapsulated in chitosan (pFNDV-CS-NPs) was investigated in pathogen free chickens (Zhao et al., 2014). Chickens administered with pFNDV-CS-NPs through intramuscular (IM) and intranasal (IN) route demonstrated peak IgG levels at fifth week post immunization and maintained relatively high IgG titers till the seventh week. In comparison, the IgG antibody titers of chickens immunized with naked NDV DNA vaccine peaked at the fourth week post immunization. Mucosal sIgA antibody titers were also found to be significantly higher while maintaining a longer sIgA secretion period in chickens administered with pFNDV-CS-NPs through the IN route compared to other groups. Lymphocyte proliferation assay was carried out in chickens on 2-, 4- and 6-weeks post immunization to assess the cell mediated immune responses. pFNDV-CS-NPs was found to enhance significantly higher T lymphocytes immunity than the control group at fourth- and sixth-week post IM and IN injection. Therefore, it can be concluded that a stronger immune response was induced by pFNDV-CS-NPs.

An investigation of the immunogenicity of multivalent DNA vaccines encapsulated in chitosan nanoparticles against *Trueperella pyogenes* was undertaken (Huang et al., 2018).

Four different genes (plo, cbpA, fmA or nanH) of T. pyogenes TP8 strain were incorporated into the pVAX1 plasmid vector to prepare the multivalent plasmid vaccines pVAX1-PC, pVAX1-PCF, pVAX1-PCFN as well as pPCFN-CpG (Fig 2.2ii). The CpG oligonucleotide (ODN)1826 motif was included in the vaccine formulation to enhance the immunity of chimeric genes. These bivalent or multivalent plasmids were compared to the chitosan encapsulated DNA vaccine pPCFN-CpG-CS-NPs through immunization of mice via intramuscular administration. The specific IgG antibody against target antigens. pPCFN-CpG-CS-NPs was found to induce the highest antibody levels in comparison with the other naked plasmid immunized mice groups. Potent lymphocyte proliferations induced by the mice group immunised with the pPCFN-CpG-CS-NPs were also supported by the ELISA analysis showing a higher IFN-γ, IL-2, and IL-4 levels observed in mice immunized with pPCFN-CpG-CS-NPs in comparison with mice immunized by naked plasmids These findings indicated that chitosan encapsulated plasmid DNA were able to provide efficient mucosal as well as cellular immune responses while coupled with CpG ODN that functions as a molecular adjuvant. Challenge study was carried out using T. pyogenes T8 and T. pyogenes T7, mice group immunized with pPCFN-CpG and pPCFN-CpG-CS-NPs both resulted in the lowest mortality rate in both challenges. The survival rate was 100% in both mice groups when challenged against T. pyogenes T8 with no clinical symptom observed for all the mice. Additionally, almost 50% of the mice immunized with pPCFN-CpG or pPCFN-CpG-CS-NPs were able to survive against the highly virulent T. pyogenes T7. In conclusion, the chitosan encapsulated chimeric gene plasmid vaccine was indicated to be able to provide more efficient protection against *T. pyogenes* infection.

Therefore, our concept of constructing a trivalent recombinant DNA vaccine against EV-A71 and CV-A16 would provide proof of concept to develop a tetravalent HFMD DNA vaccine in future by incorporation of more genes encoding for the relevant enterovirus antigens. In this study, 3 enterovirus genes were inserted into a mammalian vector

pIRES2-AcGFP1 for expression of VP1 and VP2 gene of EV-A71, as well as VP1 gene of CV-A16 in the recombinant trivalent plasmid vaccine. Both VP1 and VP2 genes of EV-A71 were included as part of our vaccine design to boost the overall neutralizing antibody response by addition of extra cross sub-genotype neutralizing epitopes.

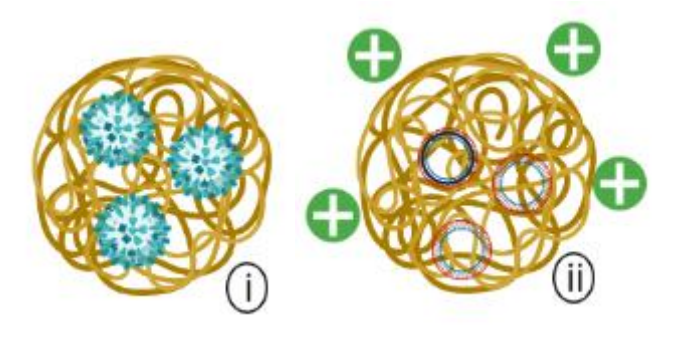


Figure 2.3: Schematic representation of i) Chitosan encapsulating inactivated whole influenza virus and ii) Chitosan encapsulating plasmid DNA vaccine. Image was generated with biorender.com.

Chapter 3 Materials and method

3.1 Mammalian and murine cell lines

3.1.1 Revival and culture of cells

Human 293T cells (ATCC-CRL-3216TM) and the murine macrophage cells J774A.1 (ATCC-TIB-67TM) were acquired from ATCC (Georgia, USA). The cell stocks were

stored in liquid nitrogen tank for long-term storage. Revival of both cell lines were carried out with the same protocol. First, vial containing the cells were thawed at room temperature followed by gentle centrifugation at 500xg for 5 min, the supernatant was discarded to remove the toxic DMSO in freeze medium. The cells were resuspended in 1 ml of prewarmed complete media [Dulbecco's Modified Eagles Medium (DMEM) (Invitrogen, USA) comprising 10% fetal bovine serum (FBS) (Invitrogen, USA) and 1% antibiotic [(Penicillin/Streptomycin) (GIBCO, Invitrogen, USA)] and transferred into a T25 culture flask (25cm²) (Thermofischer, USA) containing 4ml of complete media. The cell lines should be passaged for at least two more generations before being subjected for future studies.

3.1.2 Subculture and maintenance of cell lines

3.1.2.1 293T cells

293T cells were maintained in T75 culture flask (75cm²) (Thermofischer, USA) supplemented with complete media [Dulbecco's Modified Eagles Medium (DMEM) (Invitrogen, USA) comprising 10% fetal bovine serum (FBS) (Invitrogen, USA) and 1% antibiotic [(Penicillin/Streptomycin) (GIBCO, Invitrogen, USA)], grown at 37°C in 5% CO2 until 80%-90% confluency was reached. 293T are adherent cells that require trypsinization during sub-culturing process. First, media in the flask were discarded using a serological pipette followed by addition of 1x phosphate buffer saline (PBS) to gently rinse the cells and remove any residual media. PBS was discarded and 1.5ml of trypsin EDTA (1x) was added, the flask was placed in incubator at 37°C until the cells were fully detached. Equal volume of complete media was added into the flask to inactivate the trypsin. Cell suspension was transferred into a tube for centrifugation at 1,000xg for 5 min, the supernatant was discarded. Cell pellet was resuspended with 1ml of complete media and transferred back into the flask, complete media was added to topped it up to total volume of 10ml.

3.1.2.2 J774A.1 cells

J774A.1 murine macrophage cells were maintained in T25 culture flask (25cm²) (Thermofischer, USA) supplemented with complete media [Dulbecco's Modified Eagles Medium (DMEM) (Invitrogen, USA) comprising 10% fetal bovine serum (FBS) (Invitrogen, USA) and 1% antibiotic [(Penicillin/Streptomycin) (GIBCO, Invitrogen, USA)], grown at 37°C in 5% CO2 until 80%-90% confluency was reached. J774A.1 are suspension cells which would be loosely attached to the walls of flask upon confluency. Old culture media was first discarded followed by addition of 3ml fresh media into the flask, cells at bottom of the flask was gently scraped off using a cell scraper. 1 ml of the cell suspension would be added into a new flask and topped up to final volume of 5ml with fresh complete media.

3.1.3 Storage of 293T and J774A.1

Cryopreservation of both 293T and J774A.1 cell lines were carried out using similar methods periodically to ensure the cell lines used in experiments were not more than 30 passages. The old culture media was discarded and confluent monolayer of 293T and J774A.1 cells were washed with 1x PBS. 293T cells were detached using 1.5ml of trypsin EDTA, J774A.1 cells were detached through gentle cell scraping instead. The cells were added with 2ml of media followed by centrifugation at 800xg for 10min, the supernatant was discarded. The cell pellet of both cell lines was resuspended in 1ml of freezing medium (90% FBS, 10% DMSO). The vials containing cell suspensions were kept in Mr. FrostyTM freezing container at -80°C for 48h before being transferred for long term storage in liquid nitrogen tank.

3.2 Construction of recombinant plasmid DNA

pIRES2-AcGFP1 expression vector (Thermo Fisher Scientific) was used to construct DNA plasmid using VP1 and VP2 genes of Enterovirus 71 (EV-A71) virus strain

5865/Sin/000009 (GenBank accession number: AF316321) and VP1 gene of Coxsackievirus 16 (CV-A16) virus strain G10 (GenBank accession number: U05876). The VP1 and VP2 genes were synthesized and cloned into the pIRES2-AcGFP1 vector's multiple cloning site (MCS) located downstream of the CMV promoter (GenScript, USA). The trivalent plasmid comprised of the VP1, VP2 genes of EV-A71 and VP1 gene of CV-A16 (pIRES2/VP1s/A71/A16/VP2/A71). A FLAG-tag, HA-tag and His-tag were also cloned in close proximity to VP1, VP2 genes of EV-A71 and VP1 gene of CV-A16, respectively.

3.3 Transformation of trivalent plasmid into E. coli

A single colony of *Escherichia coli* strain TOP10 was grown in LB broth to an optical density of 0.4~0.5 at OD600nm and resuspended in ice-cold ultrapure H₂O. The pIRES-VP121 trivalent plasmid was transformed into *E. coli* competent cells using heat shock method as described by Sambrook *et al.* (1989). The transformed cultures were plated onto LB plates containing kanamycin (50 μg/ml). Kanamycin resistant colonies harbouring the DNA vaccine were isolated and stored at -80°C the presence of trivalent plasmids was confirmed by PCR and DNA sequencing.

3.4 Plasmid isolation and purification

Following the manufacturer's recommended protocol, the overnight culture of recombinant *E. coli* harbouring trivalent plasmid were subjected to plasmid extraction using Maxi Plasmid Purification Kit (QIAGEN, Calif., USA) involving centrifugation and column filtering. Extracted plasmids were diluted with TE buffer and stored at -20°C for future experiments. Plasmid concentrations were measured using NanoDropTM One/OneC Microvolume UV-Vis Spectrophotometer (Thermo ScientificTM).

3.5 Transfection of 293T cells with the recombinant DNA plasmid

293T cells (ATCC-CRL-3216TM) were seeded into 6-well plate (5x10⁵cfu/ml) and incubated overnight in complete media [Dulbecco's Modified Eagles Medium (DMEM) (Invitrogen, USA) comprising 10% fetal bovine serum (FBS) (Invitrogen, USA) and 1% antibiotic [(Penicillin/Streptomycin) (GIBCO, Invitrogen, USA)] at 37°C. Upon reaching 60-80% cell confluency, transfection was carried out according to the manufacturer's protocol using XfectTM Transfection Reagent (TAKARA Bio, USA). Cells were washed with PBS and added with 100μl of transfection mixture per well. The transfection mixture was first added with desired concentration of plasmid DNA, followed by XfectTM polymer (0.3μl per μg of pDNA) and topped up with XfectTM buffer to a final volume of 100μl. Cells were cultured in DMEM media with 2% FBS and 1% antibiotic, incubated at 37°C in an incubator containing 5% CO₂.

3.6 Confirmation of plasmid and protein expression in vitro

The pIRES2-AcGFP1 plasmid is consisted with a green fluorescent protein (AcGFP1) from *Aequorea coerulescens* with an excitation range of 475~505nm. Fluorescence microscopy was carried out using Nikon Inverted Microscope Eclipse Ti-S (Nikon, Japan) to confirm the success of plasmid transfection, blue light was used for excitation and green light was observed to be emitted.

For confirmation of viral VP1 and VP2 protein expression by the trivalent pIRES2-VP121 plasmid, SDS gel electrophoresis and western blot were carried out. Twenty-four and fourty-eight hours after transfection of 293T cells in 24 well plates, cells were harvested through scraping of the wells and kept in microcentrifuge tube. The tube was centrifuged for 300rpm for 5 minutes and the supernatant (media) was discarded. 1x PBS was added to wash the cells followed by centrifugation for 5 minutes at 300rpm, the supernatant was discarded. The cell pellet was then resuspended in 100µl of RIPA buffer, The tube was

kept on ice for 1 hour and vortexed every 15 minutes to ensure the cells were completely lysed. Equal amount of protein lysates was loaded into each well of the SDS gel followed by electro-blotting onto Immun-Blot® PVDF Membrane (Biorad, US). The membrane was blocked in TBST buffer (5% BSA) for 1 hour at room temperature followed by incubation of primary antibodies at 4°C overnight. Incubation was carried out using monoclonal antibody targeting the specific EV-A71 VP1 protein (RRID: AB_930697) and polyclonal antibody targeting the EV-A71 VP2 protein (RRID: AB_2866733), both antibodies were purchased from Invitrogen (Thermo Fisher Scientific, USA). Monoclonal His tag antibody (#SC-8036, Santa cruz, US) was employed to detect the CV-A16 VP1 protein. The membranes were each subsequently incubated in goat anti mouse (EV-A71 VP1, CV-A16 VP1 detection) (#HAF007, R&D Systems, Minneapolis, USA) or goat anti rabbit (EV-A71 VP2 detection) (#HAF008, R&D Systems, Minneapolis, USA) secondary antibody conjugated with HRP. Signals were developed with WesternBright ECL HRP substrate (Advansta, US) and images were captured with Syngene™ G: BOX Chemi XX9 (Syngene, UK).

3.7 Preparation of chitosan solutions and plasmid DNA-TPP solutions

Both the preparation and synthesis of chitosan TPP nanoparticles were devised from a study reported by Kuen et al. (2017) with slight modifications according to other studies (Nunes et al., 2022). Commercial low molecular weight chitosan (50-190kDa) with deacetylation degree of 75-85% was purchased from Sigma-Aldrich (Sigma-Aldrich (M) Sdn Bhd). Chitosan powder (5mg) was first dissolved in 5ml of acetic acid (1%) for preparation of 1mg/ml chitosan solution by magnetic stirring on a hot plate for ~16 hours at room temperature. The chitosan solution was then diluted with 5 ml of ddH2O to a final concentration of 0.5mg/ml and stirred for 1 hour with a magnetic bar. The chitosan

solution was subsequently adjusted to a final pH of 5.0 using 1M NaOH and filtered using a 0.25µm cellulose acetate syringe filter (Bioflow Lifescience, Malaysia).

Sodium tripolyphosphate (TPP) purchased from Sigma-Aldrich (Sigma-Aldrich (M) Sdn Bhd) was dissolved in ddH2O to reach a final concentration of 0.7mg/ml. The TPP solution was then adjusted to pH2 using 1M HCL. For experiments encapsulating the plasmid DNA, plasmid stock was diluted in 200µl of TPP solution to reach the required concentration.

3.8 Synthesis of chitosan TPP nanoparticles (chitosan NPs) through ionic gelation

Chitosan NPs encapsulating plasmid DNA were prepared through ionotropic gelation method with chitosan acting as the polymer and TPP acting as the crosslinker. Chitosan solution (600ul) was prepared in a 10 ml universal bottle and the plasmid-TPP solution was added dropwise at a constant rate of 60µl/min using a pipette. To ensure the consistency of chitosan NPs that were synthesized, 10µl of TPP-plasmid solution was added every 10s using 100µl pipette tips for all experiments. At the same time, chitosan solution was stirred on a magnetic hotplate at constant rate of 750rpm until all the TPP-plasmid solution was consumed and the final product was stirred for another 30 min at room temperature. For positive control, blank chitosan NPs were prepared with the same method, but TPP solution was added without the addition of plasmid DNA instead. These chitosan TPP NPs encapsulating plasmid DNA were named as CS-TPP-NPs (pIRES-VP121) while blank chitosan NPs were named as blank-CS-TPP-NPs.

3.9 Characterization of the chitosan encapsulating plasmid DNA

3.9.1 Encapsulationg efficacy of the nanospheres

Estimation of plasmid DNA encapsulated in the chitosan NPs was carried out using the protocol described by Nunes et al. (2021). The CS-TPP-NPs (pIRES-VP121) solution

was subjected to centrifugation at 10,000 rpm at 4°C for 20 min, DNA concentration in the supernatant would be measured using the NanoDropTM One/OneC Microvolume UV-Vis Spectrophotometer (Thermo ScientificTM). Therefore, indirect encapsulation efficiency (iEE%) could be calculated by using the following formula where c (total) was the nucleic acid concentration used during the chitosan encapsulation process and c(sp) was the DNA concentration of supernatant measured after centrifugation:

$$iEE\% = \frac{c(total) - c(sp)}{c(total)}$$

3.9.2 Morphology, size, polydispersity index, and zeta potential of the chitosan NPs

The average size, polydispersity index (PDI) of blank-CS-TPP-NPs and CS-TPP-NPs (pIRES-VP121) were measured through dynamic light scattering using The LitesizerTM 500 by Anton Paar (Anton Paar Malaysia Sdn Bhd). The experiment was repeated three times independently to ensure consistency of the data collected.

The Litesizer™ 500 was also used to measure the zeta potential of blank-CS-TPP-NPs and CS-TPP-NPs (pIRES-VP121) using novel patented electrophoretic light scattering optics known as the Continuously Monitored Phase-Analysis Light Scattering (cmPALS, European patent EP2 735 870). Experiments were repeated three times independently and readings were done in triplicates to ensure consistency of the data collected.

The morphology of blank-CS-TPP-NPs and CS-TPP-NPs (pIRES-VP121) were evaluated using scanning electron microscopy (SEM). Briefly, the blank-CS-TPP-NPs and CS-TPP-NPs (pIRES-VP121) solution were diluted from 1:10 to 1:100 in ddH₂O. An aliquot (10µl) of the diluted solution was pipetted onto a 10mm cover slip and air dried in the biosafety cabinet (BSC) for 1 to 2 hours. The cover slip was then attached to double

sided adhesive carbon tape and subjected to sputter coating with platinum using the SPT-20 - Ion Sputter Coater (COXEM, Korea). A scanning electron microscope TESCAN VEGA3 (TESCAN, USA) was used to capture the morphology of the chitosan samples at various magnifications.

3.10 Transfection of chitosan encapsulated pIRES-VP121

Transfection of chitosan-DNA complexes was carried out following study by Nimesh et. al (2010) with slight modifications (Nimesh et al., 2010). DMEM media supplemented with 10% FBS was first prepared at pH 6.5 and pH 7.4 respectively with 1M HCL. J774A.1 macrophage cells (ATCC-TIB-67™) were seeded in 24-well culture plate at concentration of 1x10⁵ cfu/ml for 24h. Formulated CS-TPP-NPs (pIRES-VP121) was centrifuged for 10,000 xg for 10 min, the pellet was resuspended in transfection media (pH6.5, supplemented with 10% FBS) to a concentration of 5µg pDNA/ml. Upon reaching 60% confluency, the seeded J774A.1 cells were washed with PBS and 1ml of the diluted chitosan-DNA complexes were added to each well. At 8h post transfection, the cells were washed with PBS and 1ml of DMEM media (pH 7.4, supplemented with 10% FBS) was added to each well. At 24h,48h and 72h post transfection, Nikon Inverted Microscope Eclipse Ti-S (Nikon, Japan) was used to confirm the success of plasmid transfection, blue light was used for excitation and green light was observed to be emitted.

3.11 Hemolysis assay

ICR mice blood was collected in heparin tube and centrifuged for 5 minutes at 500xg, the yellowish plasma layer (upper layer) and the lower reddish hematocrit levels were both marked on the tube. Micropipette was used to gently discard the plasma into bleach filled biohazard waste. 150mM NaCl solution was added up to the original line that was marked for the plasma layer, followed by mixing through gently inverting the tube and centrifugation for 5 minutes at 500xg. The supernatant was once again discarded and

filled to the line of original plasma layer using PBS (pH 7.4), the tube was gently inverted to mix. 1 ml of the prepared erythrocytes was diluted to a 1:50 ratio using PBS which would be ready for hemolysis assay. Samples diluted to 400µg/ml with PBS, including chitosan polymer solution, blank CS-TPP-NPs, and CS-TPP-NPs (pIRES-VP121) were each added to microcentrifuge tubes containing the prepared erythrocytes. Equal amount of triton-x and PBS would be added to the prepared erythrocytes serving as the positive and negative control, respectively. Sample tubes were centrifuged for 5 minutes at 500xg followed by transferring of 100µl of supernatant into 96 well plate for absorbance reading at 527nm. The hemolysis rate of each sample was calculated using the formula below:

$$Hemolysis (\%) = \frac{sample (OD) - negative \ control \ (OD)}{positive \ control \ (OD) - negative \ control \ (OD)}$$

3.12 Cytotoxic assay of chitosan NPs

J774A.1 cell line (ATCC® TIB-67TM) was purchased from ATCC and cultured in DMEM media with 10% FBS and 1% antibiotic [(Penicillin/Streptomycin) (GIBCO, Invitrogen, USA)]. Cell viability assay were carried out using CellTiter 96® AQueous One Solution Cell Proliferation Assay (MTS) (PROMEGA, USA) following the manufacturer's protocol. MTS assay was performed in 96 well plates seeded with 1x10^{λ5} of J774A.1 cells per well. Half-fold serial dilutions of the blank-CS-TPP-NPs and CS-TPP-NPs (pIRES-VP121) with a final concentration of (100, 200 and 400 μg/mL) was carried out using DMEM media (2% FBS and 1% antibiotic) as the diluent. Diluted chitosan NPs solution were pipetted into respective wells of the seeded 96 well plate followed by

incubation at 37°C, 5% CO₂. At 48h post incubation, 20ul of the MTS reagent was added into each of the respective wells while avoiding light exposure and again incubated for 1 h at 37°C, 5% CO₂. After the incubation, the absorbance of each sample within the 96 well plate was read at 490nm using a microplate reader [Infinite® 200 PRO (TECAN, Switzerland)].

3.13 Stability of plasmid DNA in the chitosan-NPs

Stability of CS-TPP-NPs (pIRES-VP121) was evaluated based on the protocol described by Huang et al. (2018). An aliquot of DNase I (1.0 U/mL) was used to incubate 1) suspension of chitosan NPs encapsulating pDNA (2μg), 2) naked plasmid DNA (2μg) (5.0 mmol/L Na₂SO⁴) and 3) blank-CS-TPP-NPs for 30 min at 37°C, respectively. Termination solutions (400 mmol/L NaCl, 100 mmol/L ethylenediaminetetraacetic acid [EDTA], pH 8.0) were added for 10 min at 65°C to terminate the reaction. Lysozyme (0.2U/mL) and chitosanase (0.2 U/mL) (Merck, USA) were added followed by incubation for 4h in a water bath at 37°C. Agarose gel electrophoresis (0.8%) was carried out to analyse the integrity of plasmid DNA encapsulated in chitosan NP with the blank-CS-TPP-NPs and naked pDNA both serving as negative controls.

3.14 Mice immunization

The ICR mice (3 weeks old) used in this study were divided into 2 sets (set A and B) each containing 3 groups (n=4). The 3 groups of mice in set A (**Fig. 4.15a**) were administered with: 1) naked pDNA (50µg) and 2) naked pDNA (100µg) through intramuscular route with the third group of naïve mice serving as the negative control. A single booster was administered at 2 weeks post-immunization. The 3 groups of mice in set B (**Fig. 4.15b**) were administered with: 1) naked pDNA (100µg) and 2) CS-TPP-NPs (pIRES-VP121) (100µg) through intramuscular route with the third group of naïve mice serving as the negative control. A total of 2 booster doses were administered at a 2-week interval post-

immunization. At day 35 (Set A) and day 49 (Set B) respectively, the blood and spleen of mice were harvested. Immune sera would be collected by centrifugation of blood at 6000xg for 15 minutes, the sera were stored at -80°C for future use.

3.15 Neutralizing antibody assay

In vitro microneutralization test was carried out in Rhabdomyosarcoma (RD) cells of skeletal muscle origin to detect the presence of neutralizing antibodies in immune sera following the protocol of Foo et al. (2007). The complement in mouse serum samples was first inactivated by incubation at 56 °C for 30 min. Two-fold serial dilutions (1:2, 1:4, 1:8 and 1:16) of sera (50µl) were mixed with equal volumes of enteroviruses EV-A71 or CV-A16 in 96 well microtiter plate and RD cells $(5x10^4cfu/ml)$ would be seeded after 2 hours. The plates were incubated at 37 °C and cell CPE condition would be monitored daily up to 96h, the highest dilution of serum that was able to inhibit viral growth would be read as the neutralizing antibody titer. Assays were performed in quadruplicates to ensure consistency of data. Enteroviruses that were used in neutralization assay includes wild type EV-A71 sub-genotype B4 (GenBank accession number: AF376067.1) and CV-A16/N132 sub-genotype B1, as well as mouse-adapted virus (MAV) strains of EV-A71 sub-genotype B3 (GenBank accession number: OP585372.1) and CV-A16/N132 subgenotype B1 (GenBank accession number: OP651899.1) which were all acquired from collaboration with University Malaya (UM) (Ong et al., 2008; Ong et al., 2010; Hooi et al., 2020). Monoclonal EV-A71 antibodies derived from splenocytes of mice immunized with EV-A71 sub-genotype B3 (GenBank accession number: OP585372.1) would serve as positive controls against the wild type and MAV EV-A71 enteroviruses (Tan et al., 2016).

3.16 Flow cytometry

Splenic tissues harvested from mice were passed through a 70µm cell strainer while applying force through the piston of sterile syringe and occasional rinsing with RPMI-1640 media. The spleen cells collected in a 50ml falcon tube were centrifuged at 3000x rpm for 3 min, 4°C. The supernatant was discarded followed by gentle tapping of the tube to dislodge the pellet, red blood cell (RBC) lysis buffer was added followed by incubation at RT for 4 min. Complete RPM1media (10%FBS, 1% antibiotic) was added to neutralize the RBC lysis buffer. The tube was centrifuged at 3000x rpm for 3 min, 4 °C. The supernatant was discarded followed by resuspension of pellet in warm complete RPMI for cell counting.

The splenocytes were diluted by 10-fold and stained with equal amount of trypan blue. Hemocytometer was used for counting of the stained splenocytes and unstained live cells followed by calculation of cell concentration using the following formula:

$$viable\ cells\ (cells/ml) = \frac{Total\ no.\ of\ live\ cells}{No.\ of\ quadrants} \times dilution\ factor \times 10^4$$

 4×10^{6} cells were seeded into each well of a 24-well plate followed by stimulation with 50 ng/ml of PMA, 1µg/ml of Ionomycin and golgi plug, the plate was placed in a cell incubator for 5h at 37°C.

The cells in 24-well plate were each pipetted into different centrifuge tubes and 500 μl of FACS buffer (PBS containing 1% FBS) were added into each well to wash off the remaining cells. The tubes were centrifuged at 3000x rpm for 3 min, 4°C. Viability stain master mix was prepared by mixing BD HorizonTM fixable viability stain 780 (FVS-780) and FACS buffer to a 1:200 ratio, the supernatant from each tube was discarded and resuspended with 50μl of the viability stain master mix. The tubes were incubated in dark for 10-15 min at RT, 300μl of FACS buffer was added to remove excessive stain. The tubes were centrifuged at 3000x rpm for 3 min, 4°C. Surface stain master mix (CD3, CD4 and CD8) was prepared by mixing all the surface stains (anti-CD3 APC conjugated

antibody/ anti-CD4 BV786 APC conjugated antibody/ anti-CD8 BB515 conjugated antibody) and the FACS buffer at a 1:200 ratio. The supernatant from each tube was discarded and resuspended with 50µl of the surface stain master mix. The tubes were incubated in dark for 20-30 min on ice, 300µl of FACS buffer was added to remove excessive stain. The tubes were centrifuged at 3000x rpm for 3 min, 4°C. The supernatant from each tube was discarded and resuspended with 100 µl of CytofixTM fixation buffer (BD biosciences, NJ, USA) followed by incubation for 20-30 min on ice. 300 µl of BD Perm/WashTM Buffer (BD biosciences, NJ, USA) was added to each tube and the tubes were centrifuged at 4000x rpm for 3 min, 4°C. Intracellular stain master mix (IFN-y) was prepared by mixing the anti-IFN-γ PerCP conjugated antibody and the BD Perm/WashTM Buffer (BD biosciences, NJ, USA) at a 1:400 ratio. Antibodies used for surface staining and intracellular cytokine staining (ICS) were all acquired from BD biosciences (NJ, USA). The supernatant from each tube was discarded and resuspended with 100µl of the intracellular stain master mix. The tubes were incubated in dark for 40-60 min on ice, 300µl of FACS buffer was added to remove excessive stain. The tubes were centrifuged at 3000x rpm for 3 min, 4°C. The supernatant from each tube was discarded and the pellet resuspended with 300-500µl of FACS buffer. The solutions from each tube were transferred to FACS tube on ice and ready to be read by the BD FACSCelestaTM flow cytometer (BD biosciences, NJ, USA). Flow cytometry results were analysed through Kaluza analysis software (RRID:SCR_016182) (Beckman Coulter, Kaluza, Brea, CA, USA). The seeding and processing of mice splenocytes in each experimental groups were carried out in quadruplicates.

3.17 ELISA

Enzyme-linked immunosorbent assay (ELISA) kit for IFN- γ detection was purchased from (Mabtech AB, Sweden) and ELISA was carried out following the manufacturer's protocol. An aliquote (100 μ l) of mouse antibodies (mAb) AN18 (1 μ g/ml, diluted in PBS) was added to each well of the ELISA plate, followed by incubation overnight at 4°C. The

plate was emptied and 200μl of incubation buffer (PBS containing 0.1% BSA and 0.05% Tween 20) was added to each well followed by incubation at RT for 1h. The plates were washed 5 times using 300μl of wash buffer (PBS containing 0.05% Tween 20) for each wash. Splenocytes or standards were diluted in incubation buffer and added to the plates (100μl/well) followed by incubation for 2h at RT. The plates were washed 5 times using 300μl wash buffer (PBS, 0.05% Tween 20) for each wash. Diluted streptavidin-HRP (100μl) (1:1000, diluted with incubation buffer) was added to each well followed by incubation for 1h at RT. The plates were washed 5 times using 300μl wash buffer (PBS containing 0.05% Tween 20) for each wash. An aliquot of TMB substrate (100μl) was added to each well, followed by incubation for 15min at RT and 100μl of H₂SO₄ (0.2M) was added to each well to stop the reaction. The absorbance of ELISA plate was recorded at 450nm using the microplate reader Infinite® 200 PRO (TECAN, Switzerland).

3.18 Statistical analysis

GraphPad Prism software (GraphPad Software version 7.3, USA) was used to carry out statistical analysis of data from flow cytometry and ELISA assays. Data were presented in mean \pm standard error of mean from mice (n=4) in each group. Unpaired t-test was performed to determine the statistical significance of data. A statistical level like p < 0.05 is considered as significant.

3.19 Ethics statement

All animal studies were approved and carried out in accordance with the guideline approved by the Animal Institutional Animal Care and Use Committee (Approval code: 2022-230113-/SUNWAY/R/YJS) of University Malaya and Sunway Research Ethics Committee (Approval code: PGSUREC2020/069). All mice were housed in a temperature-controlled biosafety level 2 (BSL-2) animal facility at the Animal Experimentation Unit located in University of Malaya.

CHAPTER 4 RESULTS

4.1 Design and construction of the trivalent plasmid vaccine candidate

The VP1 and VP2 genes of EV-A71 as well as VP1 gene of CV-A16 were successfully cloned into the eukaryotic pIRES-VP121 vector through confirmation by gene sequencing. The recombinant plasmid was generated using SnapGene viewer (version 6.2.1) based on the sequencing results (**Fig. 4.1**). All 3 genes inserted in pIRES-VP121 were expressed independently as the EV-A71 VP1 gene located downstream of the human CMV promoter would be expressed through cap dependent translation. Expression of EV-A71 VP2 and CV-A16 VP1 protein were dependent on the internal ribosome entry site (IRES) sequences IRES1 and IRES2, respectively through cap independent translation (**Fig. 4.2**). Additionally, a FLAG tag, HA tag and 6x His tag was each linked to the end of EV-A71 VP1, EV-A71 VP2 and CV-A16 VP1 gene, respectively (**Fig. 4.2**).

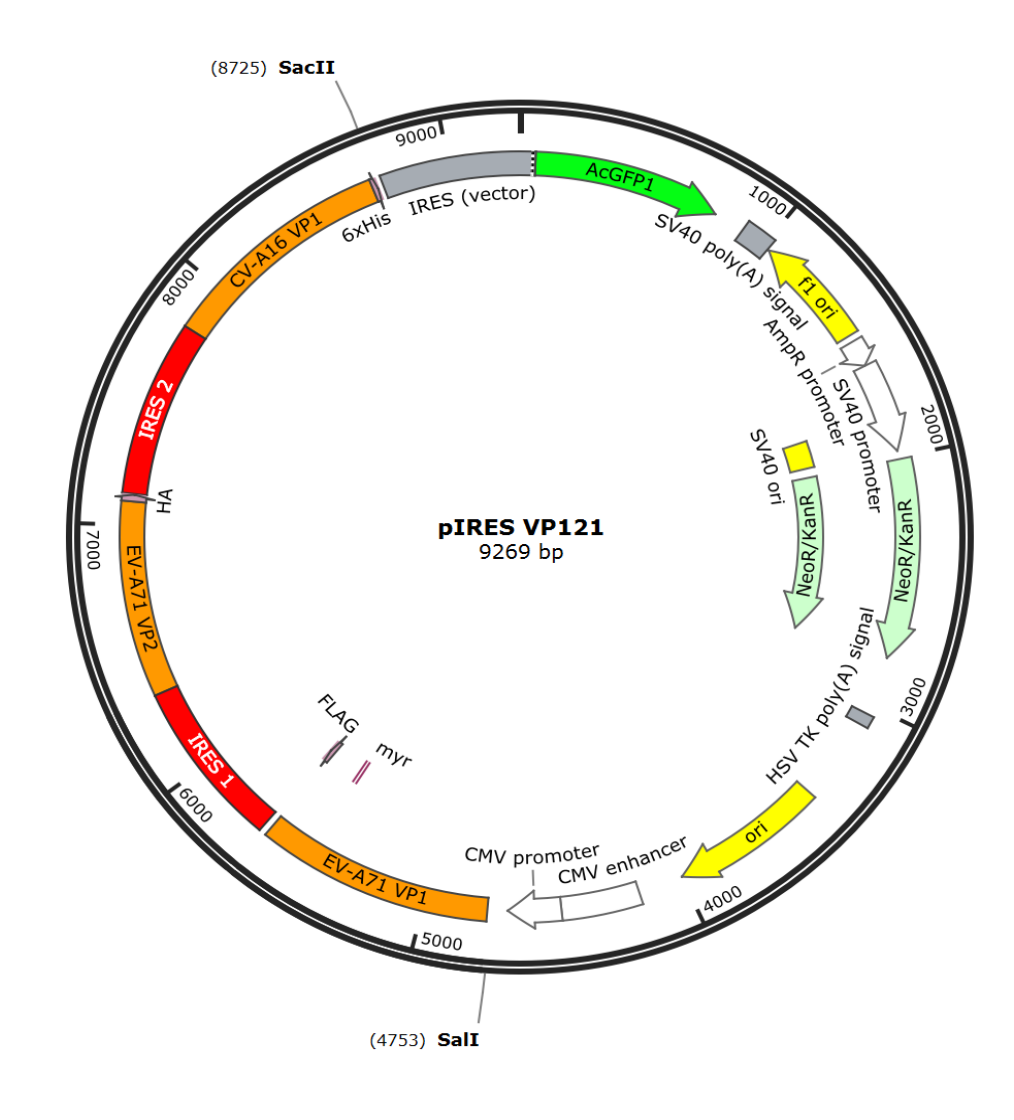


Figure 4.1: Recombinant pIRES VP121 trivalent plasmid construct harbouring the pIRES2-AcGFP1 plasmid vector carrying VP1, VP2 genes of EV-A71 and VP1 gene of CV-A16.

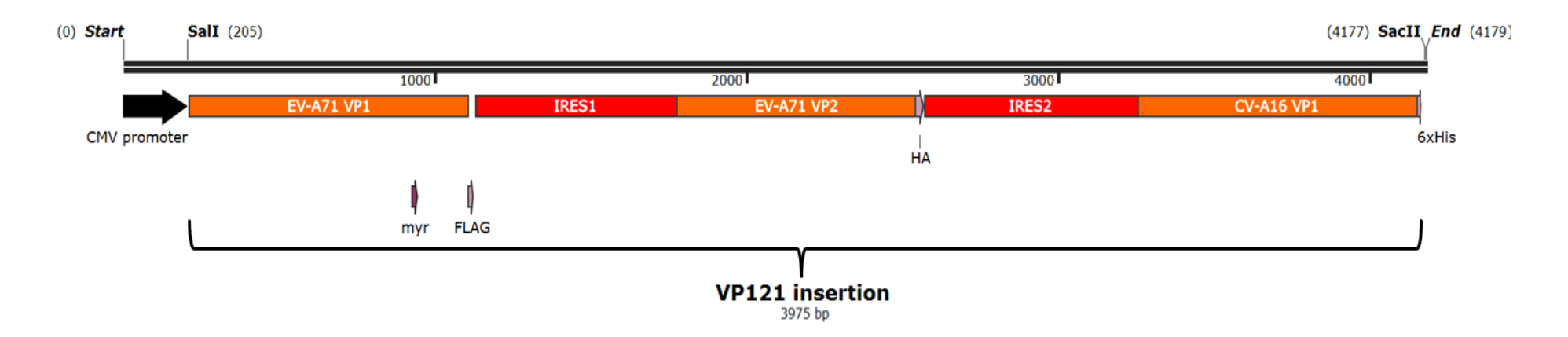


Figure 4.2: Gene sequences inserted into the multiple cloning site of the pIRES2-AcGFP1 plasmid vector.

4.2 Sequencing of the VP121 genes inserted

DNA sequencing was carried out through Firstbase sequencing service provided by Apical (Apical, Singapore) to confirm the genomic sequence of plasmid vaccine candidate pIRES-VP121. VP1, VP2 genes of EV-A71 and VP1 gene of CV-A16 were successfully cloned into the plasmid vector pIRES2-AcGFP1 along with two IRES sequence which would allow cap-independent translation of the viral genes EV-A71 VP2 and CV-A16 VP1 downstream of the CMV promoter and EV-A71 VP1 gene. The FLAG tag, HA tag and His tag sequences attached to the end of each of the three enterovirus genes were also successfully detected (**Fig. 4.3**).

EV-A71 VP1

SalI

Flag taq GATTACAAGGACGATGACGATAAG

SbfI BcII

EV-A71 VP2

ATC TCTCCAAGCGCCGAGGCATGCGGATACAGCGATAGGGTTGCCCAGCTGACCATCGGCAACTCCACAATCACC
ACACAGGAGGCCGCCAATATCATCGTGGGCTACGGCGAGTGGCCCTCCTATTGTTCTGACGATGACGCCACCGCC
GTGGATAAGCCAACAAGGCCCGACGTGTCTGTGAACAGATTCTACACCCTGGATACAAAGCTGTGGGAGAAGAGC
TCCAAGGGCTGGTATTGGAAGTTTCCTGACGTGCTGACCGAGACAGGCGTGTTCGGCCAGAACGCCCAGTTTCAC
TACCTGTATCGGTCTGGCTTCTGCATCCACGTGCAGTGTAATGCCAGCAAGTTTCACCAGGGCGCCCTGCTGGTG
GCAATCCTGCCCGAGTATGTGATCGGAACCGTGCAGGAGGAACCGGAACAGAGGATAGCCACCCCCTTACAAG
CAGACACAGCCTGGAGCAGATGGATTCGAGCTGCAGCACCCATATGTGCTGGACGCCGGCATCCCTATCTCCCAG
CTGACCGTGTGCCCACACCAGTGGATCAACCTGCGGACCAACAATTGTGCCACAATCATCGTGCCTTACATGAAT
ACACTGCCATTCGACTCCGCCCTGAACCACTGCAATTTTGGCCTGGTGGTGCCTATCTCTCCACTGGATTTC
GACCAGGGCCCCCCCGTGATCCCTATCACCATCACCTGGCCCCCATGTGCTCCGAGTTTGCAGGCCTGAGG

HA tag

CAGGCAGTGACCCAG<mark>TACCCATATGATGTGCCCGACTATGCC</mark>

Figure 4.3: Complete sequence of the genes inserted into the multiple cloning site.

51

IRES

CV-A16 VP1

Figure 4.3 continued: Complete sequence of the genes inserted into the multiple cloning site.

4.3 Expression of the recombinant plasmid pIRES VP121 in 293T cells

IRES I

The pIRES2-AcGFP1 plasmid vector is consisted of a gene encoding the green fluorescent protein (AcGFP1) from *Aequorea coerulescens* and it fluoresces within an excitation range of 475~505nm. Fluorescent microscopy was carried out to confirm plasmid transfection, blue light was used for excitation and green light was emitted. Green fluorescence signal was emitted by 293T cells at 48 hours after transfection with the recombinant pIRES-VP121 plasmid at 1μg (**Fig. 4.4f**), 2μg (**Fig. 4.4g**) and 3μg (**Fig. 4.4h**), respectively, in comparison to the non-transfected 293T cells (**Fig. 4.4e**) (negative control). Dose dependent relationship between the amount of pDNA used in transfection and fluorescence signal intensity was observed. There was an apparent increase of fluorescence intensity as the concentration of the recombinant plasmid used for transfection was increased from 1μg to 3μg (**Fig. 4.4f**, **4.4g** and **4.4h**).

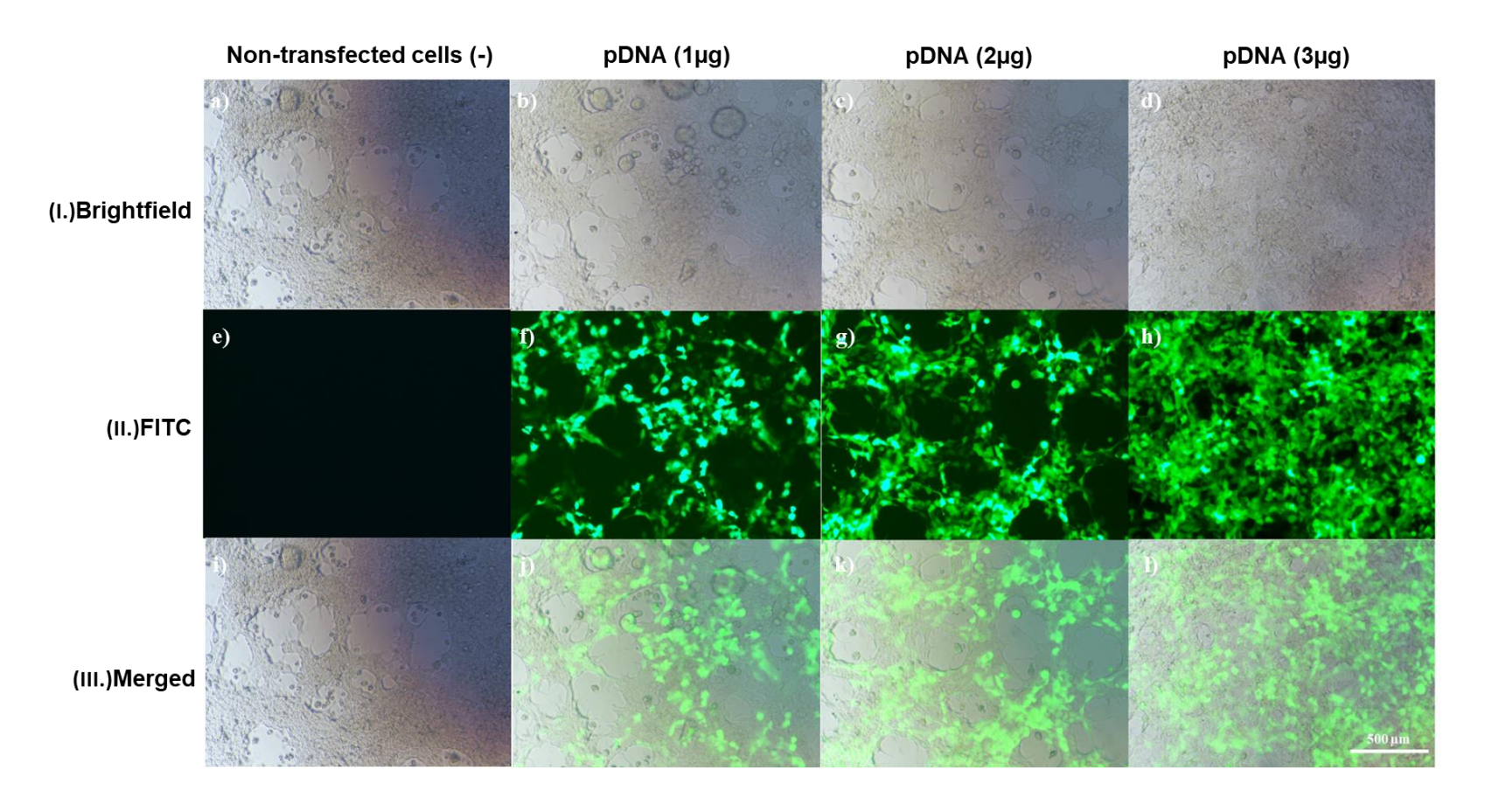


Figure 4.4: Fluorescent microscopy images of 293T cells transfected with 1μg (b, f, j), 2μg (c, g, k) and 3μg (d, h, l) of pIRES-VP121 recombinant plasmid with non-transfected cells (a, e, i) serving as the negative control. From top to bottom, Images were captured under 20x magnification (500 μm scale bar) in (I) brightfield, (II) FITC and (III) merged channels respectively.

4.4 Viral protein expressions of pIRES VP121 in 293T mammalian cells

HEK 293T cells were transfected with the pIRES-VP121 recombinant plasmid. At 24h and 48h post transfection, 293T cells were lysed and subsequently analysed for protein expression based on SDS page, with the non-transfected 293T cells serving as the negative control. However, SDS page results were inconclusive as there were no clear protein bands observed. This could be due to the unpurified lysate proteins causing a high amount of background bands (**Fig. 4.5a, 4.5b**). Therefore, western blot was carried out using 293T cell lysates at 48h post transfection. Detection was carried out with specific antibodies that target the 3 enteroviruses genes or tags that were inserted into the pIRES-VP121 plasmid.

Western blot using monoclonal anti EV-A71 VP1 antibody revealed the presence of a protein band at ~35kDa indicating the expression of EV-A71 VP1 protein (**Fig. 4.6A**). From the western blot, dose dependent relationship between the amount of pDNA used in transfection and the intensity of bands in western blot were also observed from lane 1 (1µg pDNA) to lane 6 (10µg pDNA) (**Fig. 4.6A**). No bands were observed in the non-transfected cells as shown in lanes labelled as negative control. Western blot generated after incubation with polyclonal EV-A71 VP2 antibody showed a clear protein band at ~28kDa with faint background bands (**Fig. 4.6B**). Since the EV-A71 VP2 was detected using polyclonal antibodies, it might cross react with non-target antigens thereby causing the protein backgrounds. Western blot image generated after incubation with anti-His-tag antibody showed a clear protein band of ~35kDa at **lane C1** and **C2**, indicating the expression of the CV-A16 VP1 protein. No 35kDa band was observed in **lane C3** for the non-transfected 293T cells serving as the negative control (**Fig. 4.6C**).

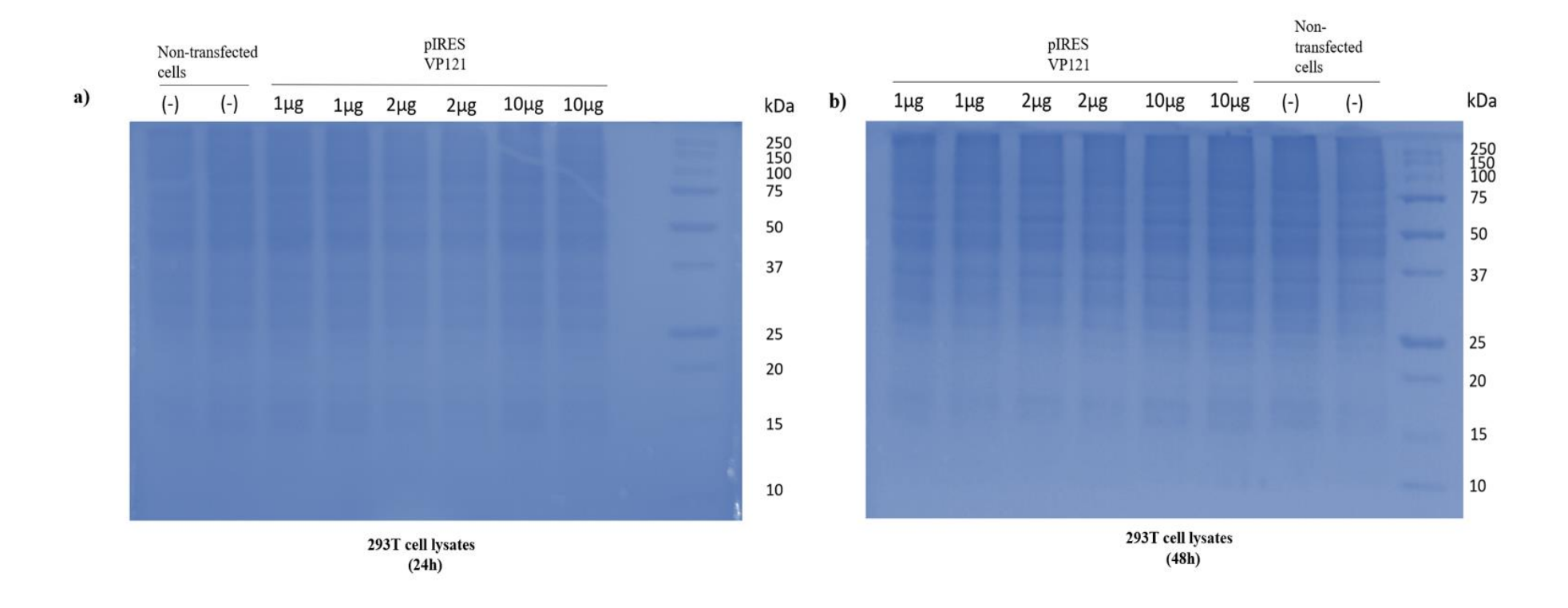


Figure 4.5: SDS PAGE gels loaded with 293T cell lysates harvested at 24h (a) and 48h (b) after transfection with 1μg,2 μg and 10 μg of recombinant pIRES-VP121, with non-transfected 293T cell lysates that served as negative controls. *Protein ladder: Precision Plus ProteinTM unstained protein standards (Bio-Rad, California, USA)

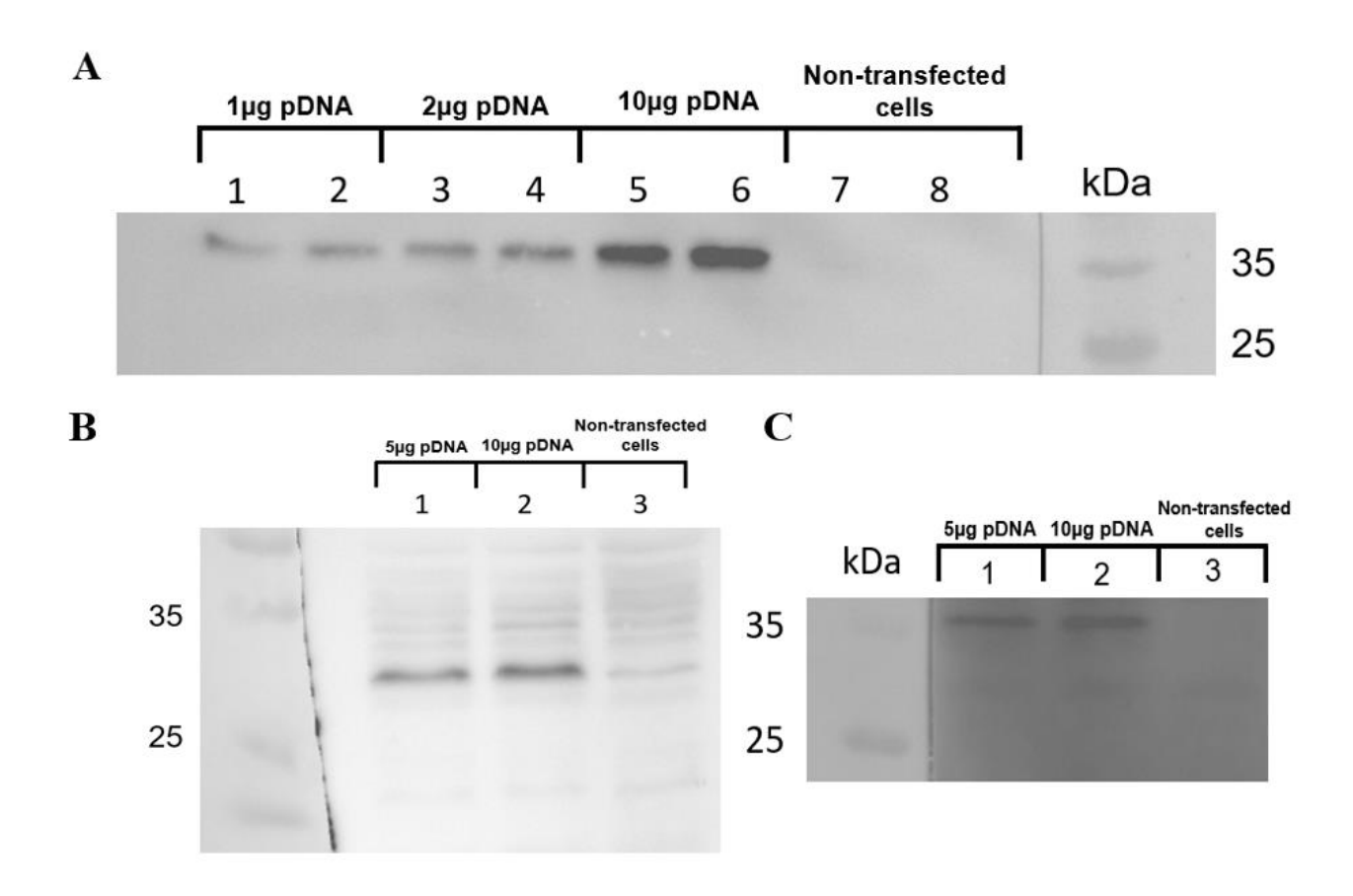


Figure 4.6: Western blots of recombinant protein expression by 293T cells transfected with pIRES-VP121 trivalent pDNA. Western blot analysis was carried out using primary A) EV-A71 VP1 monoclonal antibody, B) EV-A71 VP2 polyclonal antibody and C) His tag antibody. *Protein ladder: PM2610 (Smobio, Taiwan).

4.5 Characterization of the chitosan TPP nanoparticles

4.5.1 Encapsulation efficiency of chitosan nanoparticles correlate to the concentration of plasmid encapsulated

Encapsulation efficiency of the chitosan TPP nanoparticles encapsulating recombinant plasmid CS-TPP-NPs (pIRES-VP121) was evaluated by encapsulating pDNA at different concentrations. After high-speed centrifugation at 10,000xg, the pDNA present in the supernatant is considered as the amount of pDNA that was not encapsulated. The indirect encapsulation efficiency of CS-TPP-NPs (pIRES-VP121) was observed to increase from ~70% to 90% with the increment of pDNA concentration from 50 to 100μg during the encapsulation process (**Table 4.1**). Therefore, the maximum encapsulation efficiency of 90% was achieved by encapsulating 100μg of pIRES-VP121 using chitosan TPP nanoparticles.

Table 4.1: Encapsulation efficiency of chitosan TPP nanoparticles encapsulating different concentration of plasmid DNA.

| Samples | pDNA (μg) | Encapsulation Efficiency (%) | Encapsulated pDNA (μg) |
|--------------------------|-----------|-------------------------------------|------------------------|
| Blank-CS-TPP-NPs | - | - | |
| CS-TPP-NPs (pIRES-VP121) | 50 | 70 ± 5 | |
| CS-TPP-NPs (pIRES-VP121) | 100 | 90 ± 10 | |

^{*}Blank-CS-TPP-NPs referred to the empty chitosan TPP nanoparticles

4.5.2 Morphology, size, polydispersity index, and zeta potential of the chitosan TPP NPs

SEM images of the CS-TPP-NPs (pIRES-VP121) have shown uniform morphology with some spherical and oval shaped chitosan NPs being observed (Fig. 4.7). The average size of Chitosan TPP NPs encapsulating 50µg and 100µg pDNA were detected to be at ~180nm and ~190nm each while both being monodisperse (PDI\leq0.25) (Fig 4.8B, 4.8C). Instead, the blank chitosan TPP NPs serving as control had a smaller size in comparison with CS-TPP-NPs (pIRES-VP121) at ~145nm. The blank chitosan-TPP NPs also displayed favourable monodisperse characteristics with PDI value of ~0.25. (Fig. 4.8A). Blank chitosan-TPP nanoparticles exhibited the highest surface charge out of all 3 samples with an average zeta potential of ~+15mV (Fig. 4.9A). CS-TPP-NPs (pIRES-VP121) encapsulating 50µg and 100 µg of pDNA were also shown to have weak cationic charge with zeta potential of ~+12.5mV (Fig. 4.9B) and ~+10.5mV (Fig. 4.9C), respectively. Overall, there was no significant zeta potential differences between the blank nanoparticles (Fig. 4.9A) being observed when compared to the CS-TPP-NPs (pIRES-VP121) encapsulating 50µg (Fig. 4.9B) or 100µg (Fig. 4.9C) of pDNA respectively. Data acquired from zetasizer validating the size, PDI and zeta potential of chitosan TPP nanoparticles (experiments carried out three times independently) were averaged and compiled (Table 4.2).

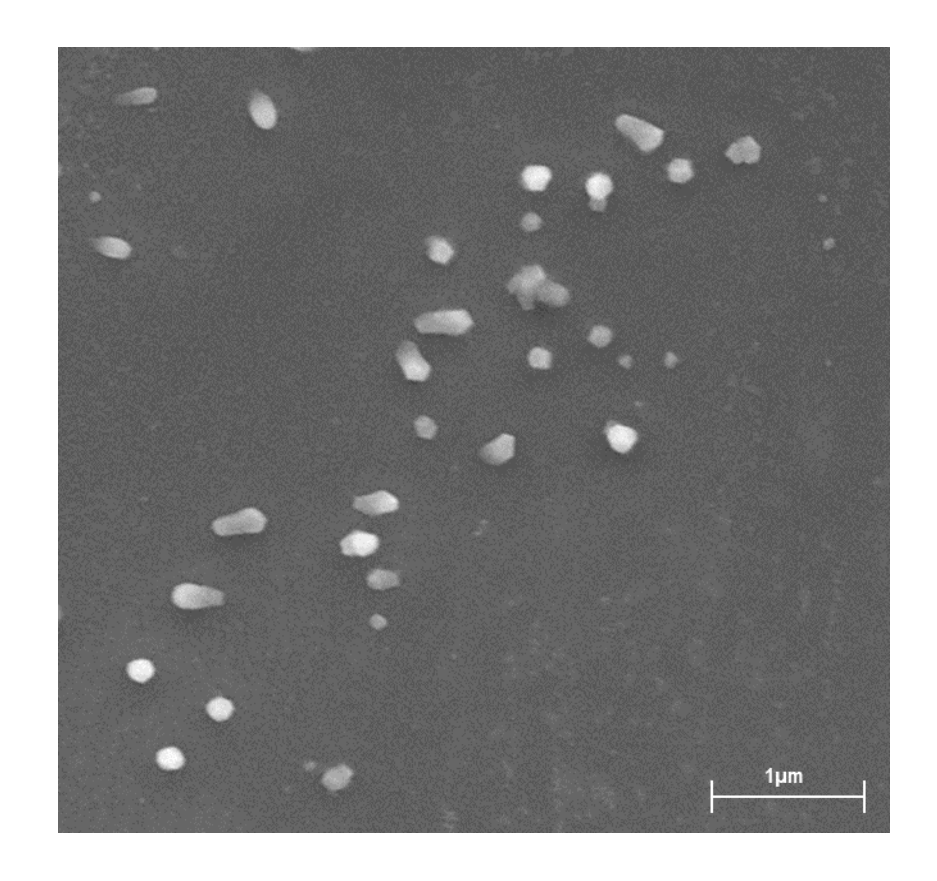


Figure 4.7: Morphology of the CS-TPP-NPs (pIRES-VP121) were visualized from SEM imaging: CS-TPP-NPs(pIRES-VP121) (100μg) at magnification of 12kx (1μm scale bar).

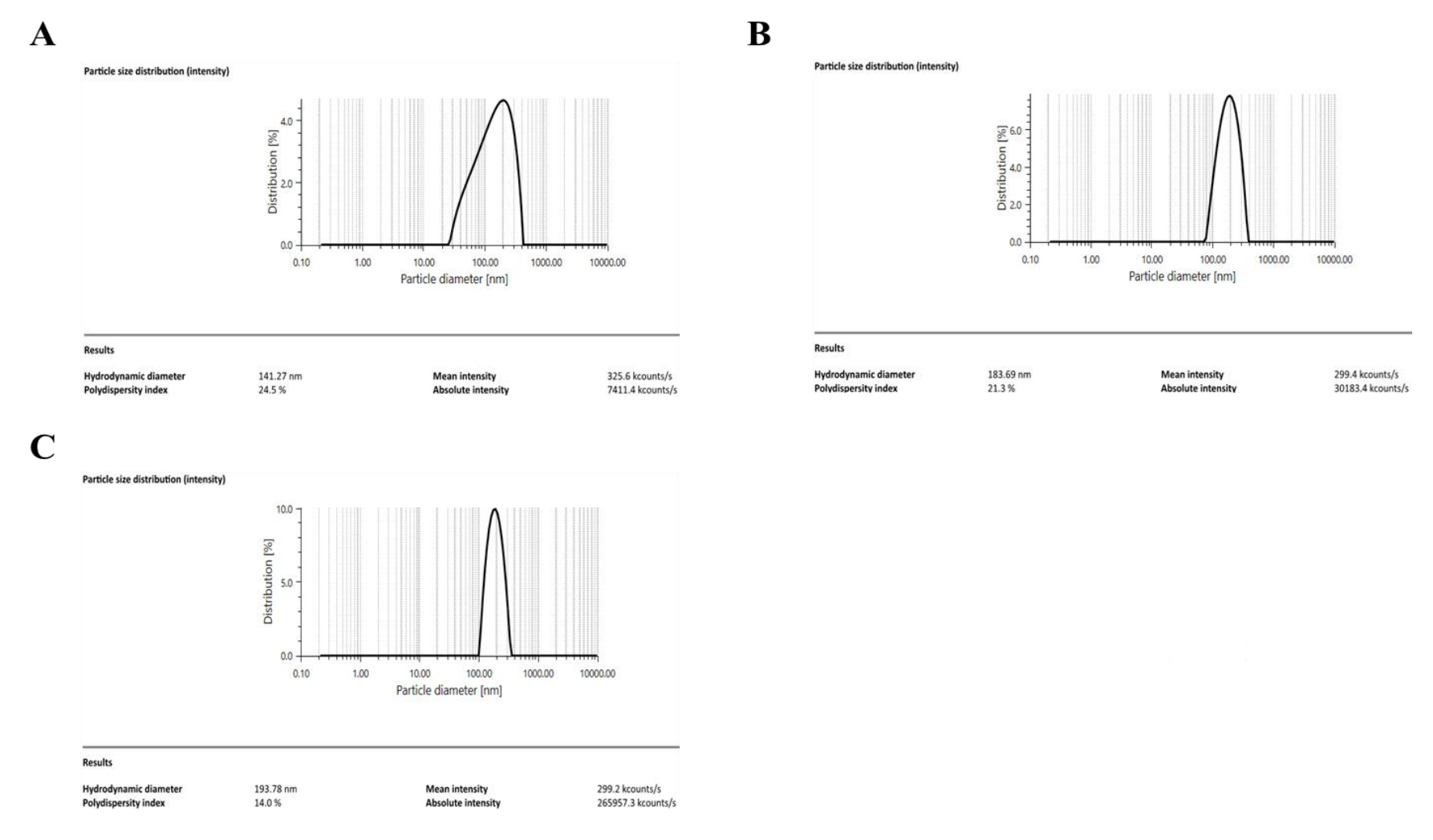


Figure 4.8: Average diameter and polydispersity index of A) blank CS-TPP-NPs, B) CS-TPP-NPs (pIRES-VP121) (50µg pDNA) and C) CS-TPP-NPs (pIRES-VP121) (100µg pDNA).

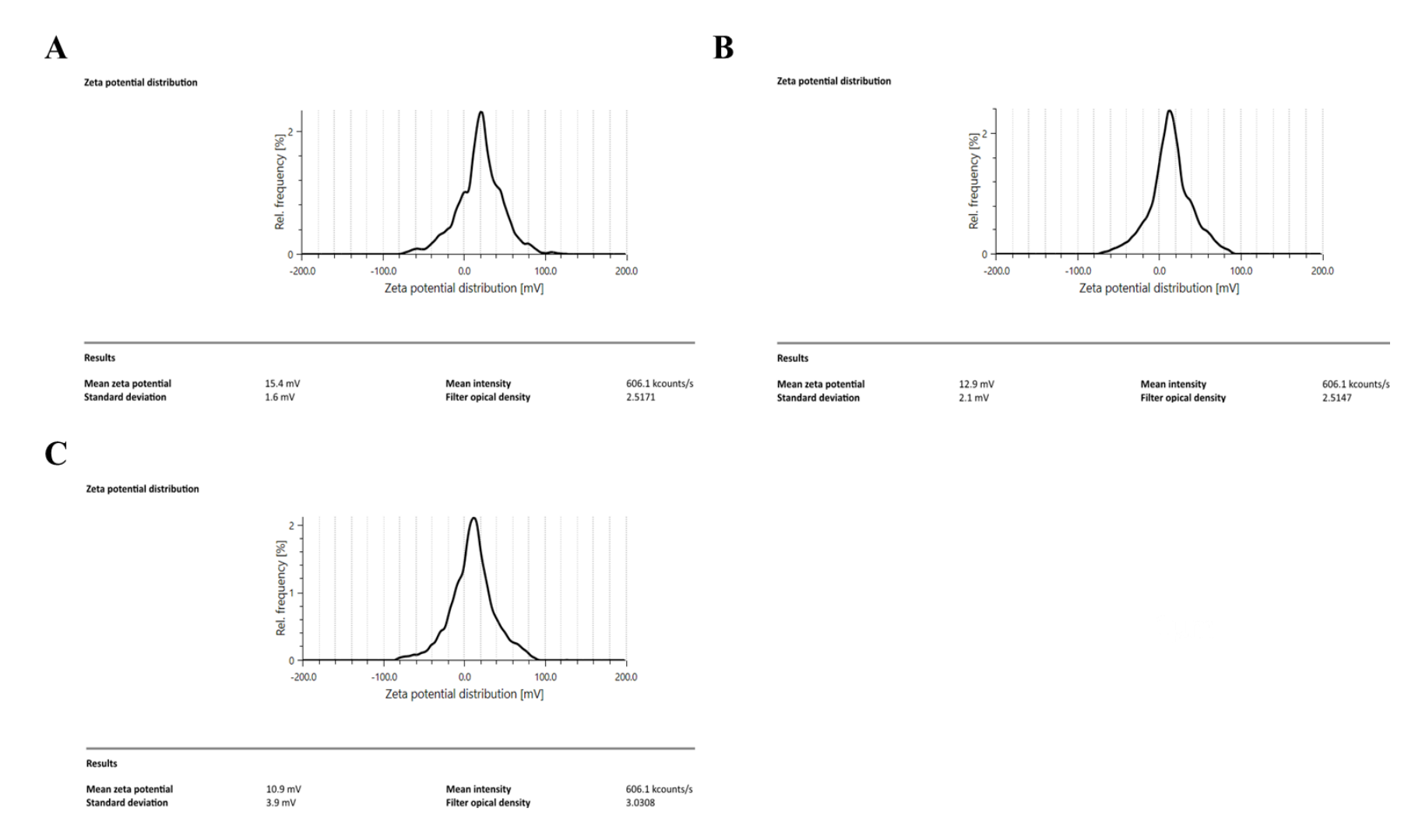


Figure 4.9: Zeta potential of A) blank CS-TPP-NPs, B) CS-TPP-NPs (pIRES-VP121) (50μg pDNA) and C) CS-TPP-NPs (pIRES-VP121) 100μg pDNA)

Table 4.2: Characteristics of Chitosan TPP nanoparticle formulations encapsulating different concentrations of recombinant plasmid DNA pIRES-VP121.

| Samples | pDNA (μg) | Mean size (nm) | Polydispersity index | Zeta potential (mV) |
|--------------------------|-----------|----------------|----------------------|---------------------|
| | | | (PDI) | |
| Blank-CS-TPP-NPs | - | 140 ± (5) | $0.25 \pm (0.01)$ | +15 ± (0.5) |
| CS-TPP-NPs (pIRES-VP121) | 50 | $180 \pm (10)$ | $0.21 \pm (0.01)$ | $+12.5 \pm (0.5)$ |
| CS-TPP-NPs (pIRES-VP121) | 100 | $190 \pm (10)$ | $0.14 \pm (0.01)$ | $+10.5 \pm (0.4)$ |

^{*}Data were derived from experiments repeated 3 times independently to ensure consistency.

4.6 Chitosan TPP NPs were able to protect encapsulated pDNA from digestion by DNase I

In order to study the stability of pDNA after being formulated into CS-TPP-NPs (pIRES-VP121), the protective capabilities of chitosan TPP nanoparticles were evaluated by incubation with DNase I followed by chitosanase solution (**Fig. 4.1**). The pDNA encapsulated in chitosan TPP NPs were not degraded by DNase I as an intact band of ~9000bp was observed at the same position as the untreated pDNA (**Fig. 4.1**, **lane 1 and lane 4**) after incubation of DNase I and chitosanase. A clear band was observed on the well (**Fig. 4.1**, **lane 6**) just like the untreated chitosan nanoparticles (**Fig. 4.1**, **lane 2**) as the CS-TPP-NPs (pIRES-VP121) complexes were unable to migrate in agarose. This indicates that the CS-TPP-NPs (pIRES-VP121) were not degraded by DNase I incubation. Instead, naked pDNA incubated with DNase I (**Fig. 4.1**, **lane 5**) alone or incubated with DNase I followed by chitosanase (**Fig. 4.1**, **lane 7**) were completely degraded with no bands being observed. Therefore, we conclude that encapsulation with chitosan TPP nanoparticles were able to protect the trivalent plasmid vaccine from DNase I degradation.

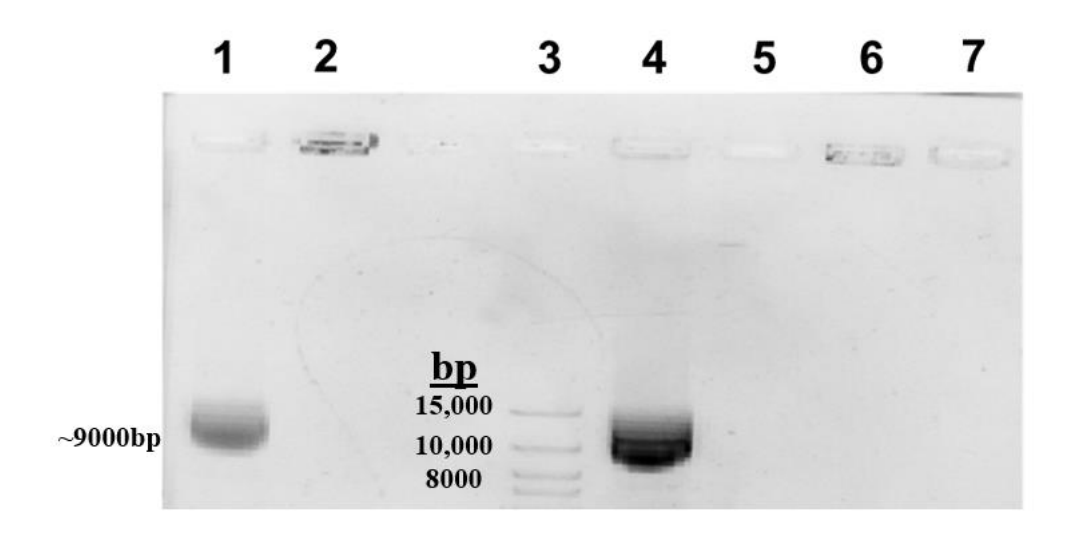


Figure 4.10: Agarose gel electrophoresis image of plasmid DNA and CS-TPP-NPs (pIRES-VP121) complex: Lane 1: untreated pDNA (control); lane 2: untreated CS-TPP-NPs (pIRES-VP121); lane 3: DNA marker - TrackItTM 1 Kb Plus DNA Ladder (Thermofisher, USA); lane 4: CS-TPP-NPs (pIRES-VP121) treated with DNase I followed by chitosanase; lane 5: pDNA treated with DNase I followed by chitosanase; lane 6: CS-TPP-NPs (pIRES-VP121) treated with DNase I; lane 7: pDNA treated with DNase I

4.7 Chitosan TPP NPs were suitable nanocarriers for cellular uptake of pDNA into murine macrophage cells.

To verify expression of the trivalent plasmid vaccine candidate encapsulated by chitosan TPP NPs in murine cells prior to immunization in mice, fluorescent microscopy was performed on J774A.1 murine macrophage cells transfected with chitosan TPP nanoparticles encapsulating pDNA. J774A.1 cells transfected for 48h with pDNA using XfectTM transfection served as the positive control (**Fig. 4.11h**) and J774A.1 cells transfected or incubated with naked pDNA alone served as the negative control (**Fig. 4.11e**). Significant fluorescent signals were first observed in J774A.1 cells at 48h post transfection (**Fig. 4.11f**). Additionally, fluorescent signal intensity was observed to have increased at 72h post transfection (**Fig. 4.11g**). Taken together, these data suggested that chitosan TPP NPs were able to be taken up by murine macrophage cells, followed with successful expression of the encapsulated pDNA. However, the transfection efficiency of chitosan TPP NPs were observed to be less significant in comparison with cells transfected using the commercial transfection kit as evident from the differences in fluorescent signal intensity (**Fig. 4.11f, 4.11g and 4.11h**).

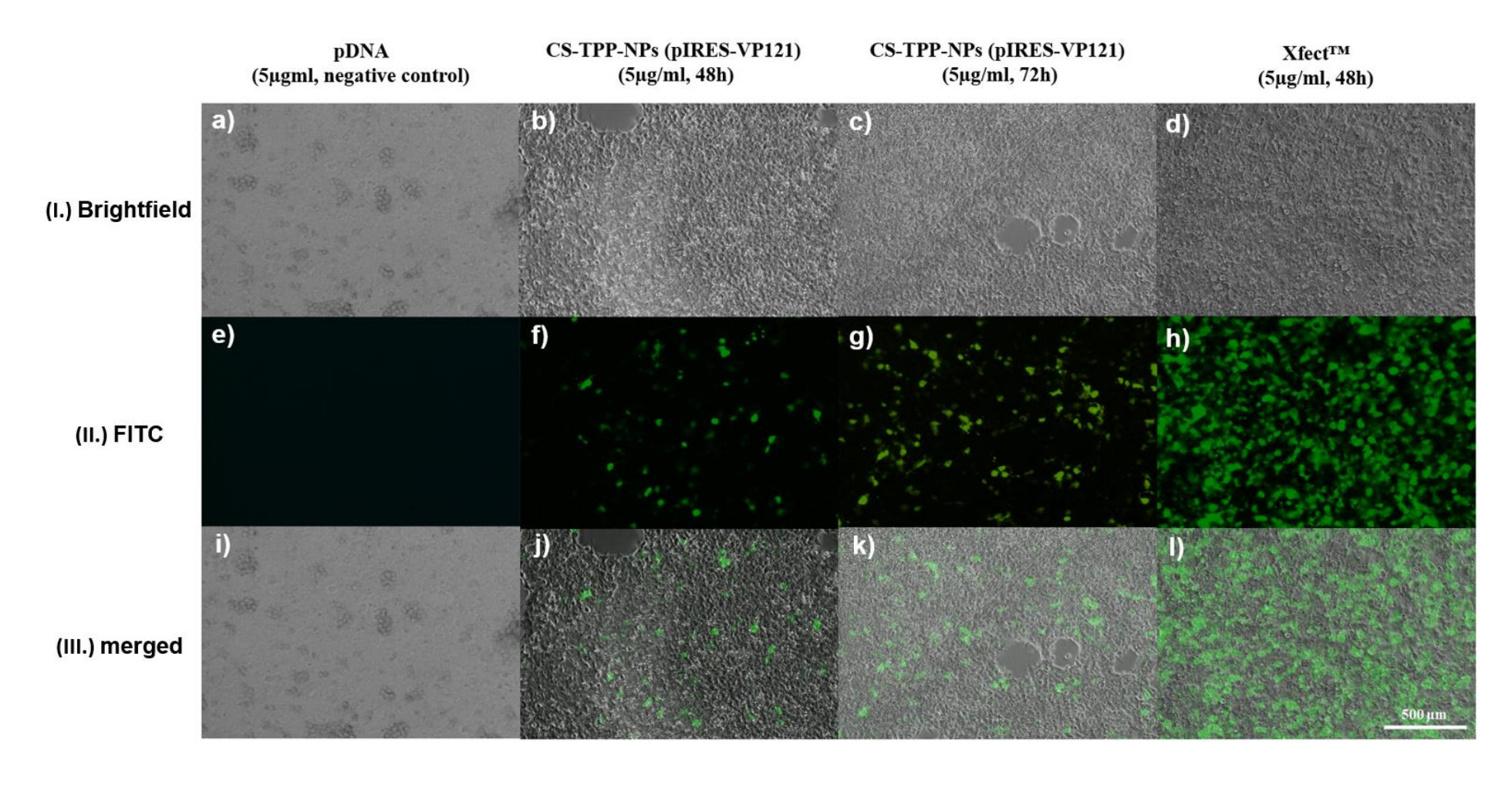


Figure 4.11: Fluorescent microscopy images of J774A.1 macrophage transfected with naked pDNA (a, e, i), CS-TPP-NPs (pIRES-VP121) (5μg/ml, 48h) (b, f, j), CS-TPP-NPs (pIRES-VP121) (5μg/ml, 72h) (c, g, k) and XfectTM reagent (5μg/ml, 48h) (d, h, l) were captured under 10x magnification (scale bar 500μm); I. images from BF channel, II. images from FITC channel and III. images merged from the FITC and BF channel.

4.8 Chitosan TPP NPs and chitosan polymer did not have hemolytic effects on RBCs of ICR mice even at high concentrations.

To ensure the safety of chitosan TPP nanoparticles encapsulating pDNA prior to administration in murine models, the hemolytic properties of chitosan TPP NPs were evaluated in RBCs harvested from ICR mice (**Fig. 4.12**). CS-TPP-NPs (pIRES-VP121), blank chitosan NPs and chitosan polymer solution at a concentration of 400µg/ml were observed to have no hemolytic effects on RBCs as the color of the supernatants from sample tube a, b and c remained the same as the negative control (tube e) after centrifugation. Instead, red color supernatant was observed in the positive control (tube d) which indicates the effect of hemolytic agent Triton X-100.

Absorbance of hemolysis assay measured at 527nm have also revealed the exact degree of hemolysis after incubation with CS-TPP-NPs (pIRES-VP121), blank chitosan NPs and chitosan polymer solution (**Fig. 4.13**). Results showed that all 3 samples did not induce hemolysis rate of more than 5%. We concluded that CS-TPP-NPs (pIRES-VP121) would not induce hemolysis upon injection in mice as only hemolytic degree (>5%) was considered significant according to ASTM E2524-08 standards (Jesus et al., 2020).

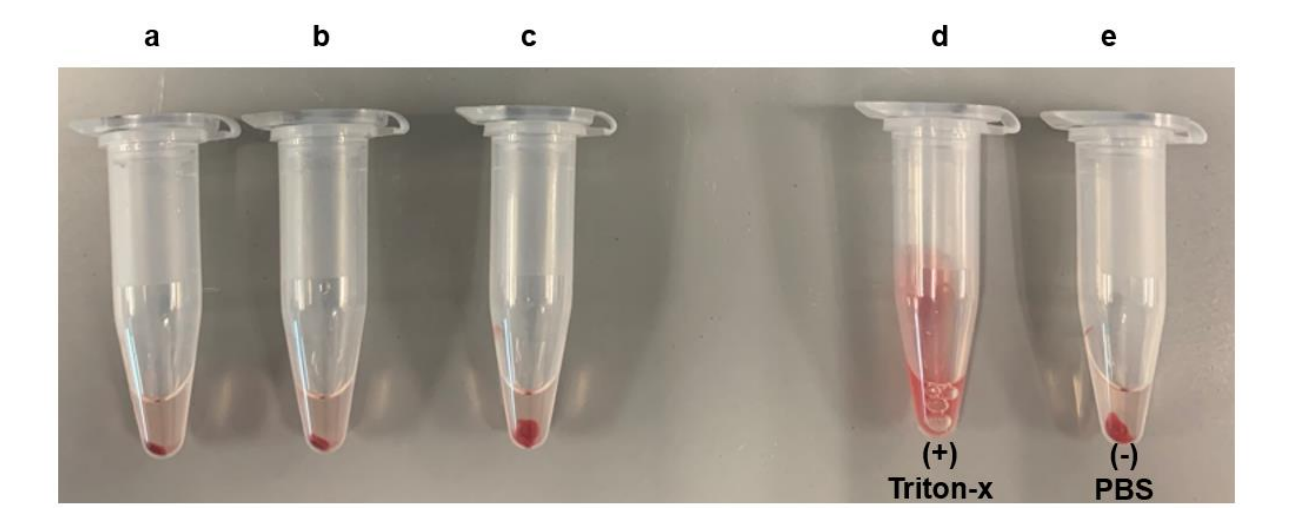


Figure 4.12: Murine RBCs were incubated with (a) blank Chitosan TPP NPs, (b) CS-TPP-NPs (pIRES-VP121) and (c) chitosan polymer at a concentration of 400μg/ml. (d) Triton-X and (e) PBS solution mixed with RBCs served as the positive and negative control, respectively. Hemolysis images of samples were taken after OD reading. Experiments were performed in quadruplicates for each sample.

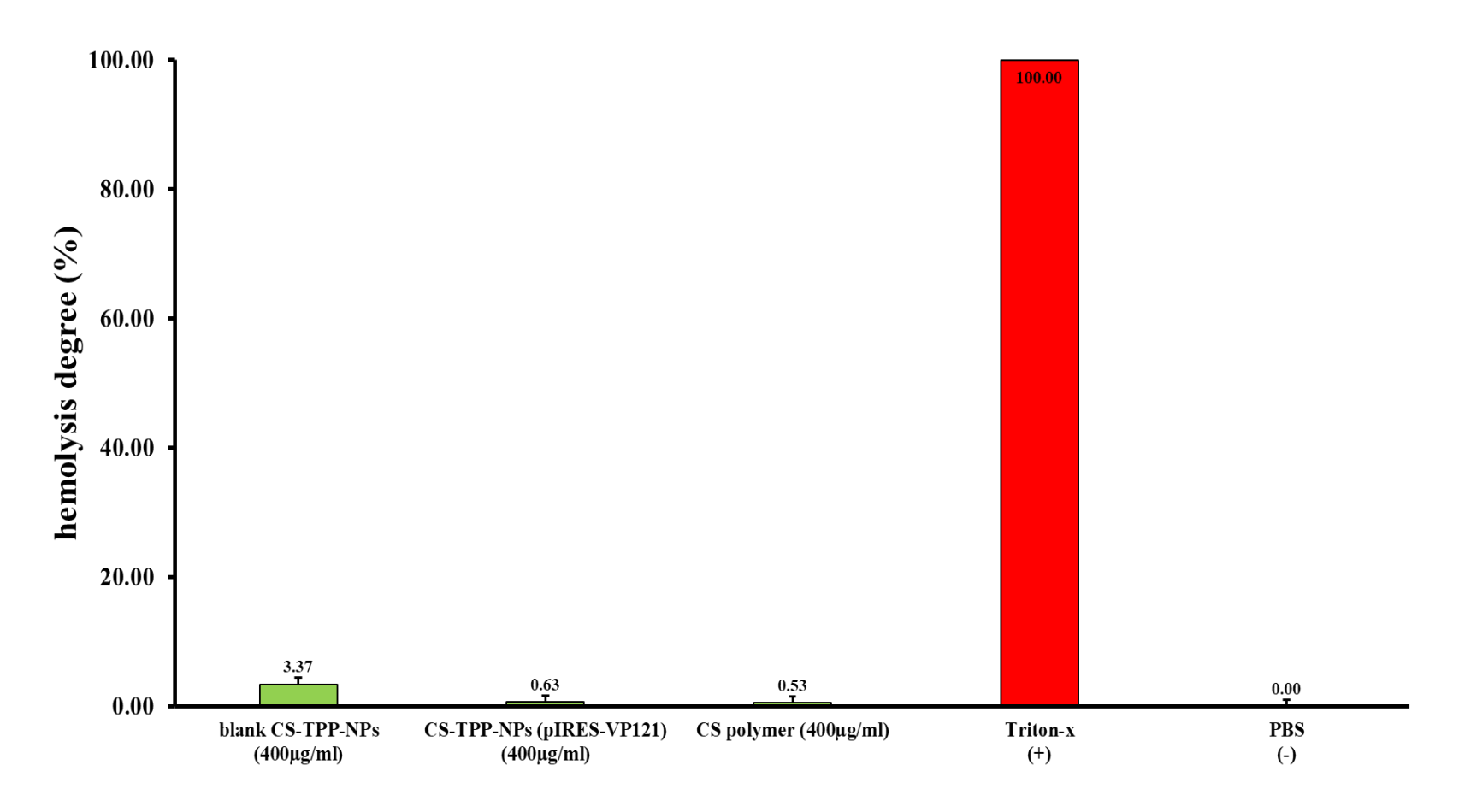


Figure 4.13: Hemolysis rate of HCR mice red blood cells (RBCs) following incubations with blank Chitosan NPs, CS-TPP-NPs (pIRES-VP121), and chitosan polymer at a concentration of 400μ g/ml. Experiment was performed in quadruplicates for each sample, data were presented as mean \pm SD with error bar indicating the standard deviation. Triton-x represents 100% hemolysis (positive control) and PBS represents the absence of hemolysis (negative control).

4.9 Chitosan TPP nanoparticles and chitosan polymer were not cytotoxic in murine macrophage cells.

MTS metabolic activity assay was carried out with the chitosan polymer, blank CS-TPP-NPs, and CS-TPP-NPs (pIRES-VP121) over different concentrations ($100\mu g/ml$, $200\mu g/ml$, and $400\mu g/ml$). Chitosan polymer was observed to induce the highest cytotoxicity (~20%) out of all 3 samples including CS-TPP-NPs (pIRES-VP121), blank chitosan NPs and chitosan polymer solution. However, results showed that all 3 samples could be considered as non-cytotoxic as the cell viability of J774A.1 murine macrophages did not drop below 80% across all 3 samples even when incubated at the highest concentration of $400\mu g/ml$ (**Fig. 4.14**). Therefore, immunization of mice could be carried out without the risk of cytotoxic effects.

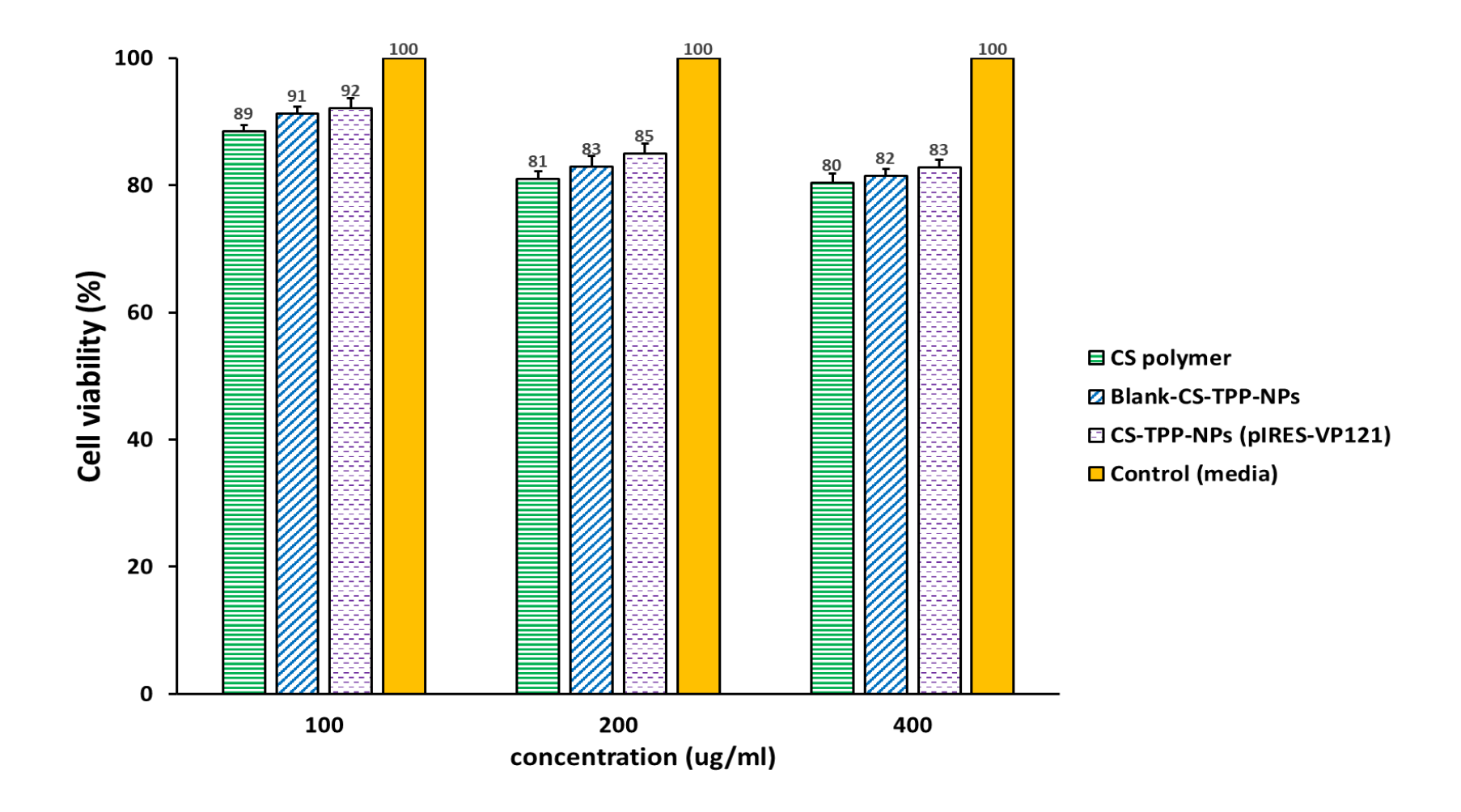


Figure 4.14: J774A.1 mice macrophages evaluated by MTS assay after 48h incubation with blank Chitosan NPs, CS-TPP-NPs (pIRES-VP121) and chitosan polymer at different concentrations ($400\mu g/ml$, $200\mu g/ml$, $100\mu g/ml$). Experiments were performed three times independently with similar results, media alone served as the control. Data was presented as mean \pm SD, error bar indicates the standard deviation.

4.10 Chitosan TPP NPs encapsulation of the trivalent pDNA vaccine candidate enhanced cellular immune response.

Flow cytometry was performed to investigate the changes of CD4⁺ and CD8⁺ T cells lymphocyte populations in the splenocytes harvested from mice immunized with a single booster dose at 2 weeks interval (**Fig. 4.15A**). The CD3⁺CD4⁺ and CD3⁺CD8⁺ T cells populations were identified in kaluza software using specific gating strategy (**Fig. 4.16**). In mice immunized with 50 μg of naked pDNA and followed with single booster dose, a slight population increase of CD4⁺ and CD8⁺ T cells expressing IFN-γ was observed when compared with the naïve mice group (**Fig. 4.17B**). In contrast, there was a significant increment (~2-fold) of IFN-γ expressing CD4⁺ T cells in group of mice immunized with 100μg of naked pDNA when compared to the group of mice that received 50 μg of naked pDNA (**Fig. 4.17B**). Comparison between the two vaccinated mice groups have also shown an almost two-fold increment of CD8⁺ T cells expressing IFN-γ (**Fig. 4.18B**). We have concluded that there is a dose dependent relationship between the amount of vaccine administered and the degree of cellular immune response elicited in immunized mice.

Flow cytometry was used to assess the percentage population of IFN- γ secreting CD4⁺ (**Fig. 4.19A**) and CD8⁺ (**Fig. 4.20A**) T cells of splenocytes harvested from mice immunized with naked pDNA (100 µg), CS-TPP-NPs (pIRES-VP121) (100µg pDNA), with naïve mice group serving as negative control. Mice in group B received a total of 2 booster doses post-immunization at a two-week interval (**Fig. 4.15B**).

There was a slight increase observed in IFN-γ secreting CD4⁺ (**Fig. 4.19B**) and CD8⁺ (**Fig. 4.20B**) populations of splenocytes from mice vaccinated with 100μg of naked pDNA in comparison with the naïve mice group. Highest percentage of CD4⁺ and CD8⁺ T cells expressing IFN-γ were observed in mice group immunized with CS-TPP-NPs (pIRES-VP121) (100μg pDNA) when compared to the naïve mice splenocytes (~2 fold increment).

To conclude, encapsulation of trivalent plasmid vaccine pIRES-VP121 in chitosan nanoparticles was able to boost T cell IFN- γ response in murine models.

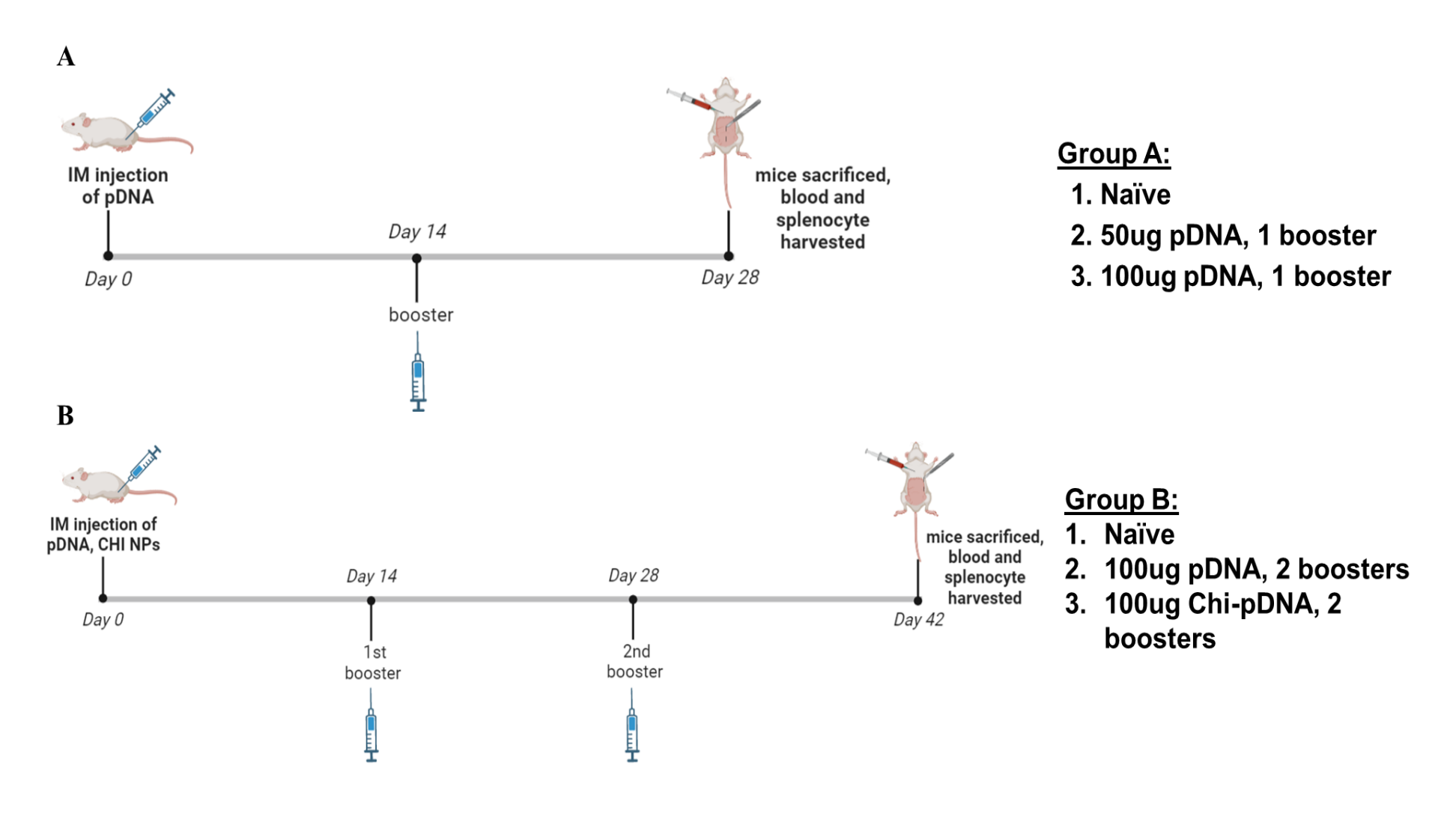


Figure 4.15: Timeline of A) groups of mice receiving a single booster dose post-immunization B) groups of mice receiving two booster doses post-immunization. Image was generated using Biorender.com.

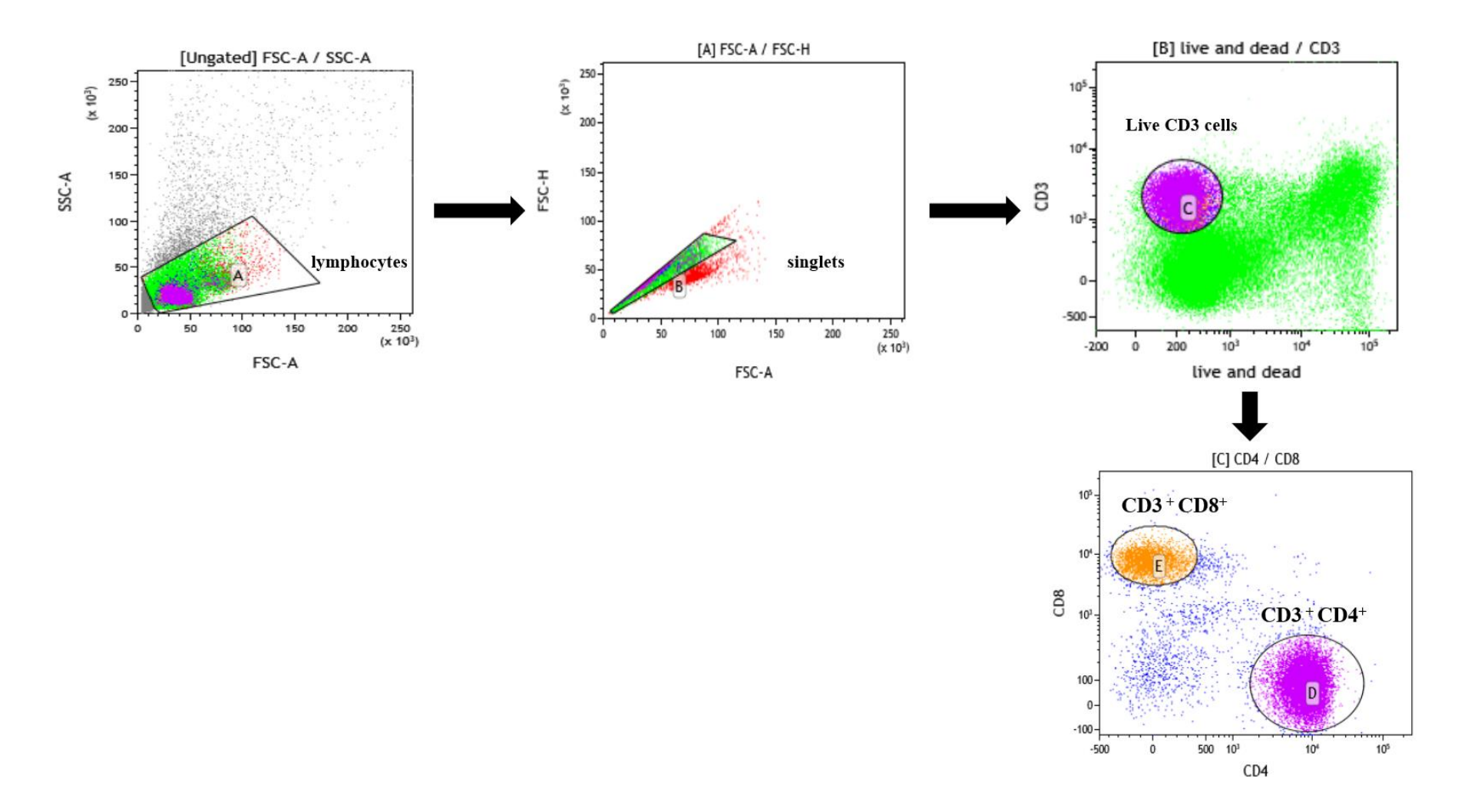


Figure 4.16: Gating strategy performed in Kaluza software to identify the live CD3⁺CD4⁺ and live CD3⁺CD8⁺ T cells populations.

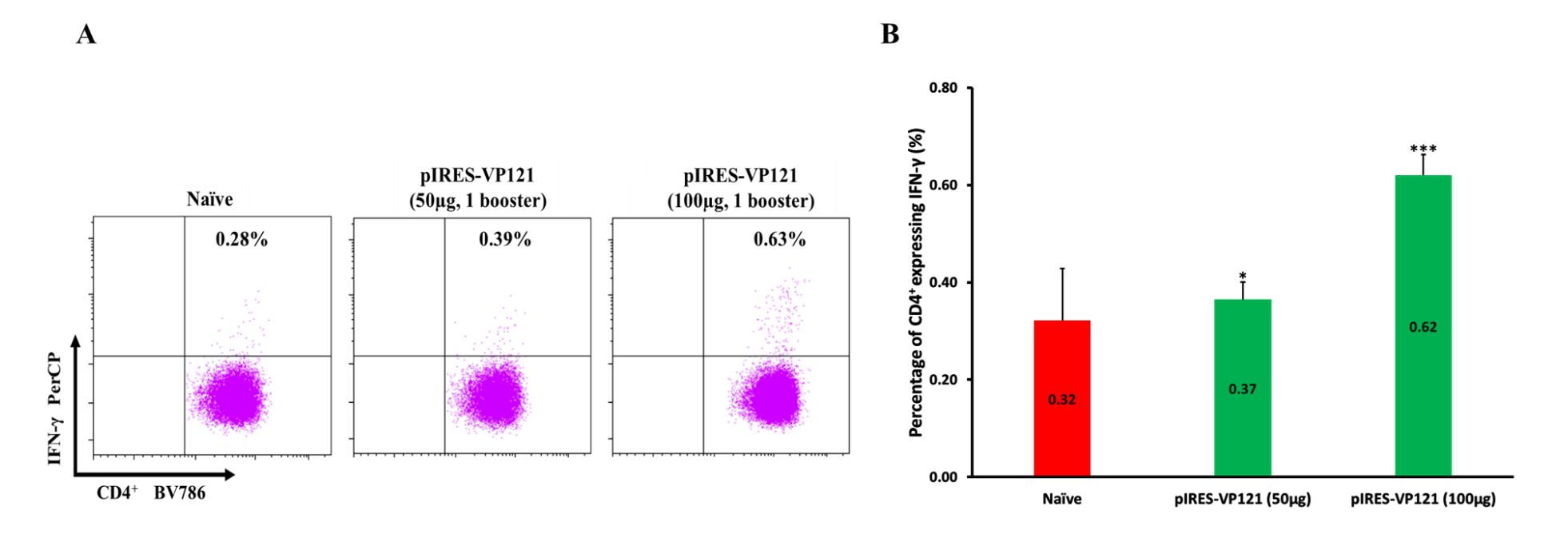


Figure 4.17: Dot plots from flow cytometry analysis (A) showing the subsets of IFN- γ expressing CD4⁺ T cells from splenocytes of naïve mice and mice immunized with 50μg or 100μg of naked pDNA, followed by 1 booster dose. IFN- γ expressing CD4⁺ from each group of mice (population %) were presented on bar chart (B) indicating mean \pm SD with error bar representing the standard deviation. Statistical significance was analysed with unpaired t-test: $*P \le 0.05$ against naïve splenocytes, $**P \le 0.01$ against naïve splenocytes and $****P \le 0.001$ against naïve splenocytes. Experiment was performed in quadruplicates for each sample.

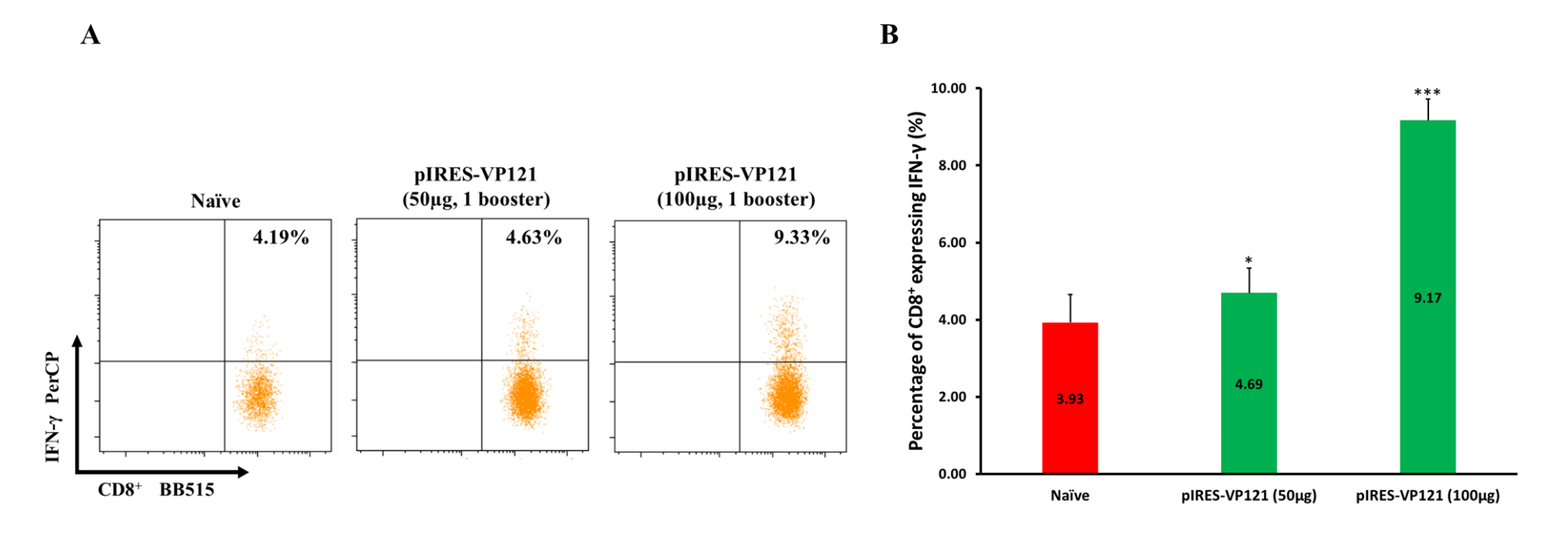


Figure 4.18: Dot plots from flow cytometry analysis (A) showing the subsets of IFN- γ expressing CD8⁺ T cells from splenocytes of naïve mice and mice immunized with 50μg or 100μg of naked pDNA, followed by 1 booster dose. IFN- γ expressing CD8⁺ from each group of mice (population %) were presented on bar chart (B) indicating mean \pm SD with error bar representing the standard deviation. Statistical significance was analysed with unpaired t-test: *P≤0.05 against naïve splenocytes, **P≤0.01 against naïve splenocytes and ****P≤0.001 against naïve splenocytes. Experiment was performed in quadruplicates for each sample.

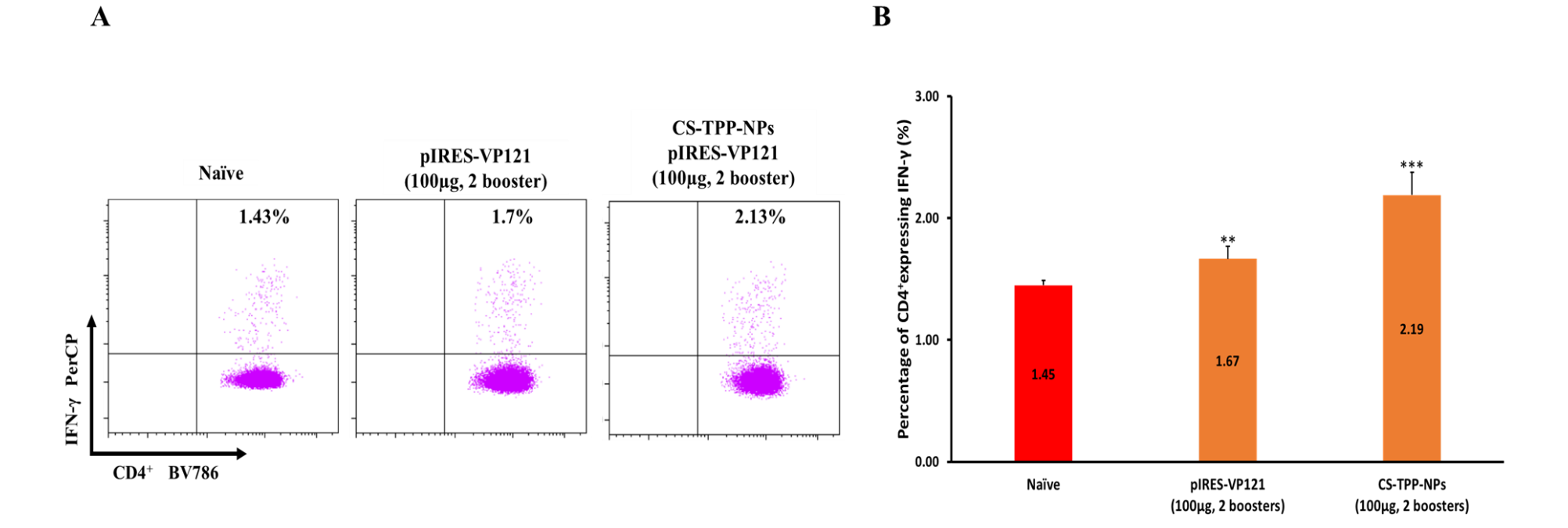


Figure 4.19: Dot plots from flow cytometry analysis (A) showing the subsets of IFN- γ expressing CD4⁺ T cells from splenocytes of naïve mice, mice immunized with naked pDNA (100μg, 2 booster) and CHI-pDNA-NPs (100μg, 2 booster). IFN- γ expressing CD4⁺ from each group of mice (population %) were presented on bar chart (B) indicating mean \pm SD with error bar representing the standard deviation. Statistical significance was analysed with unpaired t-test: *P≤0.05 against naïve splenocytes, **P≤0.01 against naïve splenocytes, ***P≤0.001 against naïve splenocytes and *****P≤0.0001 against naïve splenocytes. Experiment was performed in quadruplicates for each sample.

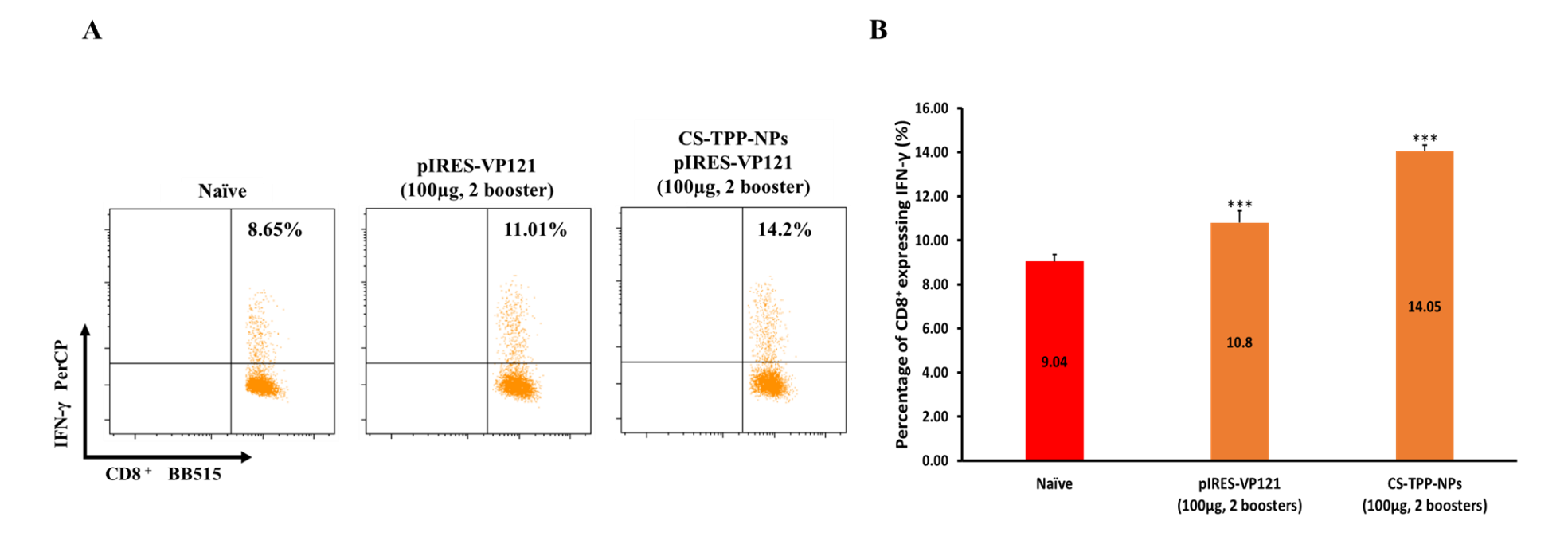


Figure 4.20: Dot plots from flow cytometry analysis (A) showing the subsets of IFN- γ expressing CD8⁺ T cells from splenocytes of naïve mice, mice immunized with naked pDNA (100μg, 2 booster) and CHI-pDNA-NPs (100μg, 2 booster). IFN- γ expressing CD8⁺ from each group of mice (population %) were presented on bar chart (B) indicating mean \pm SD with error bar representing the standard deviation. Statistical significance was analysed with unpaired t-test: *P≤0.05 against naïve splenocytes, **P≤0.01 against naïve splenocytes and ****P≤0.0001 against naïve splenocytes. Experiment was performed in quadruplicates for each sample.

4.11 Chitosan encapsulation of pIRES-VP121 enhanced the levels of IFN-γ secretion

IFN-γ concentrations secreted by the splenocytes from immunized mice were quantified using ELISA assays. Results showed a dose dependent relationship between the amount of naked pDNA vaccine administered and the magnitude of IFN-y response. A gradual increase of IFN-y levels at 0.05pg/ml was observed, starting from mice immunized with 50µg naked pDNA followed with a single booster at 2 weeks interval. The amount of naked pDNA administered was increased to 100µg at day 0, followed by a booster at 2 weeks later and IFN- γ secreted was observed to have a ~2-fold increment (0.11pg/ml). When mice were immunized with 100µg of naked pDNA but further administered with 2 booster doses at 2 weeks intervals, there was only a slight increase in IFN-γ production at 0.13pg/ml. The IFN- γ expression pattern of mice immunized with the naked plasmid vaccine further supported the findings from flow cytometry analysis. However, mice immunized with the CS-TPP-NPs (pIRES-VP121) followed by 2 booster doses (2 weeks interval) exhibited significantly higher concentration of IFN-γ levels (1.91pg/ml). There was ~15-fold of IFN-γ increment in comparison to all groups of mice immunized with the naked pDNA alone (Fig. 4.21). The measurements from ELISA analysis provided further evidence that chitosan TPP nanoparticles enhanced cellular immune response of the trivalent recombinant plasmid vaccine candidate.

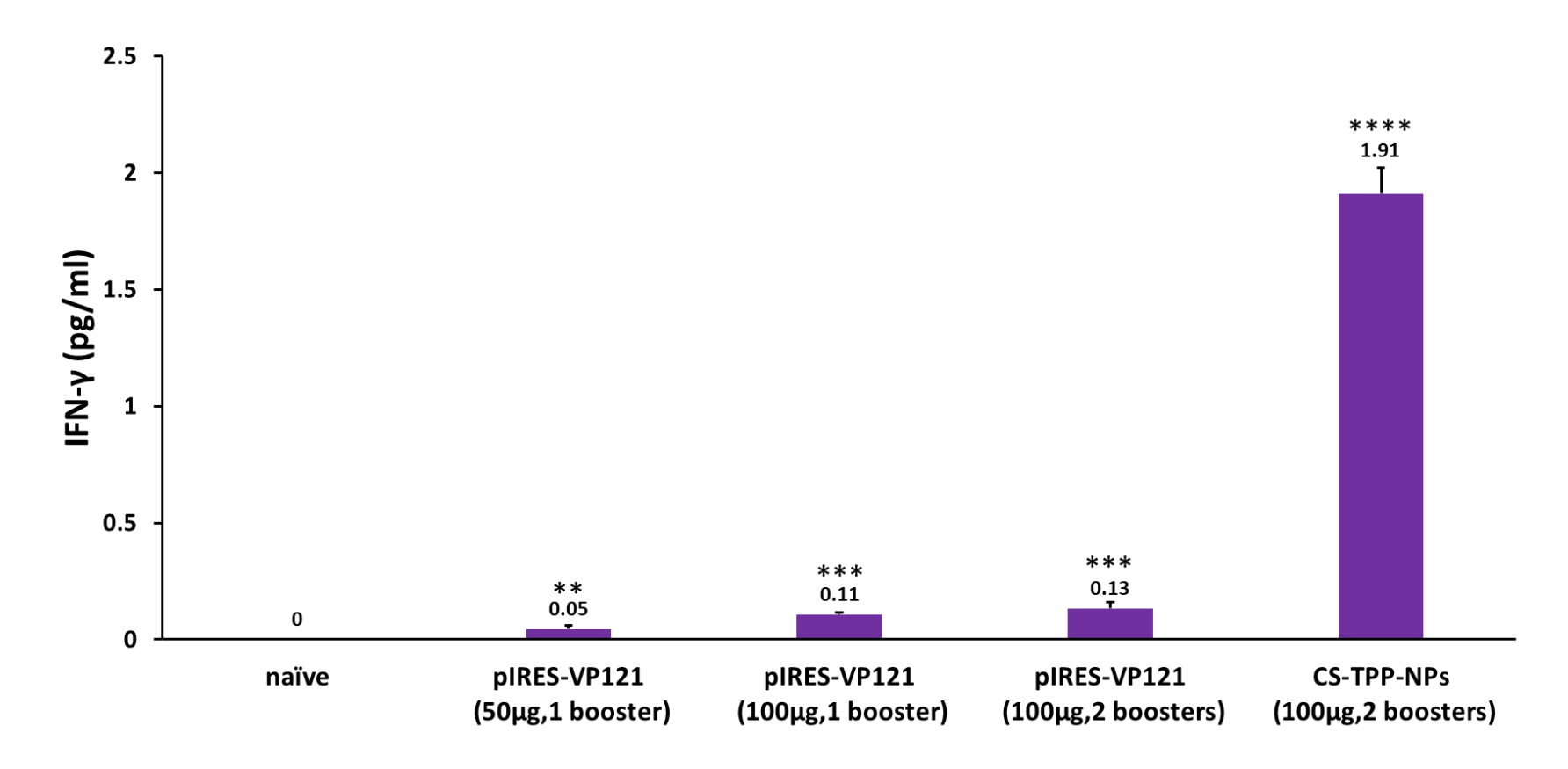


Figure 4.21: The amount of IFN- γ (pg/ml) secreted by splenocytes from mice immunized with 50μg pDNA, 100μg pDNA at one booster dose, 100μg pDNA or CS-TPP-NPs (pIRES-VP121) at two booster doses in comparison with the naïve mice from ELISA assay. Experiment was carried out in triplicates and repeated 3 times independently using the same settings. Data were presented as mean \pm SD and error bar indicates standard deviation. Significance value was analysed with unpaired T test: *P≤0.05, **P≤0.01, ***P≤0.001 and ****P≤0.0001 against naïve splenocytes.

4.12 Chitosan encapsulation of pIRES-VP121 enhanced neutralization against the wild-type EV-A71 and CV-A16

RD cells were incubated with antisera harvested from mice immunized with the naked pIRES-VP121 and CS-TPP-NPs (pIRES-VP121) at a total of 3 doses in experimental group B (**Fig. 4.15b**). The neutralizing efficacy of immunized mice sera at 1:16 dilution was determined by a classical read-out of the cytopathic effects (CPE) in monolayer RD cells. RD cells were each infected with four different enteroviruses including the wild-type EV-A71 B4, mouse-adapted EV-A71 B3 (MAV), wild-type CV-A16 N/132 and mouse-adapted CV-A16 N/132 (MAV) to determine the neutralizing capabilities of immune sera. Naïve sera and purified EV-A71 monoclonal antibodies would serve as the negative and positive control, respectively. EV-A71 monoclonal antibodies were able to inhibit CPE manifestations in RD cells infected with the wild type (**Fig. 4.22m**) or MAV (**Fig. 4.22n**) strains of EV-A71 to below 5% (**Fig. 4.23**).

RD cells incubated with sera from naïve mice were observed to show 80-90 % CPE indicating severe cell death upon infection of wild-type EV-A71 (Fig. 4.22a) or CV-A16 (Fig. 4.22d). Against MAV strains of EV-A71(Fig. 4.22g) and CV-A16 (Fig. 4.22j), RD cells incubated with naïve sera also produced extensive CPE (80-90%) (Fig 4.23). Sera of mice immunized with the naked plasmid DNA exhibited 30% and 50% CPE in RD cells against infection of wild-type EV-A71 (Fig. 4.22b) and CV-A16 (Fig. 4.22e), respectively. However, these sera failed to protect RD cells from mouse-adapted EV-A71 (Fig. 4.22h) and CV-A16 (Fig. 4.22k) infections as CPE of 75~80% was observed (Fig. 4.23). However, mice immunized with CS-TPP-NPs (pIRES-VP121) were able to produce sera that could inhibit CPE to 10% and 15% in RD cells infected with the wild-type EV-A71(Fig. 4.22c) and CV-A16 (Fig. 4.22f), respectively. In contrary, there were no significant neutralizing effects elicited by the chitosan TPP encapsulated pDNA vaccine in RD cells infected with either MAV EV-A71 (Fig. 4.22i) or CV-A16 (Fig. 4.22l). Both RD cell sample wells exhibited CPE percentage remaining at ~60% (Fig. 4.23).

To conclude our findings, encapsulation of trivalent pDNA vaccine candidate in chitosan TPP nanoparticles were able to improve its neutralizing efficacy against wild-type EV-A71 and CV-A16 in comparison with the naked pIRES-VP121. However, immunization of mice with the trivalent pIRES-VP121 vaccine candidate produced sera which was unable to neutralize both MAV strains of EV-A71 and CV-A16 even with encapsulation of chitosan TPP NPs.

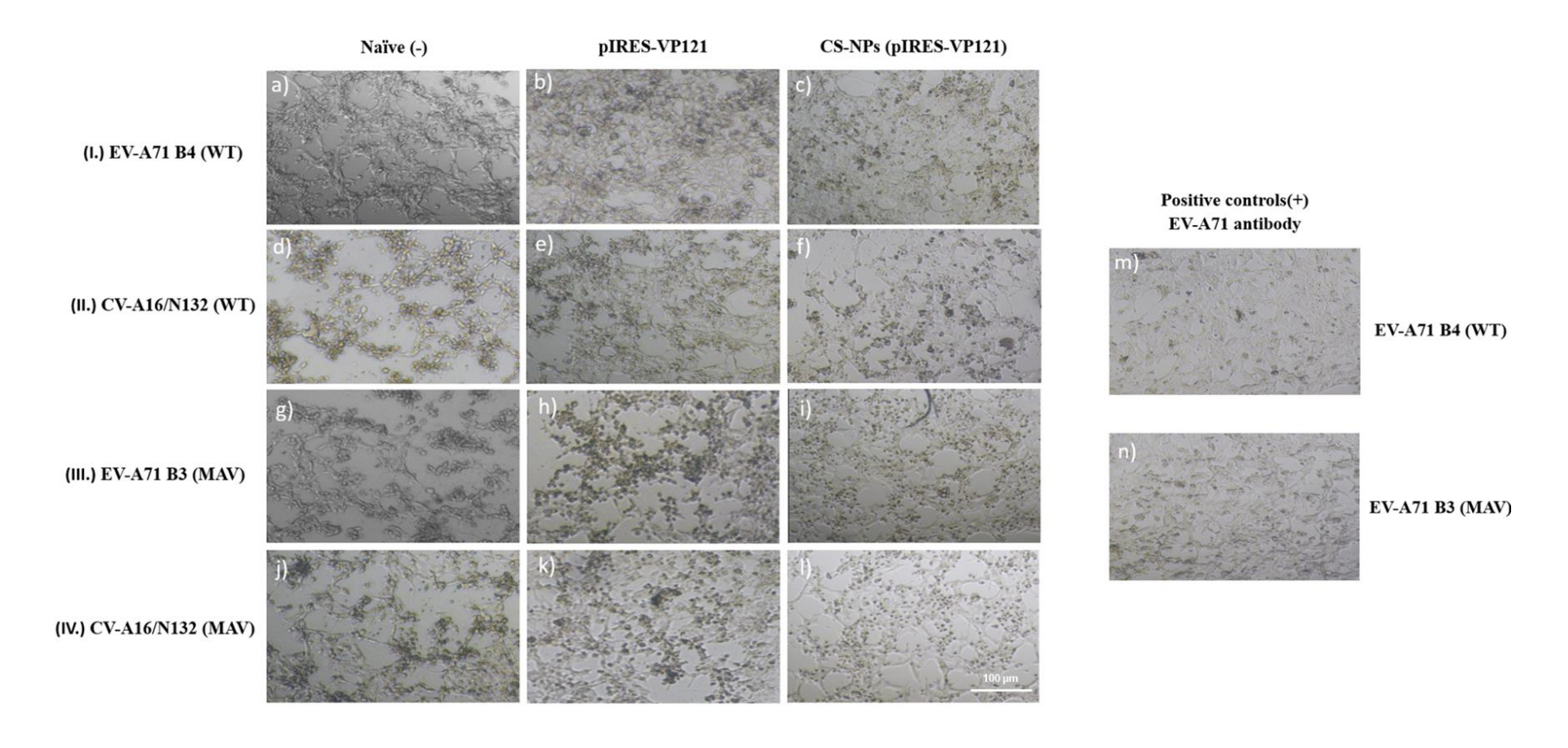


Figure 4.22: Representative micrographs showing the CPE condition of RD cells at 96h post infection with (I.) wild type EV-A71 B4, (II.) wild type CV-A16/N132, (III.) EV-A71 B3 (MAV) and (IV.) CV-A16/N132 (MAV), respectively. RD cells were also incubated with 1:16 dilution of naïve mice sera (a,d,g,j), sera of mice immunized with naked pIRES-VP121 (b,e,h,k), and antisera of mice immunized with CS-TPP-NPs (pIRES-VP121) (c,f,i,l), respectively prior to enterovirus infection. RD cells incubated with monoclonal EV-A71 antibodies (m,n) followed by incubation with wild-type or mouse adapted EV-A71 would serve as the positive controls. Images were taken at 5x magnification with 100μm scale bar.

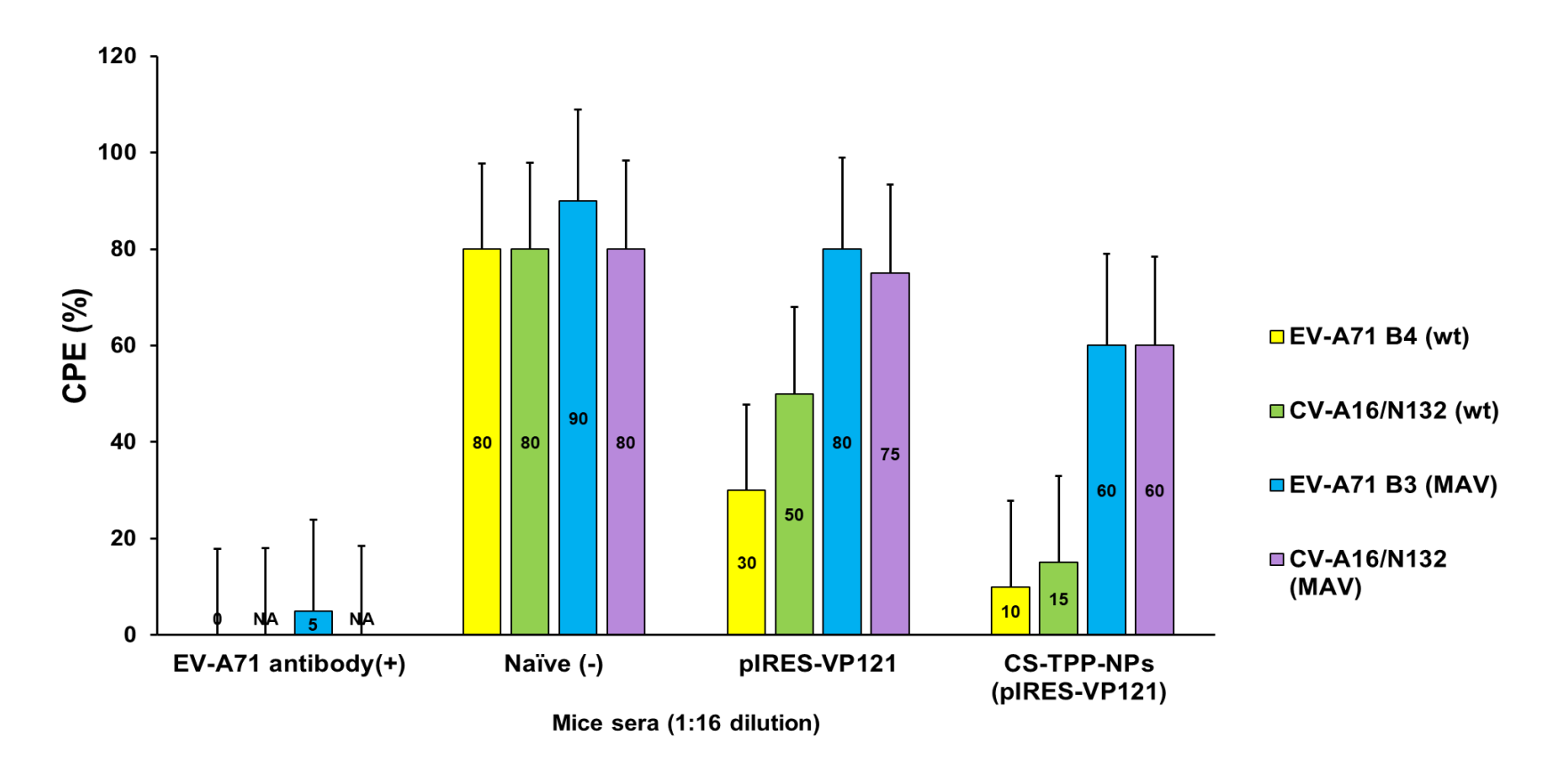


Figure 4.23: CPE present in RD cells post incubation with murine sera (1:16) derived from mice immunized with 3 doses of naked pIRES-VP121, CS-TPP-NPs (pIRES-VP121) and infected with an equal amount of wild-type EV-A71, CV-A16 and mouse adapted EV-A71, CV-A16 enteroviruses. Naïve murine sera and EV-A71 monoclonal antibodies incubated with an equal volume of wild-type and mouse adapted EV-A71, CV-A16 enteroviruses served as the positive and negative controls, respectively. Neutralizing assay was carried out in triplicates for each sample, data was presented as mean ± SD and error bar indicates the standard deviation. * NA= not tested.

4.13 Molecular analysis of wild type and mouse adapted EV-A71, CV-A16

The VP1 regions of EV-A71 and CV-A16 and VP2 region of EV-A71 was aligned using clustal omega followed by snapgene software (version 7.0) to investigate the nucleotide and amino acid differences between both wild type and mouse adapted enteroviruses (Goujon et al., 2010). Genome alignment of EV-A71 B4 (wild-type) and EV-A71 B3 (MAV) revealed a total of 57 nucleotide differences in the VP1 region and 37 nucleotide differences in VP2 region, respectively. Protein alignment of EV-A71 VP1 region revealed a total of 3 amino acid differences at residue 145 (Q-E), 147 (F-E) and 292 (T-K), respectively (Fig. 4.24A). A single amino acid residue change was identified at position 149 (K-I) in alignment results between the wild-type EV-A71 B4 and MAV EV-A71 B3 VP2 protein (Fig. 4.24B). There was a single nucleotide change identified in genome alignment of wild type and MAV CV-A16/N132 VP1 DNA sequences (Fig. 4.24C). However, there were no amino acid change discovered at the VP1 region of both CV-A16/N132 enteroviruses.

| Α | EV-A71 B4 (wild-type) | RKVELFTYMRFDAEFTFVACTPTGQVFPQLLQYMFVPPGAPKPESRESLAWQTATNPSVF | 180 |
|---|-------------------------|---|------------|
| | EV-A71 B3 (MAV) | RKVELFTYMRFDAEFTFVACTPTGEVVPQLLQYMFVPPGAPKPESRESLAWQTATNPSVF * * | 180 |
| | EV-A71 B4 (wild-type) | SKSKYPLVVRIYMRMKHVRAWIPRPMRNQNYLFKANPNYAGNSIKPTGTSRTAITTL | 297 |
| | EV-A71 B3 (MAV) | SKSKYPLVVRIYMRMKHVRAWIPRPMRNQNYLFKANPNYAGNSIKPTGTSRKAITTL * | 297 |
| В | | ALLVAILPEYVIGTVAGGTGTEDSHPPYKQTQPGADGFELQHPYVLDAGIPISQLTVCPH ALLVAILPEYVIGTVAGGTGTEDSHPPYIQTQPGADGFELQHPYVLDAGIPISQLTVCPH * | 180 180 |
| С | CV-A16/N132 (wild-type) | GGGGATCCCATCGCAGACATGATCGACCAGACCGTGAACAATCAAGTGAATCGCTCCTTA | 60 |
| | CV-A16/N132 (MAV) | GGGGATCCCATCGCAGACATGATCGACCAGACTGTGAACAATCAAGTGAATCGCTCCTTA * | 60 |

Figure 4.24: A) VP1 protein alignment between EV-A71 B4 (wild-type) and EV-A71 B3 (MAV) revealed a total of 3 amino acid differences at position 145 (Q-E), 147 (F-E) and 292 (T-K), respectively. B) VP2 protein alignment between EV-A71 B4 (wild-type) and EV-A71 B3 (MAV) revealed single amino acid difference at position 149 (K-I). C) VP1 genome alignment between CV-A16 N132 (wild-type) and CV-A16 N132 (MAV) revealed single nucleotide change at position 33 (C-T).

CHAPTER 5 DISCUSSION

Hand foot and mouth disease has been a global plague since the 1990s in Asia pacific region. Currently, the monovalent inactivated vaccine commercially available in China was not able to protect against the other enteroviruses serotypes and cross EV-A71 genotype protection were not evaluated as well. The only HFMD pDNA vaccine study published was by Tung et al.(2007) experimenting with a monovalent EV-A71 plasmid vaccine candidate that was able to neutralize against homologous EV-A71 B4 live virus (Tung et al., 2007). Therefore, our design of trivalent plasmid HFMD vaccine candidate would lay down the foundation for future design of multivalent HFMD DNA vaccine.

Upon internalization, DNA vaccines would be transcripted into mRNA in the nucleus and later transferred to the cytoplasm for translation into protein (Bai et al., 2017). Eukaryotic mRNAs translation to protein were mainly initiated through a cap-dependent manner as ribosome would bind to the 5' cap of genome (Cooper & Hausman, 2000). However, specific internal ribosome entry site (IRES) sequences were discovered to be able to direct the internal binding of 40s ribosomal subunits to downstream AUG start codon thereby initiating the translation process in a cap-independent manner (Ambrosini et al., 2021). IRES sequence was first discovered in the noncoding region (5' UTR) of poliovirus followed by (picornavirus) encephalomyocarditis virus (EMCV) mRNA (Pelletier & Sonenberg, 1988; Jang & Wimmer, 1990). To date, poliovirus and EMCV derived IRES elements were commonly used in commercial and experimental construction of polycistronic vectors for expression of heterologous proteins, gene transfer or gene therapy (Hennecke et al., 2001; Bochkov & Palmenberg, 2006).

It is observed that the protein lysates of transfected 293T cells successfully cross reacted with EV-A71 VP2 antibody and His-tag antibody (CV-A16 VP1 detection) producing a ~28kDa and ~35 kDa band respectively. However, the relative band intensities of both blots were observed to be significantly weaker in comparison to the band detected on the

EV-A71 VP1 blot despite the same concentration of pDNA (10μg) was used in transfection and same amount of protein lysates were loaded during SDS gel electrophoresis. The pIRES-VP121 tricistronic vaccine candidate was designed with two IRES sequences (IRES1 and IRES2) that were almost identical, both derived from a pTrident vector and alignment with NCBI BLAST database showed >90% homology with human poliovirus 1 (Fussenegger et al., 1998; Lee et al., 2020). The reduced expression of recombinant protein translated through mediation of IRES elements in comparison to protein expressed by cap dependent translation were well recorded in previous studies. Lower translation efficiency (~3 fold) was reported in a second cistron translated by poliovirus derived IRES sequence when compared to cap dependent translation (Dirks et al., 1994). Another study also reported 3-to-10-fold lower cytokine protein expression by the second poliovirus IRES dependent cistron in a bicistronic setting, in contrast to monocistronic translation of same gene (Hennecke et al., 2001). The concentration of EV-A71 VP2 and CV-A16 VP1 recombinant proteins could be lower in comparison with the EV-A71 VP1 protein expressed by cap dependent mechanism.

Due to its biodegradable, biocompatible and non-toxic nature, chitosan derivatives have been widely utilized in the drug formulation and pharmaceutical industry (Boroumand et al., 2021). Chitosan was known to enhance the penetration of loaded drugs and improve intracellular uptake by opening of tight intercellular junctions (van der Lubben et al., 2001; Wang et al., 2017). Chitosan is capable of transmucosal delivery such as oral or nasal administration routes due to its mucoadhesive properties (Watts et al., 2014; TM et al., 2018). The mucoadhesive nature of chitosan also allowed prolonged adhesion or contact time with bloodstream capillaries, thereby improving the uptake of plasmid vaccine or antigenic proteins (Gupta et al., 2006).

The indirect encapsulation efficiency of Chitosan TPP nanoparticles was observed to have a \sim 20% increment when the pDNA concentration was increased from 50 μ g to 100 μ g. The

same trend was observed in a previous study where increasing the pDNA concentration leads to higher encapsulation efficiency of chitosan TPP nanoparticles (Nunes et al., 2021). Chitosan TPP nanoparticles encapsulating 100µg of recombinant pDNA were visualized with a spherical morphology and an average diameter of ~190nm. Oval and spherical shaped nanoparticles at sub 200nm were described in several literatures to be ideal for transfection or cellular uptake in comparison with rod shaped nanoparticles (Chithrani et al., 2006; Zhang et al., 2008). However, the SEM images displayed a few Chitosan NPs to be of larger size while having a longer, uneven structure and clustering between NPs were also observed. This occurrence could be due to agglomeration of chitosan-TPP NPs during formulation or after dilution in ddH₂O (pH of system: 6.5~7) for better visualization under SEM. Chitosan had a pKa of 6.3 and is therefore easily soluble in low pH environment while being insoluble in basic environment. Selfaggregation of chitosan was also reported at pH of 6.0-6.5 in several publications (Kumar et al., 2004; Othman et al., 2018). This phenomenon was further supported by previous study stating physiological or slightly alkaline pH environment being able to disrupt the colloidal stability of chitosan/TPP NPs due to chitosan's pH-dependent nature (Cai et al., 2020). Clustering between CS-TPP NPs into macroscopic aggregates during the formulation process would be attributed to the crosslinker TPP which is a flocculating agent that promotes the aggregation between particles (Masarudin et al., 2015; Huang & Lapitsky, 2017).

There was also an increase in the size of NPs upon addition of pDNA which was expected and reported in a previous study (Nunes et al., 2022). The CS-TPP-NPs (pIRES-VP121) (100µg pDNA) had a PDI value of ~0.14 indicating the chitosan TPP nanoparticles population to be highly monodisperse. In common practice of polymer-based nanoparticles, PDI values of 0.2 and below were deemed as generally acceptable (Clarke, 2013). Chitosan nanoparticles with low PDI value were described with higher stability while high PDI nanoparticles would have lower stability (Masarudin et al., 2015). In this

study, majority of the chitosan TPP nanoparticles encapsulating pDNA formulated through ionic gelation method were uniform in size with only a small fraction of the nanoparticles being agglomerated.

High zeta potential values indicated stability of the nanosuspension due to repulsion of similar electrostatic charges created between nanoparticles, aggregation and formation of precipitates would then be minimal (Hallaj-Nezhadi et al., 2011; Nunes et al., 2022). Generally, suspensions of nanoparticles with pronounced zeta potential either above +10mV or below -10mV were reported to have good stability (Al-nemrawi et al., 2018). Chitosan TPP nanoparticles in this work were all cationic holding similar charges between +10.5 to +15 mV, indicating the stability of nanosuspension. As expected, chitosan TPP NPs surface zeta potential value decreased upon addition of pDNA. The global negative charge of nanosuspension could increase due to the anionic phosphate backbone of pDNA (Iswanti et al., 2019; Ma et al., 2019); non-encapsulated free pDNA could also adhere to the surface of already formed chitosan TPP NPs during ionic gelation. Increased concentration of DNA encapsulated was also reported to reduce zeta potential of chitosan NPs suspension system previously (Hallaj-Nezhadi et al., 2011). The positive charges of chitosan were reported to facilitate the increment of paracellular permeability and reduction of trans-epithelial electrical resistance of cell monolayers upon adherence to cell membrane (Bowman & Leong, 2006; Guadarrama-Escobar et al., 2023). Efficient gene delivery would be achieved as intracellular uptake was improved by electrostatic attraction between positively charged chitosan TPP nanoparticles and the anionic cell membrane (Hallaj-Nezhadi et al., 2011; Valente et al., 2021).

Chitosan TPP NPs in this study successfully mediated the internalization and expression of plasmid pIRES-VP121 in murine macrophage J774A.1 cells and the strongest expression of fluorescence signal was observed at 72h post transfection. Plasmid/chitosan complex have been reported in multiple studies with lower transfection level when compared with commercially available plasmid carriers including lipofectamine and PEI

(MacLaughlin et al., 1998; Hashimoto et al., 2006; Fernández Fernández et al., 2016). Therefore, the transfection of CS-TPP-NPs (pIRES-VP121) took inspiration from a previous study reporting ~42% of cells being transfected and protein expression higher than lipofectamine (Nimesh et al., 2010). The author reported that optimal cellular uptake and gene expression was achieved through transfection media at pH 6.5 (10% serum), followed by replacement of pH 7.4 media (10% serum) at 8,12 or 24h post transfection. Similar studies by Sato et al.(2001) and Zhao et al.(2006) both reported higher transfection or expression levels of chitosan-DNA complexes at a slightly acidic environment (pH 6.8~7.0) as opposed to transfection medium with higher pH (pH 7.4~7.6) (Sato et al., 2001; Zhao et al., 2006).

Due to the pKa of chitosan being ~6.5, transfection media at a more acidic pH would lead to higher degree of chitosan protonation thereby promoting the adherence to anionic cell surface and plasmid DNA (Anthonsen & Smidsrød, 1995; Filion et al., 2007; Nimesh et al., 2010). In contrast, the zeta potential of chitosan/DNA nanosuspension were reported to decrease at a more basic pH due to amine group neutralization (Ishii et al., 2001; Mao et al., 2001; Lavertu et al., 2006). Additionally, TPP being buffered in a high pH environment with less positive (H+) ions would be more cross-reactive thereby promoting self-aggregation between chitosan-TPP NPs which leads to size increment and reduced cellular uptake (Masarudin et al., 2015). Nimesh et al. (2010) also stated that replacement of media to pH 7.4 after 8,12 or 24h post transfection with pH6.5 media would allow the cells to return to their metabolically active state for efficient processing of internalized chitosan/DNA complex (Nimesh et al., 2010). Reduced cell viability and cell metabolism at slightly lower pH environment were previously reported in multiple studies (Sauer et al., 2000; Nimesh et al., 2010; Kang et al., 2012).

However, CS-TPP-NPs (pIRES-VP121) in this study failed to exhibit stronger GFP expression in comparison to the Xfect[™] Transfection Reagent (TAKARA Bio, USA). Aside from the pH environment, transfection efficiency of chitosan-plasmid complex was

also highly dependent on the NPs size and cell line (Aibani et al., 2021). A previous study shown that dendritic cells and RAW 264.7 macrophage favoured the uptake of 1μm chitosan nanoparticles in comparison to smaller sized (300nm) and larger sized (3 μm) NPs (Koppolu & Zaharoff, 2013). There was no significant fluorescent signal being observed in J774A.1 cells at 24h post transfection (unpublished image) and maximum GFP expression was observed at 72h post transfection instead of 48h. A possible explanation was that the chitosan we used had a higher molecular weight (MW) (50-190 kDa) in comparison with Nimesh et.al (2010) (10 kDa). In general, chitosan with high MW would have higher stability and slow degradation in vivo was well recorded (Nakamura, 1992; Mucha & Pawlak, 2002).

Generally, cationic polymers were found with the highest cytotoxicity followed by polymers with neutral or negative charges (Jevprasesphant et al., 2003; McConnell et al., 2016). Cationic polymers would undergo strong electrostatic attraction with anionic plasma membrane proteins, triggering the disruption of cell membrane integrity and eventually cell membrane rupture (Fischer et al., 2003). Size-dependent cytotoxicity of NPs were more profound at lower ranged-size below 100nm due to their relatively higher surface area to volume ratio (Sahu et al., 2016; Moraru et al., 2020). Smaller sized-NPs were able to be taken up easily in large quantities, thereby inducing higher secretion of hydrolytic enzymes and reactive oxygen species (ROS) as part of the cellular mechanism in removing foreign substances. Prolonged ROS production would trigger chronic inflammation and oxidative stress leading to cell death (Huang et al., 2017; Moraru et al., 2020). Several studies have shown ultrafine NPs (<100nm) to induce higher levels of ROS in comparison to their larger NPs counterpart (Stone et al., 1998; Wilson et al., 2002; Sioutas et al., 2005). A review by Frigaard et al. (2022) compiled the findings of 25 articles investigating the ex-vivo (4), in-vivo (1) and in-vitro (20) cytotoxicity of chitosan-TPP nanoparticles (Frigaard et al., 2022). More than 80% cell viability was reported by 24 papers evaluating the in vitro cytotoxicity of chitosan TPP nanoparticles with

concentrations and size over the range of 0.01-10,000 µg/ml and 126-1000nm, respectively. The only study with low cell viability was reported by Ye et al. (2013), Calu-6 cells were incubated with 250 and 500 µg/ml of freeze-dried chitosan TPP nanoparticles for 24h (Ye et al., 2013). The explanation given was due to the anti-tumor apoptosis induced by chitosan as calu-6 was derived from lung cancer cell line (Qi & Xu, 2006; Abedian et al., 2019). As expected, our chitosan-TPP NPs encapsulating pDNA with spherical morphology at ~190nm while being mildly cationic (+10 mV) was found to be non-cytotoxic when tested against murine macrophage cell line J774A.1 for up to 48h. Nunes et. al (2022) have reported similar findings where chitosan-TPP NPs at <180nm carrying zeta of ~+20mV did not exhibit cytotoxicity in RAW macrophage cells (Nunes et al., 2022) Additionally, CS-TPP-NPs complexes and chitosan polymer in this study were found to be non-hemolytic upon incubation in ICR mice red blood cells.

Our study attempt to mimic the physiological challenges including DNase I, chitosanase and lysozyme that were faced by CS-TPP-NPs (pIRES-VP121) (100µg pDNA) upon intramuscular administration in murine models. Degradation of DNA in blood was well established and multiple authors have reported a higher yield of circulating DNA in cancer patients with lower blood DNase activity (Herriott et al., 1961; Tamkovich et al., 2006; Cherepanova et al., 2008). Deoxyribonuclease I (DNAse I) is the most prominent nuclease present in blood and its components including the plasma and serum. DNase I is responsible for the nucleolysis of extracellular DNA circulating in the serum, which were mainly derived from blood cells and tissues that underwent necrosis, apoptosis, or during the formation of neutrophils extracellular traps (NETosis) (Hartmann, 2017; Lauková et al., 2020). Chitosan was known to be degraded in vivo mainly by a non-specific protease-lysozyme that was present within leucocytes and lysosomes (Lončarević et al., 2017; Ferraboschi et al., 2021). Chitosanase, glucosidase, proteases and colonic bacterial enzymes were also able to break down chitosan in human body (Shukla et al., 2022). The transportation of chitosan particles across cell membrane were

mainly mediated through an active endocytosis mechanism involving two different pathways (phagocytosis and pinocytosis) (Foroozandeh & Aziz, 2018; Aibani et al., 2021). If taken up by macrophage or dendritic cells, both uptake pathways would lead to delivery of cargo to lysosome for digestion and processing of antigens for presentation (Hipolito et al., 2018). Previous studies have reported the protective capabilities of chitosan-DNA complexes at preventing DNase I degradation in vitro (Tan et al., 2009; Tu et al., 2013). As expected, CS-TPP-NPs (pIRES-VP121) were able to protect the encapsulated plasmid DNA from cleavage of DNase I. Chitosan degradation with chitosanase and lysozyme further revealed an intact DNA band on agarose gel.

Flow cytometry data in this study showed a dose dependent relationship as the concentration of naked pDNA increased from 50μg to 100μg, the frequency of IFN-γ secreting CD4+ and CD8 T cells also increased. The highest population of IFN-γ secreting CD4+ and CD8+T cells was observed in mice immunized with three dosages of CS-TPP-NPs (pIRES-VP121) (100μg pDNA). A previous study reported similar results where cytokine (IFN-γ) expressing CD4+ and CD8+T cells population was the highest in groups vaccinated with antigens coupled with chitosan compared to mice receiving antigens alone (Highton et al., 2016). Chitosan-TPP nanoparticles encapsulating OVA also resulted in the highest number of IFN-γ expressing CD8+T cells in comparison to antigens alone (Han et al., 2016).

A dose dependent relationship was also observed between the IFN- γ secreted by splenocytes and the naked pDNA concentration used in vaccination. Mice groups vaccinated with three dosages of 100 μ g naked pDNA also expressed higher IFN- γ levels in comparison to mice vaccinated with two dosages of 100 μ g naked pDNA. However, IFN- γ secretion by splenocytes of mice vaccinated with three dosages of CS-TPP-NPs (pIRES-VP121) had increment up to ~15 fold over the second highest group which received three dosages of naked pDNA (100 μ g). A study by Heffernan et al. (2011) reported a 9-10-fold increment of IFN- γ secretion in splenocytes of mice receiving

antigens coupled with chitosan solutions and IL-12 (Heffernan et al., 2011). The significant increment of IFN- γ levels in vaccinated groups receiving three dosages of CS-TPP-NPs(pIRES-VP121) was inconsistent with flow cytometry results that only observed a gradual increase of IFN- γ secreting CD4+ and CD8+ T cells in comparison to the other vaccinated groups. The secretion of interferon-gamma (IFN- γ) was mainly by activated lymphocytes including the CD4+ T helper cells and CD8+ cytotoxic T cells, natural killer (NK) cells and $\gamma\delta$ T cells (Corthay et al., 2005; Ribot et al., 2009; Keppel et al., 2015; Castro et al., 2018). In addition, B cells, natural killer T cells and antigen-presenting cells (APCs) were also able to secrete IFN- γ but at a lesser extent (Darwich et al., 2009; Bao et al., 2014). Therefore, the 15-fold increment of IFN- γ concentration detected in ELISA assay post immunization with CS-TPP-NPs (pIRES-VP121) (100 μ g pDNA) was due to ELISA kit quantifying the total concentration in murine splenocytes. In contrast, flow cytometry was quantifying the percentage of IFN- γ expressing CD4+ and CD8+ T lymphocytes. Therefore, ELISA results in this study were directly correlated with data obtained from flow cytometry.

Neutralizing data shown that serum (1:16) derived from immunization with naked pIRES-VP121, and CS-TPP-NPs(pIRES-VP121) were able to inhibit CPE manifestations upon wild-type EV-A71 B4 infection. Serum at 1:2, 1:4 and 1:8 dilution was causing poor cell growth and cell death possibly due to high serum concentration. Tung et al. (2007) reported similar results where serum at 1:2 and 1:4 dilutions were causing cell death without CPE (Tung et al., 2007). Extremely high or low serum concentration have been reported to inhibit cell proliferation previously (M. Liu et al., 2011).

However, serum of mice vaccinated with naked pDNA, and chitosan NPs encapsulated pDNA failed to exhibit neutralization effects against the mouse adapted strain of EV-A71 B3. A possible explanation might be that the mouse adapted EV-A71 B3 was more virulent in comparison with the wild-type EV-A71 B4. Previously, Ong et al. (2010) carried out a formaldehyde whole-virus inactivated vaccine (IV) study, wild-type EV-

A71 B4, wild-type EV-A71 B3 and its mouse adapted counterpart were designed into 3 different IV (MAV) (Ong et al., 2010). Mice sera post immunization with the 3 IVs were tested against clinical isolates of EV-A71 sub-genotype B3, B4, C1, C2, C3, C4 and C5. Sera of mice immunized with IVs derived from wild-type EV-A71 B3 and B4 displayed neutralizing titers of 1:32 against infection with wild-type EV-A71 B4 virus, both antisera was ineffective against EV-A71 sub-genotype C1-C5. In contrast, antisera generated from vaccination with EV-A71 B3 (MAV) IV not only displayed significantly higher neutralizing titers of 1:512 against EV-A71 genotype B3 and B4 but was able to cross-neutralize against all EV-A71 sub-genotypes C1-C5. Therefore, genome and protein alignments of the VP1 and VP2 regions were carried out to identify possible nucleotide or amino acid differences that would contribute to the stronger immunogenicity of EV-A71 B3 MAV virus.

Amino acid residue 145 of VP1 capsid protein (VP1-145) of EV-A71 was identified to be important for antigenic phenotyping and determination as it is in close contact with SCARB2 and PSGL-1 receptor binding amino acid residues (Huang et al., 2015). Human scavenger receptor B2 (hSCARB2) was established as the most important receptor for infection of all EV-A71 enterovirus strains (Hu et al., 2023). hSCARB2 mediates the virion attachment to cell surface, followed by internalization and uncoating of the virion (Fujii et al., 2018). PSGL-1 is also a key EV-A71 receptors that was involved in attachment but not the uncoating process (Yamayoshi et al., 2013). PSGL-1 is important for the neurologic and pulmonary invasion of EV-A71 as PSGL-1 was only found on immune cells including dendritic, lymphoid, and myeloid cells (Zarbock et al., 2009; Gu et al., 2017). Substitutions of VP1-145Q/G to E have been an implication of mouse-adapted virulence as multiple studies have reported VP1-145E to be more virulent in neonatal murine models (Wang et al., 2004; Chua et al., 2008; Wang et al., 2011; Huang et al., 2012; Zaini & McMinn, 2012). VP1-Q145E have been reported by Huang et al.

(2012) to enhance viral binding to murine neuroblast cells. The author also reported a combination of two mutations between VP1-145E and VP2-K149M which enhanced the accumulation of viral RNA leading to increased viral cytotoxicity with in vivo mouse lethality (Huang et al., 2012). VP1-Q145E mutation was also found to be able to reduce the antiviral efficacy of Suramin by ~30 fold (Ren et al., 2017). Suramin is an FDAapproved medication for parasites that could inhibit the viral entry of EV-A71 (Ren et al., 2014). Suramin have shown promising results in mice and monkey models with reduced mortality rate upon challenged with lethal strains of EV-A71 (Ren et al., 2017). VP1-145E was also responsible for viremia coupled with neuropathogenesis development in a non-human primate model (Kataoka et al., 2015). In vitro neutralization assay had revealed VP1-145E EV-A71 to be relatively resistant to two polyclonal EV-A71 neutralizing antibodies in comparison with VP1-145G EV-A71 virus (Fujii et al., 2018). VP2-149 residue is positioned at an established cross-sub-genotype linear neutralizing epitope VP2-28 (136-150aa) which is highly conserved (C. C. Liu et al., 2011). VP2-28 was also speculated to form a potential receptor binding site (C. C. Liu et al., 2011; Zaini et al., 2012; Fujii et al., 2013). VP2-K149I hydrophobic isoleucine mutation was reported to be responsible for enhanced virulence of EV-A71 in neonatal mice by Wang et al. (2004) and Chua et al. (2008) (Wang et al., 2004; Chua et al., 2008). This VP2-149I EV-A71 mutant virus could be circulating in humans at a low frequency as it has been isolated from human samples previously without adaptation in mice (Xu et al., 2017). Chua et al. (2008) have also reported enhanced viral replication in CHO cells due to VP2-149I mutation (Chua et al., 2008). Artificial introduction of VP2- K149I mutation in EV-A71 C4 enterovirus transformed the avirulent strain to be highly virulent in 14-day old mice (Xu et al., 2017). Xu et al. (2017) also speculated that the VP2-K149I mutation being located at VP2-28 could have improved the binding with murine PSGL-1 transmembrane receptor thereby improving the cross-species transmission of EV-A71.

Antisera of mice (1:16) immunized with naked pDNA alone or CS-TPP-NPs (pIRES-VP121) exhibited neutralizing effects against the wild-type CV-A16/N132 enterovirus but not against its MAV counterpart. Protein alignment revealed the VP1 amino acid sequence of wild-type and MAV strain of CV-A16/N132 to be identical. However, it is possible that there were nucleotide or amino acid mutations on the other capsid proteins (VP2-VP4) which could have contributed to enhanced virulence. Therefore, the exact reason of pIRES-VP121 and CS-TPP-NPs(pIRES-VP121) vaccination being able to neutralize the wild-type CV-A16/N132 but not its MAV counterpart remained elusive.

CHAPTER 6 CONCLUSION

Recombinant plasmid pIRES-VP121 in this study was able to express viral capsid proteins by all 3 genes at a sufficient concentration in mammalian 293T cells. Chitosan nanoparticles was deployed as a self-adjuvanting nanocarrier for the trivalent pDNA due to it being non-toxic and biodegradable. Ionotropic gelation deployed in this study successfully generated chitosan TPP nanoparticles encapsulating the trivalent recombinant plasmid at sub 200nm, which was non-cytotoxic, non-hemolytic and capable of transfecting murine macrophage in vitro. Chitosan encapsulation of the plasmid pIRES-VP121 prevented plasmid degradation by DNase I in vitro. CS-TPP-NPs (pIRES-VP121) as a candidate vaccine displayed the strongest cellular immune response in vivo in comparison with naked pIRES-VP121 alone. Neutralizing results of antisera of mice vaccinated with CS-TPP-NPs (pIRES-VP121) displayed the highest neutralization efficacy in comparison with naked pDNA against wild-type EV-A71 and CV-A16 enteroviruses. However, sera derived from CS-TPP-NPs (pIRES-VP121) and naked pIRES-VP121 mice immunization did not exhibit cross-neutralization against the mouse-

adapted strains of EV-A71 and CV-A16. Sequence alignments revealed several nucleotide and amino acid differences/mutations between the wild-type and mouse adapted strains of EV-A71 and CV-A16. These differences could have contributed to the increased virulence of mouse-adapted strains of enteroviruses alone or in combination with other unknown factors which would require further investigation. Overall, the CS-TPP-NPs (pIRES-VP121) could serve as a useful prototype for future development of a multivalent HFMD plasmid vaccine with stronger cross-reactive immunogenicity.

CHAPTER 7 BIBLIOGRAPHICAL REFERENCES

- Abedian, Z., Moghadamnia, A. A., Zabihi, E., Pourbagher, R., Ghasemi, M., Nouri, H. R., . . . Jenabian, N. (2019). Anticancer properties of chitosan against osteosarcoma, breast cancer and cervical cancer cell lines. *Caspian J Intern Med*, 10(4), 439-446. https://doi.org/10.22088/cjim.10.4.439
- Aderibigbe, B. A., & Naki, T. (2019). Chitosan-Based Nanocarriers for Nose to Brain Delivery. Applied Sciences, 9(11).
- Aibani, N., Rai, R., Patel, P., Cuddihy, G., & Wasan, E. K. (2021). Chitosan Nanoparticles at the Biological Interface: Implications for Drug Delivery. *Pharmaceutics*, 13(10). https://doi.org/10.3390/pharmaceutics13101686
- Al-Allaf, F. A., Abduljaleel, Z., Athar, M., Taher, M. M., Khan, W., Mehmet, H., . . . Bouazzaoui, A. (2019). Modifying inter-cistronic sequence significantly enhances IRES dependent second gene expression in bicistronic vector: Construction of optimised cassette for gene therapy of familial hypercholesterolemia. *Noncoding RNA Res*, 4(1), 1-14. https://doi.org/10.1016/j.ncrna.2018.11.005
- Al-nemrawi, N., Alsharif, S., & Dave, R. (2018). Preparation of chitosan-tpp nanoparticles: The influence of chitosan polymeric properties and formulation variables. *International Journal of Applied Pharmaceutics*, 10, 60. https://doi.org/10.22159/ijap.2018v10i5.26375
- Alving, C. R. (2002). Design and selection of vaccine adjuvants: animal models and human trials. Vaccine, 20 Suppl 3, S56-64. https://doi.org/10.1016/s0264-410x(02)00174-3
- Ambrosini, C., Garilli, F., Quattrone, A. J. P. i. M. B., & Science, T. (2021). Reprogramming translation for gene therapy. In *Curing Genetic Diseases Through Genome Reprogramming* (Vol. 182, pp. 439-476).
- Anasir, M. I., & Poh, C. L. (2019). Advances in Antigenic Peptide-Based Vaccine and Neutralizing Antibodies against Viruses Causing Hand, Foot, and Mouth Disease. *Int J Mol Sci*, 20(6). https://doi.org/10.3390/ijms20061256
- Ang, L. W., Koh, B. K., Chan, K. P., Chua, L. T., James, L., & Goh, K. T. (2009). Epidemiology and control of hand, foot and mouth disease in Singapore, 2001-2007. *Ann Acad Med Singap*, 38(2), 106-112.
- Ang, L. W., Tay, J., Phoon, M. C., Hsu, J. P., Cutter, J., James, L., . . . Chow, V. T. (2015). Seroepidemiology of Coxsackievirus A6, Coxsackievirus A16, and Enterovirus 71 Infections among Children and Adolescents in Singapore, 2008-2010. PLoS One, 10(5), e0127999. https://doi.org/10.1371/journal.pone.0127999
- Anthonsen, M. W., & Smidsrød, O. (1995). Hydrogen ion titration of chitosans with varying degrees of N-acetylation by monitoring induced 1H-NMR chemical shifts. *Carbohydr Polym*, 26(4), 303-305. https://doi.org/https://doi.org/10.1016/0144-8617(95)00010-5
- Arita, M., Nagata, N., Iwata, N., Ami, Y., Suzaki, Y., Mizuta, K., . . . Shimizu, H. (2007). An attenuated strain of enterovirus 71 belonging to genotype a showed a broad spectrum of antigenicity with attenuated neurovirulence in cynomolgus monkeys. *J Virol*, *81*(17), 9386-9395. https://doi.org/10.1128/jvi.02856-06
- Arita, M., Shimizu, H., Nagata, N., Ami, Y., Suzaki, Y., Sata, T., . . . Miyamura, T. (2005). Temperature-sensitive mutants of enterovirus 71 show attenuation in cynomolgus monkeys. *J Gen Virol*, 86(Pt 5), 1391-1401. https://doi.org/10.1099/vir.0.80784-0
- Aswathyraj, S., Arunkumar, G., Alidjinou, E. K., & Hober, D. (2016). Hand, foot and mouth disease (HFMD): emerging epidemiology and the need for a vaccine strategy. *Med Microbiol Immunol*, 205(5), 397-407. https://doi.org/10.1007/s00430-016-0465-y
- Aw-Yong, K. L., Sam, I. C., Koh, M. T., & Chan, Y. F. (2016). Immunodominant IgM and IgG Epitopes Recognized by Antibodies Induced in Enterovirus A71-Associated Hand, Foot and Mouth Disease Patients. *PLoS One*, *11*(11), e0165659. https://doi.org/10.1371/journal.pone.0165659

- Bai, H., Lester, G. M. S., Petishnok, L. C., & Dean, D. A. (2017). Cytoplasmic transport and nuclear import of plasmid DNA. *Biosci Rep*, 37(6). https://doi.org/10.1042/bsr20160616
- Bande, F., Arshad, S. S., Bejo, M. H., Omar, A. R., Moeini, H., Khadkodaei, S., . . . Anka, I. A. (2020). Development and immunogenic potentials of chitosan-saponin encapsulated DNA vaccine against avian infectious bronchitis coronavirus. *Microb Pathog*, *149*, 104560. https://doi.org/10.1016/j.micpath.2020.104560
- Bao, Y., Liu, X., Han, C., Xu, S., Xie, B., Zhang, Q., . . . Cao, X. (2014). Identification of IFN-γ-producing innate B cells. *Cell Res*, 24(2), 161-176. https://doi.org/10.1038/cr.2013.155
- Barinov, A., Galgano, A., Krenn, G., Tanchot, C., Vasseur, F., & Rocha, B. (2017). CD4/CD8/Dendritic cell complexes in the spleen: CD8+ T cells can directly bind CD4+ T cells and modulate their response. *PLoS One*, *12*(7), e0180644. https://doi.org/10.1371/journal.pone.0180644
- Bochkov, Y. A., & Palmenberg, A. C. (2006). Translational efficiency of EMCV IRES in bicistronic vectors is dependent upon IRES sequence and gene location. *Biotechniques*, *41*(3), 283-284, 286, 288 passim. https://doi.org/10.2144/000112243
- Borman, A. M., Le Mercier, P., Girard, M., & Kean, K. M. (1997). Comparison of picornaviral IRES-driven internal initiation of translation in cultured cells of different origins. *Nucleic Acids Res*, 25(5), 925-932. https://doi.org/10.1093/nar/25.5.925
- Boroumand, H., Badie, F., Mazaheri, S., Seyedi, Z. S., Nahand, J. S., Nejati, M., . . . Mirzaei, H. (2021). Chitosan-Based Nanoparticles Against Viral Infections. *Front Cell Infect Microbiol*, 11, 643953. https://doi.org/10.3389/fcimb.2021.643953
- Bourgeois, C., Rocha, B., & Tanchot, C. (2002). A role for CD40 expression on CD8+ T cells in the generation of CD8+ T cell memory. *Science*, *297*(5589), 2060-2063. https://doi.org/10.1126/science.1072615
- Bowman, K., & Leong, K. W. (2006). Chitosan nanoparticles for oral drug and gene delivery. *Int J Nanomedicine*, 1(2), 117-128. https://doi.org/10.2147/nano.2006.1.2.117
- Brown, B. A., & Pallansch, M. A. (1995). Complete nucleotide sequence of enterovirus 71 is distinct from poliovirus. *Virus Res*, 39(2-3), 195-205. https://doi.org/10.1016/0168-1702(95)00087-9
- Cai, Y., Lapitsky, Y. J. C., & Biointerfaces, S. B. (2020). Biomolecular uptake effects on chitosan/tripolyphosphate micro-and nanoparticle stability. *193*, 111081.
- Cai, Y., Rodriguez, S., & Hebel, H. (2009). DNA vaccine manufacture: scale and quality. *Expert Rev Vaccines*, 8(9), 1277-1291. https://doi.org/10.1586/erv.09.84
- Caine, E. A., Fuchs, J., Das, S. C., Partidos, C. D., & Osorio, J. E. (2015). Efficacy of a Trivalent Hand, Foot, and Mouth Disease Vaccine against Enterovirus 71 and Coxsackieviruses A16 and A6 in Mice. *Viruses*, 7(11), 5919-5932. https://doi.org/10.3390/v7112916
- Cao, Y., Tan, Y. F., Wong, Y. S., Liew, M. W. J., & Venkatraman, S. (2019). Recent Advances in Chitosan-Based Carriers for Gene Delivery. *Mar Drugs*, *17*(6). https://doi.org/10.3390/md17060381
- Castro, F., Cardoso, A. P., Gonçalves, R. M., Serre, K., & Oliveira, M. J. (2018). Interferon-Gamma at the Crossroads of Tumor Immune Surveillance or Evasion. *Front Immunol*, *9*, 847. https://doi.org/10.3389/fimmu.2018.00847
- Chan, Y. F., Wee, K. L., Chiam, C. W., Khor, C. S., Chan, S. Y., Amalina, W. M., & Sam, I. C. (2012). Comparative genetic analysis of VP4, VP1 and 3D gene regions of enterovirus 71 and coxsackievirus A16 circulating in Malaysia between 1997-2008. *Trop Biomed*, 29(3), 451-466.
- Chang, P. C., Chen, S. C., & Chen, K. T. (2016). The Current Status of the Disease Caused by Enterovirus 71 Infections: Epidemiology, Pathogenesis, Molecular Epidemiology, and Vaccine Development. Int J Environ Res Public Health, 13(9). https://doi.org/10.3390/ijerph13090890
- Chen, L., Yang, H., Feng, Q. J., Yao, X. J., Zhang, H. L., Zhang, R. L., & He, Y. Q. (2015). Complete genome sequence of a coxsackievirus a16 strain, isolated from a fatal case in shenzhen,

- southern china, in 2014. *Genome Announc*, 3(2). https://doi.org/10.1128/genomeA.00391-15
- Cherepanova, A. V., Tamkovich, S. N., Bryzgunova, O. E., Vlassov, V. V., & Laktionov, P. P. (2008). Deoxyribonuclease activity and circulating DNA concentration in blood plasma of patients with prostate tumors. *Ann N Y Acad Sci*, 1137, 218-221. https://doi.org/10.1196/annals.1448.016
- Chithrani, B. D., Ghazani, A. A., & Chan, W. C. J. N. I. (2006). Determining the size and shape dependence of gold nanoparticle uptake into mammalian cells. *6*(4), 662-668.
- Chokephaibulkit, K., & Perng, G. C. (2013). Challenges for the formulation of a universal vaccine against dengue. *Exp Biol Med (Maywood)*, *238*(5), 566-578. https://doi.org/10.1177/1535370212473703
- Chong, P., Guo, M. S., Lin, F. H., Hsiao, K. N., Weng, S. Y., Chou, A. H., . . . Liu, C. C. (2012). Immunological and biochemical characterization of coxsackie virus A16 viral particles. *PLoS One*, *7*(11), e49973. https://doi.org/10.1371/journal.pone.0049973
- Chong, P., Hsieh, S. Y., Liu, C. C., Chou, A. H., Chang, J. Y., Wu, S. C., . . . Klein, M. (2012). Production of EV71 vaccine candidates. *Hum Vaccin Immunother*, 8(12), 1775-1783. https://doi.org/10.4161/hv.21739
- Chong, P., Liu, C. C., Chow, Y. H., Chou, A. H., & Klein, M. (2015). Review of enterovirus 71 vaccines. *Clin Infect Dis*, 60(5), 797-803. https://doi.org/10.1093/cid/ciu852
- Chong, P. C.-S., & Klein, M. (2018). 21 Enterovirus 71. In S. A. Plotkin, W. A. Orenstein, P. A. Offit, & K. M. Edwards (Eds.), *Plotkin's Vaccines (Seventh Edition)* (pp. 288-294.e283). Elsevier. https://doi.org/https://doi.org/10.1016/B978-0-323-35761-6.00021-3
- Chua, B. H., Phuektes, P., Sanders, S. A., Nicholls, P. K., & McMinn, P. C. (2008). The molecular basis of mouse adaptation by human enterovirus 71. *J Gen Virol*, 89(Pt 7), 1622-1632. https://doi.org/10.1099/vir.0.83676-0
- Chumakov, M., Voroshilova, M., Shindarov, L., Lavrova, I., Gracheva, L., Koroleva, G., . . . Rodin, V. (1979). Enterovirus 71 isolated from cases of epidemic poliomyelitis-like disease in Bulgaria. *Arch Virol*, 60(3-4), 329-340. https://doi.org/10.1007/bf01317504
- Clarke, S. P. (2013). Development of Hierarchical Magnetic Nanocomposite Materials for Biomedical Applications.
- Coban, C., Kobiyama, K., Aoshi, T., Takeshita, F., Horii, T., Akira, S., & Ishii, K. J. (2011). Novel strategies to improve DNA vaccine immunogenicity. *Curr Gene Ther*, *11*(6), 479-484. https://doi.org/10.2174/156652311798192815
- Coban, C., Kobiyama, K., Jounai, N., Tozuka, M., & Ishii, K. J. (2013). DNA vaccines: a simple DNA sensing matter? *Hum Vaccin Immunother*, *9*(10), 2216-2221. https://doi.org/10.4161/hv.25893
- Coller, B. A., & Clements, D. E. (2011). Dengue vaccines: progress and challenges. *Curr Opin Immunol*, 23(3), 391-398. https://doi.org/10.1016/j.coi.2011.03.005
- Cooper, G. M., & Hausman, R. J. T. C. n. e. S., MA: Sinauer Associates. (2000). The Cell: A Molecular Approach. 2nd edition. Sunderland (MA): Sinauer Associates; 2000. Translation of mRNA.
- Corthay, A., Skovseth, D. K., Lundin, K. U., Røsjø, E., Omholt, H., Hofgaard, P. O., . . . Bogen, B. (2005). Primary antitumor immune response mediated by CD4+ T cells. *Immunity*, 22(3), 371-383. https://doi.org/10.1016/j.immuni.2005.02.003
- Cullen, B. R., Lomedico, P. T., & Ju, G. (1984). Transcriptional interference in avian retroviruses-implications for the promoter insertion model of leukaemogenesis. *Nature*, *307*(5948), 241-245. https://doi.org/10.1038/307241a0
- Darwich, L., Coma, G., Peña, R., Bellido, R., Blanco, E. J., Este, J. A., . . . Bofill, M. (2009). Secretion of interferon-gamma by human macrophages demonstrated at the single-cell level after costimulation with interleukin (IL)-12 plus IL-18. *Immunology*, *126*(3), 386-393. https://doi.org/10.1111/j.1365-2567.2008.02905.x

- Dassarma, B., Tripathy, S., Chabalala, M., & Matsabisa, M. G. (2022). Challenges in Establishing Vaccine Induced Herd Immunity through Age Specific Community Vaccinations. *Aging Dis*, 13(1), 29-36. https://doi.org/10.14336/ad.2021.0611
- Deering, R. P., Kommareddy, S., Ulmer, J. B., Brito, L. A., & Geall, A. J. (2014). Nucleic acid vaccines: prospects for non-viral delivery of mRNA vaccines. *Expert Opin Drug Deliv*, 11(6), 885-899. https://doi.org/10.1517/17425247.2014.901308
- Dehghan, S., Tafaghodi, M., Bolourieh, T., Mazaheri, V., Torabi, A., Abnous, K., & Tavassoti Kheiri, M. (2014). Rabbit nasal immunization against influenza by dry-powder form of chitosan nanospheres encapsulated with influenza whole virus and adjuvants. *Int J Pharm*, 475(1-2), 1-8. https://doi.org/10.1016/j.ijpharm.2014.08.032
- den Haan, J. M., Arens, R., & van Zelm, M. C. (2014). The activation of the adaptive immune system: cross-talk between antigen-presenting cells, T cells and B cells. *Immunol Lett*, 162(2 Pt B), 103-112. https://doi.org/10.1016/j.imlet.2014.10.011
- Dirks, W., Mielke, C., Karreman, S., Haase, B., Wirth, M., Lindenmaier, W., & Hauser, H. (1994).

 Applications of Expression Vectors Containing Bicistronic Transcription Units in Mammalian Cells. In N. E. Fusenig & H. Graf, Cell Culture in Pharmaceutical Research Berlin, Heidelberg.
- Donnelly, J. J., Liu, M. A., & Ulmer, J. B. (2000). Antigen presentation and DNA vaccines. *Am J Respir Crit Care Med*, 162(4 Pt 2), S190-193. https://doi.org/10.1164/ajrccm.162.supplement3.15tac10
- Duffy, S. (2018). Why are RNA virus mutation rates so damn high? *PLoS Biol*, *16*(8), e3000003. https://doi.org/10.1371/journal.pbio.3000003
- Elieh-Ali-Komi, D., & Hamblin, M. R. (2016). Chitin and Chitosan: Production and Application of Versatile Biomedical Nanomaterials. *Int J Adv Res (Indore)*, 4(3), 411-427.
- Emerman, M., & Temin, H. M. (1984). Genes with promoters in retrovirus vectors can be independently suppressed by an epigenetic mechanism. *Cell*, *39*(3 Pt 2), 449-467.
- Emerman, M., & Temin, H. M. (1986). Quantitative analysis of gene suppression in integrated retrovirus vectors. *Mol Cell Biol*, *6*(3), 792-800. https://doi.org/10.1128/mcb.6.3.792-800.1986
- Eyckmans, T., Wollants, E., Janssens, A., Schoemans, H., Lagrou, K., Wauters, J., & Maertens, J. (2014). Coxsackievirus A16 encephalitis during obinutuzumab therapy, Belgium, 2013. *Emerg Infect Dis*, 20(5), 913-915. https://doi.org/10.3201/eid2005.131766
- Fang, C. Y., & Liu, C. C. (2018). Recent development of enterovirus A vaccine candidates for the prevention of hand, foot, and mouth disease. *Expert Rev Vaccines*, *17*(9), 819-831. https://doi.org/10.1080/14760584.2018.1510326
- Farahat, R. A., Shaheen, N., Kundu, M., Shaheen, A., & Abdelaal, A. (2022). The resurfacing of hand, foot, and mouth disease: Are we on the verge of another epidemic? *Ann Med Surg (Lond)*, 81, 104419. https://doi.org/10.1016/j.amsu.2022.104419
- Farris, E., Brown, D. M., Ramer-Tait, A. E., & Pannier, A. K. (2016). Micro- and nanoparticulates for DNA vaccine delivery. *Exp Biol Med (Maywood)*, *241*(9), 919-929. https://doi.org/10.1177/1535370216643771
- Fernández Fernández, E., Santos-Carballal, B., Weber, W. M., & Goycoolea, F. M. (2016). Chitosan as a non-viral co-transfection system in a cystic fibrosis cell line. *Int J Pharm*, 502(1-2), 1-9. https://doi.org/10.1016/j.ijpharm.2016.01.083
- Ferraboschi, P., Ciceri, S., & Grisenti, P. (2021). Applications of Lysozyme, an Innate Immune Defense Factor, as an Alternative Antibiotic. *Antibiotics (Basel)*, 10(12). https://doi.org/10.3390/antibiotics10121534
- Filion, D., Lavertu, M., & Buschmann, M. D. (2007). Ionization and solubility of chitosan solutions related to thermosensitive chitosan/glycerol-phosphate systems. *Biomacromolecules*, 8(10), 3224-3234. https://doi.org/10.1021/bm700520m
- Fischer, D., Li, Y., Ahlemeyer, B., Krieglstein, J., & Kissel, T. (2003). In vitro cytotoxicity testing of polycations: influence of polymer structure on cell viability and hemolysis. *Biomaterials*, 24(7), 1121-1131. https://doi.org/10.1016/s0142-9612(02)00445-3

- Fong, S. Y., Mori, D., Rundi, C., Yap, J. F., Jikal, M., Latip, A., . . . Ahmed, K. (2021). A five-year retrospective study on the epidemiology of hand, foot and mouth disease in Sabah, Malaysia. *Sci Rep*, 11(1), 17814. https://doi.org/10.1038/s41598-021-96083-3
- Foo, D. G., Alonso, S., Phoon, M. C., Ramachandran, N. P., Chow, V. T., & Poh, C. L. (2007). Identification of neutralizing linear epitopes from the VP1 capsid protein of Enterovirus 71 using synthetic peptides. *Virus Res*, 125(1), 61-68. https://doi.org/10.1016/j.virusres.2006.12.005
- Foroozandeh, P., & Aziz, A. A. (2018). Insight into Cellular Uptake and Intracellular Trafficking of Nanoparticles. *Nanoscale Res Lett*, *13*(1), 339. https://doi.org/10.1186/s11671-018-2728-6
- Frigaard, J., Jensen, J. L., Galtung, H. K., & Hiorth, M. (2022). The Potential of Chitosan in Nanomedicine: An Overview of the Cytotoxicity of Chitosan Based Nanoparticles. *Front Pharmacol*, 13, 880377. https://doi.org/10.3389/fphar.2022.880377
- Fröhlich, E. (2012). The role of surface charge in cellular uptake and cytotoxicity of medical nanoparticles. *Int J Nanomedicine*, *7*, 5577-5591. https://doi.org/10.2147/ijn.S36111
- Fujii, K., Nagata, N., Sato, Y., Ong, K. C., Wong, K. T., Yamayoshi, S., . . . Koike, S. (2013). Transgenic mouse model for the study of enterovirus 71 neuropathogenesis. *Proc Natl Acad Sci U S A*, 110(36), 14753-14758. https://doi.org/10.1073/pnas.1217563110
- Fujii, K., Sudaka, Y., Takashino, A., Kobayashi, K., Kataoka, C., Suzuki, T., . . . Koike, S. (2018). VP1 Amino Acid Residue 145 of Enterovirus 71 Is a Key Residue for Its Receptor Attachment and Resistance to Neutralizing Antibody during Cynomolgus Monkey Infection. *J Virol*, 92(15). https://doi.org/10.1128/jvi.00682-18
- Fujimoto, T. (2018). [Hand-Foot-and-Mouth Disease, Aseptic Meningitis, and Encephalitis Caused by Enterovirus]. *Brain Nerve*, 70(2), 121-131. https://doi.org/10.11477/mf.1416200964
- Fussenegger, M., Mazur, X., & Bailey, J. E. (1998). pTRIDENT, a novel vector family for tricistronic gene expression in mammalian cells. *Biotechnol Bioeng*, *57*(1), 1-10. https://doi.org/10.1002/(sici)1097-0290(19980105)57:1<1::aid-bit1>3.0.co;2-m
- Goujon, M., McWilliam, H., Li, W., Valentin, F., Squizzato, S., Paern, J., & Lopez, R. (2010). A new bioinformatics analysis tools framework at EMBL–EBI. *Nucleic Acids Res*, *38*(suppl_2), W695-W699. https://doi.org/10.1093/nar/gkq313 %J Nucleic Acids Research
- Gu, Y. Y., Shi, K., Yao, S., Yang, X., Liu, Y. H., Tang, L., . . . Pan, H. B. (2017). Morphological characteristics of fatal pediatric hand, foot and mouth disease: A clinicopathological study with related receptors of EV71. *Pathol Res Pract*, *213*(9), 1144-1151. https://doi.org/10.1016/j.prp.2017.07.004
- Guadarrama-Escobar, O. R., Serrano-Castañeda, P., Anguiano-Almazán, E., Vázquez-Durán, A., Peña-Juárez, M. C., Vera-Graziano, R., . . . Escobar-Chávez, J. J. (2023). Chitosan Nanoparticles as Oral Drug Carriers. *Int J Mol Sci*, 24(5). https://doi.org/10.3390/ijms24054289
- Gupta, P. N., Mahor, S., Rawat, A., Khatri, K., Goyal, A., & Vyas, S. P. (2006). Lectin anchored stabilized biodegradable nanoparticles for oral immunization 1. Development and in vitro evaluation. *Int J Pharm*, 318(1-2), 163-173. https://doi.org/10.1016/j.ijpharm.2006.03.017
- Hagiwara, A., Tagaya, I., & Yoneyama, T. (1978). Epidemic of hand, foot and mouth disease associated with enterovirus 71 infection. *Intervirology*, *9*(1), 60-63. https://doi.org/10.1159/000148922
- Hajizade, A., Ebrahimi, F., Salmanian, A.-H., Arpanaei, A., & Amani, J. (2014). Nanoparticles in Vaccine Development. *Journal of Applied Biotechnology Reports*, 1(4), 125-134. http://www.biotechrep.ir/article 69152.html
- Hallaj-Nezhadi, S., Valizadeh, H., Dastmalchi, S., Baradaran, B., Jalali, M. B., Dobakhti, F., & Lotfipour, F. (2011). Preparation of chitosan-plasmid DNA nanoparticles encoding interleukin-12 and their expression in CT-26 colon carcinoma cells. *J Pharm Pharm Sci*, 14(2), 181-195. https://doi.org/10.18433/j3tp4t

- Han, H. D., Byeon, Y., Jang, J. H., Jeon, H. N., Kim, G. H., Kim, M. G., . . . Park, Y. M. (2016). In vivo stepwise immunomodulation using chitosan nanoparticles as a platform nanotechnology for cancer immunotherapy. *Sci Rep*, *6*, 38348. https://doi.org/10.1038/srep38348
- Hartmann, G. (2017). Nucleic Acid Immunity. *Adv Immunol*, *133*, 121-169. https://doi.org/10.1016/bs.ai.2016.11.001
- Hashimoto, M., Morimoto, M., Saimoto, H., Shigemasa, Y., Yanagie, H., Eriguchi, M., & Sato, T. (2006). Gene transfer by DNA/mannosylated chitosan complexes into mouse peritoneal macrophages. *Biotechnol Lett*, 28(11), 815-821. https://doi.org/10.1007/s10529-006-9006-x
- He, F., Rui, J., Deng, Z., Zhang, Y., Qian, K., Zhu, C., . . . Zhou, X. (2021). Surveillance, Epidemiology and Impact of EV-A71 Vaccination on Hand, Foot, and Mouth Disease in Nanchang, China, 2010-2019. Front Microbiol, 12, 811553. https://doi.org/10.3389/fmicb.2021.811553
- He, X., Zhang, M., Zhao, C., Zheng, P., Zhang, X., & Xu, J. (2021). From Monovalent to Multivalent Vaccines, the Exploration for Potential Preventive Strategies Against Hand, Foot, and Mouth Disease (HFMD). *Virol Sin*, *36*(2), 167-175. https://doi.org/10.1007/s12250-020-00294-3
- He, Y. Q., Chen, L., Xu, W. B., Yang, H., Wang, H. Z., Zong, W. P., . . . Zhao, D. J. (2013). Emergence, circulation, and spatiotemporal phylogenetic analysis of coxsackievirus a6- and coxsackievirus a10-associated hand, foot, and mouth disease infections from 2008 to 2012 in Shenzhen, China. *J Clin Microbiol*, 51(11), 3560-3566. https://doi.org/10.1128/jcm.01231-13
- Heffernan, M. J., Zaharoff, D. A., Fallon, J. K., Schlom, J., & Greiner, J. W. (2011). In vivo efficacy of a chitosan/IL-12 adjuvant system for protein-based vaccines. *Biomaterials*, *32*(3), 926-932. https://doi.org/10.1016/j.biomaterials.2010.09.058
- Heinsbroek, E., & Ruitenberg, E. J. (2010). The global introduction of inactivated polio vaccine can circumvent the oral polio vaccine paradox. *Vaccine*, *28*(22), 3778-3783. https://doi.org/10.1016/j.vaccine.2010.02.095
- Hennecke, M., Kwissa, M., Metzger, K., Oumard, A., Kröger, A., Schirmbeck, R., . . . Hauser, H. (2001). Composition and arrangement of genes define the strength of IRES-driven translation in bicistronic mRNAs. *Nucleic Acids Res*, 29(16), 3327-3334. https://doi.org/10.1093/nar/29.16.3327
- Herriott, R. M., Connolly, J. H., & Gupta, S. (1961). Blood nucleases and infectious viral nucleic acids. *Nature*, 189, 817-820. https://doi.org/10.1038/189817a0
- Hewitt, E. W. (2003). The MHC class I antigen presentation pathway: strategies for viral immune evasion. *Immunology*, 110(2), 163-169. https://doi.org/10.1046/j.1365-2567.2003.01738.x
- Highton, A. J., Girardin, A., Bell, G. M., Hook, S. M., & Kemp, R. A. (2016). Chitosan gel vaccine protects against tumour growth in an intracaecal mouse model of cancer by modulating systemic immune responses. *BMC Immunol*, *17*(1), 39. https://doi.org/10.1186/s12865-016-0178-4
- Hipolito, V. E. B., Ospina-Escobar, E., & Botelho, R. J. (2018). Lysosome remodelling and adaptation during phagocyte activation. *Cell Microbiol*, 20(4). https://doi.org/10.1111/cmi.12824
- Hobson, P., Barnfield, C., Barnes, A., & Klavinskis, L. S. (2003). Mucosal immunization with DNA vaccines. *Methods*, *31*(3), 217-224. https://doi.org/10.1016/s1046-2023(03)00139-7
- Hooi, Y. T., Ong, K. C., Tan, S. H., Perera, D., & Wong, K. T. (2020). A novel orally infected hamster model for Coxsackievirus A16 hand-foot-and-mouth disease and encephalomyelitis. *Lab Invest*, 100(9), 1262-1275. https://doi.org/10.1038/s41374-020-0456-x
- Hu, K., Onintsoa Diarimalala, R., Yao, C., Li, H., & Wei, Y. (2023). EV-A71 Mechanism of Entry: Receptors/Co-Receptors, Related Pathways and Inhibitors. *Viruses*, 15(3). https://doi.org/10.3390/v15030785

- Hu, Y. F., Jia, L. P., Yu, F. Y., Liu, L. Y., Song, Q. W., Dong, H. J., . . . Zhu, R. N. (2021). Molecular epidemiology of coxsackievirus A16 circulating in children in Beijing, China from 2010 to 2019. *World J Pediatr*, 17(5), 508-516. https://doi.org/10.1007/s12519-021-00451-y
- Huang, L. M., Chiu, C. H., Chiu, N. C., Lin, C. Y., Li, M. T., Kuo, T. Y., . . . Tai, I. C. (2019). Immunogenicity, safety, cross-reaction, and immune persistence of an inactivated enterovirus A71 vaccine in children aged from two months to 11 years in Taiwan. *Vaccine*, *37*(13), 1827-1835. https://doi.org/10.1016/j.vaccine.2019.02.023
- Huang, S. W., Cheng, D., & Wang, J. R. (2019). Enterovirus A71: virulence, antigenicity, and genetic evolution over the years. *J Biomed Sci*, 26(1), 81. https://doi.org/10.1186/s12929-019-0574-1
- Huang, S. W., Cheng, H. L., Hsieh, H. Y., Chang, C. L., Tsai, H. P., Kuo, P. H., ... Wang, J. R. (2014). Mutations in the non-structural protein region contribute to intra-genotypic evolution of enterovirus 71. *J Biomed Sci*, 21(1), 33. https://doi.org/10.1186/1423-0127-21-33
- Huang, S. W., Hsu, Y. W., Smith, D. J., Kiang, D., Tsai, H. P., Lin, K. H., . . . Wang, J. R. (2009). Reemergence of enterovirus 71 in 2008 in taiwan: dynamics of genetic and antigenic evolution from 1998 to 2008. *J Clin Microbiol*, 47(11), 3653-3662. https://doi.org/10.1128/jcm.00630-09
- Huang, S. W., Tai, C. H., Fonville, J. M., Lin, C. H., Wang, S. M., Liu, C. C., . . . Wang, J. R. (2015). Mapping Enterovirus A71 Antigenic Determinants from Viral Evolution. *J Virol*, 89(22), 11500-11506. https://doi.org/10.1128/jvi.02035-15
- Huang, S. W., Wang, Y. F., Yu, C. K., Su, I. J., & Wang, J. R. (2012). Mutations in VP2 and VP1 capsid proteins increase infectivity and mouse lethality of enterovirus 71 by virus binding and RNA accumulation enhancement. *Virology*, *422*(1), 132-143. https://doi.org/10.1016/j.virol.2011.10.015
- Huang, T., Song, X., Jing, J., Zhao, K., Shen, Y., Zhang, X., & Yue, B. (2018). Chitosan-DNA nanoparticles enhanced the immunogenicity of multivalent DNA vaccination on mice against Trueperella pyogenes infection. *J Nanobiotechnology*, 16(1), 8. https://doi.org/10.1186/s12951-018-0337-2
- Huang, Y., & Lapitsky, Y. (2017). On the kinetics of chitosan/tripolyphosphate micro- and nanogel aggregation and their effects on particle polydispersity. *J Colloid Interface Sci*, 486, 27-37. https://doi.org/10.1016/j.jcis.2016.09.050
- Huang, Y. W., Cambre, M., & Lee, H. J. (2017). The Toxicity of Nanoparticles Depends on Multiple Molecular and Physicochemical Mechanisms. *Int J Mol Sci*, 18(12). https://doi.org/10.3390/ijms18122702
- Ishii, T., Okahata, Y., & Sato, T. (2001). Mechanism of cell transfection with plasmid/chitosan complexes. *Biochim Biophys Acta*, *1514*(1), 51-64. https://doi.org/10.1016/s0005-2736(01)00362-5
- Iswanti, F. C., Nurulita, I., Djauzi, S., Sadikin, M., Witarto, A. B., & Yamazaki, T. (2019). Preparation, characterization, and evaluation of chitosan-based nanoparticles as CpG ODN carriers. *Biotechnology & Biotechnological Equipment*, 33(1), 390-396. https://doi.org/10.1080/13102818.2019.1578690
- Iurescia, S., Fioretti, D., & Rinaldi, M. (2014). Strategies for improving DNA vaccine performance. *Methods Mol Biol*, 1143, 21-31. https://doi.org/10.1007/978-1-4939-0410-5 3
- Iwasaki, A., Torres, C. A., Ohashi, P. S., Robinson, H. L., & Barber, B. H. (1997). The dominant role of bone marrow-derived cells in CTL induction following plasmid DNA immunization at different sites. *J Immunol*, 159(1), 11-14.
- Jang, S. K., & Wimmer, E. (1990). Cap-independent translation of encephalomyocarditis virus RNA: structural elements of the internal ribosomal entry site and involvement of a cellular 57-kD RNA-binding protein. *Genes Dev*, 4(9), 1560-1572. https://doi.org/10.1101/gad.4.9.1560
- Jazayeri, S. D., & Poh, C. L. (2019). Recent advances in delivery of veterinary DNA vaccines against avian pathogens. *Vet Res*, *50*(1), 78. https://doi.org/10.1186/s13567-019-0698-z

- Jeong, H., Choi, Y. M., Seo, H., & Kim, B. J. (2021). A Novel DNA Vaccine Against SARS-CoV-2 Encoding a Chimeric Protein of Its Receptor-Binding Domain (RBD) Fused to the Amino-Terminal Region of Hepatitis B Virus preS1 With a W4P Mutation. *Front Immunol*, 12, 637654. https://doi.org/10.3389/fimmu.2021.637654
- Jesus, S., Marques, A. P., Duarte, A., Soares, E., Costa, J. P., Colaço, M., . . . Borges, O. (2020). Chitosan Nanoparticles: Shedding Light on Immunotoxicity and Hemocompatibility. *Front Bioeng Biotechnol*, *8*, 100. https://doi.org/10.3389/fbioe.2020.00100
- Jevprasesphant, R., Penny, J., Jalal, R., Attwood, D., McKeown, N. B., & D'Emanuele, A. (2003). The influence of surface modification on the cytotoxicity of PAMAM dendrimers. *Int J Pharm*, 252(1-2), 263-266. https://doi.org/10.1016/s0378-5173(02)00623-3
- Joffre, O., Nolte, M. A., Spörri, R., & Reis e Sousa, C. (2009). Inflammatory signals in dendritic cell activation and the induction of adaptive immunity. *Immunol Rev*, 227(1), 234-247. https://doi.org/10.1111/j.1600-065X.2008.00718.x
- Joffre, O. P., Segura, E., Savina, A., & Amigorena, S. (2012). Cross-presentation by dendritic cells. Nat Rev Immunol, 12(8), 557-569. https://doi.org/10.1038/nri3254
- Kang, H. C., Samsonova, O., Kang, S. W., & Bae, Y. H. (2012). The effect of environmental pH on polymeric transfection efficiency. *Biomaterials*, 33(5), 1651-1662. https://doi.org/10.1016/j.biomaterials.2011.11.006
- Kataoka, C., Suzuki, T., Kotani, O., Iwata-Yoshikawa, N., Nagata, N., Ami, Y., . . . Shimizu, H. (2015). The Role of VP1 Amino Acid Residue 145 of Enterovirus 71 in Viral Fitness and Pathogenesis in a Cynomolgus Monkey Model. *PLoS Pathog*, 11(7), e1005033. https://doi.org/10.1371/journal.ppat.1005033
- Keppel, M. P., Saucier, N., Mah, A. Y., Vogel, T. P., & Cooper, M. A. (2015). Activation-specific metabolic requirements for NK Cell IFN-γ production. J Immunol, 194(4), 1954-1962. https://doi.org/10.4049/jimmunol.1402099
- Khan, A. S., Broderick, K. E., & Sardesai, N. Y. (2014). Clinical development of intramuscular electroporation: providing a "boost" for DNA vaccines. *Methods Mol Biol*, 1121, 279-289. https://doi.org/10.1007/978-1-4614-9632-8 25
- Koppolu, B., & Zaharoff, D. A. (2013). The effect of antigen encapsulation in chitosan particles on uptake, activation and presentation by antigen presenting cells. *Biomaterials*, *34*(9), 2359-2369. https://doi.org/10.1016/j.biomaterials.2012.11.066
- Kozak, M. (1995). Adherence to the first-AUG rule when a second AUG codon follows closely upon the first. *Proc Natl Acad Sci U S A*, *92*(15), 7134. https://doi.org/10.1073/pnas.92.15.7134
- Kuen, C. Y., Fakurazi, S., Othman, S. S., & Masarudin, M. J. (2017). Increased Loading, Efficacy and Sustained Release of Silibinin, a Poorly Soluble Drug Using Hydrophobically-Modified Chitosan Nanoparticles for Enhanced Delivery of Anticancer Drug Delivery Systems. Nanomaterials (Basel), 7(11). https://doi.org/10.3390/nano7110379
- Kumar, A., Kumar, A. J. B. S., Performance, Applications, & Kumar, M., Mustansar, HC, Eds. (2017). Chitosan as a biomedical material: Properties and applications. 139-153.
- Kumar, M. N., Muzzarelli, R. A., Muzzarelli, C., Sashiwa, H., & Domb, A. J. (2004). Chitosan chemistry and pharmaceutical perspectives. *Chem Rev*, 104(12), 6017-6084. https://doi.org/10.1021/cr030441b
- Kushnir, N., Streatfield, S. J., & Yusibov, V. (2012). Virus-like particles as a highly efficient vaccine platform: diversity of targets and production systems and advances in clinical development. *Vaccine*, *31*(1), 58-83. https://doi.org/10.1016/j.vaccine.2012.10.083
- Lalani, S., Gew, L. T., & Poh, C. L. (2021). Antiviral peptides against Enterovirus A71 causing hand, foot and mouth disease. *Peptides*, *136*, 170443. https://doi.org/10.1016/j.peptides.2020.170443
- Langer, B., Renner, M., Scherer, J., Schüle, S., & Cichutek, K. (2013). Safety assessment of biolistic DNA vaccination. *Methods Mol Biol*, *940*, 371-388. https://doi.org/10.1007/978-1-62703-110-3 27

- Laor, P., Apidechkul, T., Khunthason, S., Keawdounglek, V., Sudsandee, S., Fakkaew, K., & Siriratruengsuk, W. (2020). Association of environmental factors and high HFMD occurrence in northern Thailand. BMC Public Health, 20(1), 1829. https://doi.org/10.1186/s12889-020-09905-w
- Lauková, L., Konečná, B., Janovičová, Ľ., Vlková, B., & Celec, P. (2020). Deoxyribonucleases and Their Applications in Biomedicine. *Biomolecules*, 10(7). https://doi.org/10.3390/biom10071036
- Lavertu, M., Méthot, S., Tran-Khanh, N., & Buschmann, M. D. (2006). High efficiency gene transfer using chitosan/DNA nanoparticles with specific combinations of molecular weight and degree of deacetylation. *Biomaterials*, 27(27), 4815-4824. https://doi.org/10.1016/j.biomaterials.2006.04.029
- Lee, M. H. P., Chong, Y. M., Tay, C. G., Koh, M. T., Chem, Y. K., Noordin, N., . . . Chan, Y. F. (2021). Detection of enteroviruses during a 2018 hand, foot and mouth disease outbreak in Malaysia. *Trop Biomed*, 38(1), 150-153. https://doi.org/10.47665/tb.38.1.026
- Lee, Y. H., Pang, S. W., Revai Lechtich, E., Shah, K., Simon, S. E., Ponnusamy, S., . . . Tan, K. O. (2020). Tricistronic expression of MOAP-1, Bax and RASSF1A in cancer cells enhances chemo-sensitization that requires BH3L domain of MOAP-1. *J Cancer Res Clin Oncol*, 146(7), 1751-1764. https://doi.org/10.1007/s00432-020-03231-9
- Leirião, P., del Fresno, C., & Ardavín, C. (2012). Monocytes as effector cells: activated Ly-6C(high) mouse monocytes migrate to the lymph nodes through the lymph and cross-present antigens to CD8+ T cells. *Eur J Immunol*, 42(8), 2042-2051. https://doi.org/10.1002/eji.201142166
- Leung, C. S. (2015). Endogenous Antigen Presentation of MHC Class II Epitopes through Non-Autophagic Pathways. *Front Immunol*, *6*, 464. https://doi.org/10.3389/fimmu.2015.00464
- Li, R., Liu, L., Mo, Z., Wang, X., Xia, J., Liang, Z., . . . Li, Q. (2014). An inactivated enterovirus 71 vaccine in healthy children. *N Engl J Med*, *370*(9), 829-837. https://doi.org/10.1056/NEJMoa1303224
- Li, Y. X., Zhao, H., Cao, R. Y., Deng, Y. Q., Han, J. F., Zhu, S. Y., . . . Qin, C. F. (2014). Recombinant tandem multi-linear neutralizing epitopes of human enterovirus 71 elicited protective immunity in mice. *Virol J*, 11, 79. https://doi.org/10.1186/1743-422x-11-79
- Lim, H. X., & Poh, C. L. (2019). Insights into innate and adaptive immune responses in vaccine development against EV-A71. *Ther Adv Vaccines Immunother*, 7, 2515135519888998. https://doi.org/10.1177/2515135519888998
- Lin, Y. J., Wen, C. N., Lin, Y. Y., Hsieh, W. C., Chang, C. C., Chen, Y. H., . . . Fang, C. T. (2020). Oil-in-water emulsion adjuvants for pediatric influenza vaccines: a systematic review and meta-analysis. *Nat Commun*, 11(1), 315. https://doi.org/10.1038/s41467-019-14230-x
- Lin, Y. L., Yu, C. I., Hu, Y. C., Tsai, T. J., Kuo, Y. C., Chi, W. K., . . . Chiang, B. L. (2012). Enterovirus type 71 neutralizing antibodies in the serum of macaque monkeys immunized with EV71 virus-like particles. *Vaccine*, 30(7), 1305-1312. https://doi.org/10.1016/j.vaccine.2011.12.081
- Liu, C. C., Chou, A. H., Lien, S. P., Lin, H. Y., Liu, S. J., Chang, J. Y., . . . Chong, P. (2011). Identification and characterization of a cross-neutralization epitope of Enterovirus 71. *Vaccine*, *29*(26), 4362-4372. https://doi.org/10.1016/j.vaccine.2011.04.010
- Liu, C. C., Guo, M. S., Wu, S. R., Lin, H. Y., Yang, Y. T., Liu, W. C., . . . Chong, P. (2016). Immunological and biochemical characterizations of coxsackievirus A6 and A10 viral particles. *Antiviral Res*, 129, 58-66. https://doi.org/10.1016/j.antiviral.2016.02.008
- Liu, M., Hu, P. A., & Ding, K. X. (2011). [The effect of serum concentration on the growth, proliferation and collagen secretion in mouse L929 fibroblasts]. *Xi Bao Yu Fen Zi Mian Yi Xue Za Zhi*, 27(7), 736-739.
- Liu, M. A. (2011). DNA vaccines: an historical perspective and view to the future. *Immunol Rev,* 239(1), 62-84. https://doi.org/10.1111/j.1600-065X.2010.00980.x

- Liu, W., Wu, S., Xiong, Y., Li, T., Wen, Z., Yan, M., . . . Wu, J. (2014). Co-circulation and genomic recombination of coxsackievirus A16 and enterovirus 71 during a large outbreak of hand, foot, and mouth disease in Central China. *PLoS One*, *9*(4), e96051. https://doi.org/10.1371/journal.pone.0096051
- Lončarević, A., Ivanković, M., & Rogina, A. (2017). Lysozyme-Induced Degradation of Chitosan: The Characterisation of Degraded Chitosan Scaffolds. *Journal of Tissue Repair and Regeneration*, 1. https://doi.org/10.14302/issn.2640-6403.jtrr-17-1840
- Lu, G., Qi, J., Chen, Z., Xu, X., Gao, F., Lin, D., . . . Gao, G. F. (2011). Enterovirus 71 and coxsackievirus A16 3C proteases: binding to rupintrivir and their substrates and antihand, foot, and mouth disease virus drug design. *J Virol*, 85(19), 10319-10331. https://doi.org/10.1128/jvi.00787-11
- Ma, F., Wang, Y., & Yang, G. (2019). The Modulation of Chitosan-DNA Interaction by Concentration and pH in Solution. *Polymers (Basel)*, 11(4). https://doi.org/10.3390/polym11040646
- MacLaughlin, F. C., Mumper, R. J., Wang, J., Tagliaferri, J. M., Gill, I., Hinchcliffe, M., & Rolland, A. P. (1998). Chitosan and depolymerized chitosan oligomers as condensing carriers for in vivo plasmid delivery. *J Control Release*, *56*(1-3), 259-272. https://doi.org/10.1016/s0168-3659(98)00097-2
- Maecker, H. T., Umetsu, D. T., DeKruyff, R. H., & Levy, S. (1998). Cytotoxic T cell responses to DNA vaccination: dependence on antigen presentation via class II MHC. *J Immunol*, 161(12), 6532-6536.
- malaymail. (2023). *Weekly HFMD cases in Malaysia exceed alert level, says Health D-G*. Retrieved 30 July 2023 from https://www.malaymail.com/news/malaysia/2023/05/20/weekly-hfmd-cases-in-malaysia-exceed-alert-level-says-health-d-g/70184
- Mandary, M. B., & Poh, C. L. (2018). Changes in the EV-A71 Genome through Recombination and Spontaneous Mutations: Impact on Virulence. *Viruses*, *10*(6). https://doi.org/10.3390/v10060320
- Mao, H. Q., Roy, K., Troung-Le, V. L., Janes, K. A., Lin, K. Y., Wang, Y., . . . Leong, K. W. (2001). Chitosan-DNA nanoparticles as gene carriers: synthesis, characterization and transfection efficiency. *J Control Release*, 70(3), 399-421. https://doi.org/10.1016/s0168-3659(00)00361-8
- Mao, Q., Wang, Y., Yao, X., Bian, L., Wu, X., Xu, M., & Liang, Z. (2014). Coxsackievirus A16. *Hum Vaccin Immunother*, 10(2), 360-367. https://doi.org/10.4161/hv.27087
- Masarudin, M. J., Cutts, S. M., Evison, B. J., Phillips, D. R., & Pigram, P. J. (2015). Factors determining the stability, size distribution, and cellular accumulation of small, monodisperse chitosan nanoparticles as candidate vectors for anticancer drug delivery: application to the passive encapsulation of [(14)C]-doxorubicin. *Nanotechnol Sci Appl*, 8, 67-80. https://doi.org/10.2147/nsa.S91785
- McConnell, K. I., Shamsudeen, S., Meraz, I. M., Mahadevan, T. S., Ziemys, A., Rees, P., . . . Serda, R. E. (2016). Reduced Cationic Nanoparticle Cytotoxicity Based on Serum Masking of Surface Potential. *J Biomed Nanotechnol*, 12(1), 154-164. https://doi.org/10.1166/jbn.2016.2134
- Mizuguchi, H., Xu, Z., Ishii-Watabe, A., Uchida, E., & Hayakawa, T. (2000). IRES-dependent second gene expression is significantly lower than cap-dependent first gene expression in a bicistronic vector. *Mol Ther*, 1(4), 376-382. https://doi.org/10.1006/mthe.2000.0050
- Mizuta, K., Aoki, Y., Matoba, Y., Yahagi, K., Itagaki, T., Katsushima, F., . . . Matsuzaki, Y. (2014). Molecular epidemiology of enterovirus 71 strains isolated from children in Yamagata, Japan, between 1990 and 2013. *J Med Microbiol*, 63(Pt 10), 1356-1362. https://doi.org/10.1099/jmm.0.079699-0
- Moraru, C., Mincea, M., Menghiu, G., & Ostafe, V. (2020). Understanding the Factors Influencing Chitosan-Based Nanoparticles-Protein Corona Interaction and Drug Delivery Applications. *Molecules*, 25(20). https://doi.org/10.3390/molecules25204758

- Mucha, M., & Pawlak, A. (2002). Complex study on chitosan degradability. *Polimery/Polymers*, 47, 509-516. https://doi.org/10.14314/polimery.2002.509
- Nakamura, F. (1992). Lysozyme-catalyzed degradation properties of the conjugates between chitosans having some deacetylation degrees and methotrexate. *Yakuzaigaku*, *52*, 59-67. https://cir.nii.ac.jp/crid/1572824499522629120
- Nguyen, D. N., Green, J. J., Chan, J. M., Longer, R., & Anderson, D. G. (2009). Polymeric Materials for Gene Delivery and DNA Vaccination. *Adv Mater*, *21*(8), 847-867. https://doi.org/10.1002/adma.200801478
- Nhan, L. N. T., Hong, N. T. T., Nhu, L. N. T., Nguyet, L. A., Ny, N. T. H., Thanh, T. T., . . . Tan, L. V. (2018). Severe enterovirus A71 associated hand, foot and mouth disease, Vietnam, 2018: preliminary report of an impending outbreak. *Euro Surveill*, 23(46). https://doi.org/10.2807/1560-7917.Es.2018.23.46.1800590
- NikNadia, N., Sam, I. C., Rampal, S., WanNorAmalina, W., NurAtifah, G., Verasahib, K., . . . Chan, Y. F. (2016). Cyclical Patterns of Hand, Foot and Mouth Disease Caused by Enterovirus A71 in Malaysia. *PLoS Negl Trop Dis*, 10(3), e0004562. https://doi.org/10.1371/journal.pntd.0004562
- Nimesh, S., Thibault, M. M., Lavertu, M., & Buschmann, M. D. (2010). Enhanced gene delivery mediated by low molecular weight chitosan/DNA complexes: effect of pH and serum. *Mol Biotechnol*, 46(2), 182-196. https://doi.org/10.1007/s12033-010-9286-1
- Nishimura, Y., Lee, H., Hafenstein, S., Kataoka, C., Wakita, T., Bergelson, J. M., & Shimizu, H. (2013). Enterovirus 71 binding to PSGL-1 on leukocytes: VP1-145 acts as a molecular switch to control receptor interaction. *PLoS Pathog*, *9*(7), e1003511. https://doi.org/10.1371/journal.ppat.1003511
- Niu, Q., Liu, J., Zhao, Z., Onishi, M., Kawaguchi, A., Bandara, A., . . . Nagai-Tanima, M. (2022). Explanation of hand, foot, and mouth disease cases in Japan using Google Trends before and during the COVID-19: infodemiology study. *BMC Infect Dis*, 22(1), 806. https://doi.org/10.1186/s12879-022-07790-9
- Nouailles, G., Adler, J. M., Pennitz, P., Peidli, S., Teixeira Alves, L. G., Baumgardt, M., . . . Trimpert, J. (2023). Live-attenuated vaccine sCPD9 elicits superior mucosal and systemic immunity to SARS-CoV-2 variants in hamsters. *Nat Microbiol*, 8(5), 860-874. https://doi.org/10.1038/s41564-023-01352-8
- Nunes, R., Serra, A. S., Simaite, A., & Sousa, Â. (2022). Modulation of Chitosan-TPP Nanoparticle Properties for Plasmid DNA Vaccines Delivery. *Polymers (Basel)*, *14*(7). https://doi.org/10.3390/polym14071443
- Nunes, R., Sousa, Â., Simaite, A., Aido, A., & Buzgo, M. (2021). Sub-100 nm Chitosan-Triphosphate-DNA Nanoparticles for Delivery of DNA Vaccines. *Proceedings*, 78(1).
- O'Connell, A. K., & Douam, F. (2020). Humanized Mice for Live-Attenuated Vaccine Research: From Unmet Potential to New Promises. *Vaccines (Basel)*, 8(1). https://doi.org/10.3390/vaccines8010036
- O'Hagan, D. T., Singh, M., & Ulmer, J. B. (2004). Microparticles for the delivery of DNA vaccines. *Immunol Rev*, 199, 191-200. https://doi.org/10.1111/j.0105-2896.2004.00153.x
- Ong, K. C., Badmanathan, M., Devi, S., Leong, K. L., Cardosa, M. J., & Wong, K. T. (2008). Pathologic characterization of a murine model of human enterovirus 71 encephalomyelitis. *J Neuropathol Exp Neurol*, 67(6), 532-542. https://doi.org/10.1097/NEN.0b013e31817713e7
- Ong, K. C., Devi, S., Cardosa, M. J., & Wong, K. T. (2010). Formaldehyde-inactivated whole-virus vaccine protects a murine model of enterovirus 71 encephalomyelitis against disease. *J Virol*, 84(1), 661-665. https://doi.org/10.1128/jvi.00999-09
- Osterback, R., Vuorinen, T., Linna, M., Susi, P., Hyypiä, T., & Waris, M. (2009). Coxsackievirus A6 and hand, foot, and mouth disease, Finland. *Emerg Infect Dis*, *15*(9), 1485-1488. https://doi.org/10.3201/eid1509.090438
- Othman, N., Masarudin, M. J., Kuen, C. Y., Dasuan, N. A., Abdullah, L. C., & Md Jamil, S. N. A. (2018). Synthesis and Optimization of Chitosan Nanoparticles Loaded with L-Ascorbic

- Acid and Thymoquinone. *Nanomaterials* (Basel), 8(11). https://doi.org/10.3390/nano8110920
- Pelletier, J., & Sonenberg, N. (1988). Internal initiation of translation of eukaryotic mRNA directed by a sequence derived from poliovirus RNA. *Nature*, *334*(6180), 320-325. https://doi.org/10.1038/334320a0
- Plevka, P., Perera, R., Cardosa, J., Kuhn, R. J., & Rossmann, M. G. (2012). Crystal structure of human enterovirus 71. *Science*, 336(6086), 1274. https://doi.org/10.1126/science.1218713
- Pöyry, T., Hyypiä, T., Horsnell, C., Kinnunen, L., Hovi, T., & Stanway, G. (1994). Molecular analysis of coxsackievirus A16 reveals a new genetic group of enteroviruses. *Virology*, *202*(2), 982-987. https://doi.org/10.1006/viro.1994.1423
- Pozzetto, B., & Gaudin, O. G. (1999). COXSACKIEVIRUSES (PICORNAVIRIDAE). *Encyclopedia of Virology*, 305-311. https://doi.org/10.1006/rwvi.1999.0057
- Prabha, S., Zhou, W. Z., Panyam, J., & Labhasetwar, V. (2002). Size-dependency of nanoparticle-mediated gene transfection: studies with fractionated nanoparticles. *Int J Pharm*, 244(1-2), 105-115. https://doi.org/10.1016/s0378-5173(02)00315-0
- Prompetchara, E., Ketloy, C., Tharakhet, K., Kaewpang, P., Buranapraditkun, S., Techawiwattanaboon, T., . . . Ruxrungtham, K. (2021). DNA vaccine candidate encoding SARS-CoV-2 spike proteins elicited potent humoral and Th1 cell-mediated immune responses in mice. *PLoS One*, 16(3), e0248007. https://doi.org/10.1371/journal.pone.0248007
- Puenpa, J., Wanlapakorn, N., Vongpunsawad, S., & Poovorawan, Y. (2019). The History of Enterovirus A71 Outbreaks and Molecular Epidemiology in the Asia-Pacific Region. *J Biomed Sci*, 26(1), 75. https://doi.org/10.1186/s12929-019-0573-2
- Qi, L., & Xu, Z. (2006). In vivo antitumor activity of chitosan nanoparticles. *Bioorg Med Chem Lett*, *16*(16), 4243-4245. https://doi.org/10.1016/j.bmcl.2006.05.078
- Qin, F., Xia, F., Chen, H., Cui, B., Feng, Y., Zhang, P., . . . Luo, M. (2021). A Guide to Nucleic Acid Vaccines in the Prevention and Treatment of Infectious Diseases and Cancers: From Basic Principles to Current Applications. *Front Cell Dev Biol*, *9*, 633776. https://doi.org/10.3389/fcell.2021.633776
- Quaak, S. G., Haanen, J. B., Beijnen, J. H., & Nuijen, B. (2010). Naked plasmid DNA formulation: effect of different disaccharides on stability after lyophilisation. *AAPS PharmSciTech*, 11(1), 344-350. https://doi.org/10.1208/s12249-010-9391-2
- Randall, C. (2010). Construction of self-sufficient CYP153 chimeras.
- Rapetti, L., Meunier, S., Pontoux, C., & Tanchot, C. (2008). CD4 help regulates expression of crucial genes involved in CD8 T cell memory and sensitivity to regulatory elements. *J Immunol*, 181(1), 299-308. https://doi.org/10.4049/jimmunol.181.1.299
- Ren, P., Zheng, Y., Wang, W., Hong, L., Delpeyroux, F., Arenzana-Seisdedos, F., & Altmeyer, R. (2017). Suramin interacts with the positively charged region surrounding the 5-fold axis of the EV-A71 capsid and inhibits multiple enterovirus A. *Sci Rep*, 7, 42902. https://doi.org/10.1038/srep42902
- Ren, P., Zou, G., Bailly, B., Xu, S., Zeng, M., Chen, X., . . . Altmeyer, R. (2014). The approved pediatric drug suramin identified as a clinical candidate for the treatment of EV71 infection-suramin inhibits EV71 infection in vitro and in vivo. *Emerg Microbes Infect*, 3(9), e62. https://doi.org/10.1038/emi.2014.60
- Repass, G. L., Palmer, W. C., & Stancampiano, F. F. (2014). Hand, foot, and mouth disease: identifying and managing an acute viral syndrome. *Cleve Clin J Med*, 81(9), 537-543. https://doi.org/10.3949/ccjm.81a.13132
- Ribot, J. C., deBarros, A., Pang, D. J., Neves, J. F., Peperzak, V., Roberts, S. J., . . . Silva-Santos, B. (2009). CD27 is a thymic determinant of the balance between interferon-gamma- and interleukin 17-producing gammadelta T cell subsets. *Nat Immunol*, *10*(4), 427-436. https://doi.org/10.1038/ni.1717

- Roche, P. A., & Furuta, K. (2015). The ins and outs of MHC class II-mediated antigen processing and presentation. *Nat Rev Immunol*, *15*(4), 203-216. https://doi.org/10.1038/nri3818
- Rodpothong, P., & Auewarakul, P. (2012). Viral evolution and transmission effectiveness. *World J Virol*, 1(5), 131-134. https://doi.org/10.5501/wjv.v1.i5.131
- Roldão, A., Mellado, M. C., Castilho, L. R., Carrondo, M. J., & Alves, P. M. (2010). Virus-like particles in vaccine development. *Expert Rev Vaccines*, *9*(10), 1149-1176. https://doi.org/10.1586/erv.10.115
- Sahu, D., Kannan, G. M., Tailang, M., & Vijayaraghavan, R. (2016). In Vitro Cytotoxicity of Nanoparticles: A Comparison between Particle Size and Cell Type.
- Sanjuán, R., Nebot, M. R., Chirico, N., Mansky, L. M., & Belshaw, R. (2010). Viral mutation rates. *J Virol*, 84(19), 9733-9748. https://doi.org/10.1128/jvi.00694-10
- Sato, T., Ishii, T., & Okahata, Y. (2001). In vitro gene delivery mediated by chitosan. effect of pH, serum, and molecular mass of chitosan on the transfection efficiency. *Biomaterials*, 22(15), 2075-2080. https://doi.org/10.1016/s0142-9612(00)00385-9
- Sato, Y., Silina, K., van den Broek, M., Hirahara, K., & Yanagita, M. (2023). The roles of tertiary lymphoid structures in chronic diseases. *Nat Rev Nephrol*, 19(8), 525-537. https://doi.org/10.1038/s41581-023-00706-z
- Sauer, P. W., Burky, J. E., Wesson, M. C., Sternard, H. D., & Qu, L. (2000). A high-yielding, generic fed-batch cell culture process for production of recombinant antibodies. *Biotechnol Bioeng*, *67*(5), 585-597.
- Schmidt, N. J., Lennette, E. H., & Ho, H. H. (1974). An apparently new enterovirus isolated from patients with disease of the central nervous system. *J Infect Dis*, 129(3), 304-309. https://doi.org/10.1093/infdis/129.3.304
- Sham, N. M., Krishnarajah, I., Ibrahim, N. A., & Lye, M. S. (2014). Temporal and spatial mapping of hand, foot and mouth disease in Sarawak, Malaysia. *Geospat Health*, 8(2), 503-507. https://doi.org/10.4081/gh.2014.39
- Shen, C., Liu, Q., Zhou, Y., Ku, Z., Wang, L., Lan, K., . . . Huang, Z. (2016). Inactivated coxsackievirus A10 experimental vaccines protect mice against lethal viral challenge. *Vaccine*, *34*(41), 5005-5012. https://doi.org/10.1016/j.vaccine.2016.08.033
- Shi, J., Huang, X., Liu, Q., & Huang, Z. (2013). Identification of conserved neutralizing linear epitopes within the VP1 protein of coxsackievirus A16. *Vaccine*, *31*(17), 2130-2136. https://doi.org/10.1016/j.vaccine.2013.02.051
- Shukla, R., Vasdev, N., Ruwali, M., Hasnain, M. S., & Beg, S. (2022). Chapter 17 Chitosan for delivery of biomolecules. In M. S. Hasnain, S. Beg, & A. K. Nayak (Eds.), *Chitosan in Drug Delivery* (pp. 433-460). Academic Press. https://doi.org/https://doi.org/10.1016/B978-0-12-819336-5.00005-4
- Si, F., Wang, D., Ji, T., Zhang, Y., Zhu, S., Li, J., . . . Yan, D. (2022). Identification of the first C1 subgenotype of enterovirus 71 in the Chinese mainland in a retrospective study. *Virol J*, 19(1), 83. https://doi.org/10.1186/s12985-022-01810-5
- Sickles, G. M., Mutterer, M., Feorino, P., & Plager, H. (1955). Recently classified types of Coxsackie virus, group A; behavior in tissue culture. *Proc Soc Exp Biol Med*, *90*(2), 529-531. https://doi.org/10.3181/00379727-90-22088
- Sioutas, C., Delfino, R. J., & Singh, M. (2005). Exposure assessment for atmospheric ultrafine particles (UFPs) and implications in epidemiologic research. *Environ Health Perspect*, 113(8), 947-955. https://doi.org/10.1289/ehp.7939
- Slingluff, C. L., Jr., Petroni, G. R., Chianese-Bullock, K. A., Wages, N. A., Olson, W. C., Smith, K. T., . . . Hall, E. H. (2021). Trial to evaluate the immunogenicity and safety of a melanoma helper peptide vaccine plus incomplete Freund's adjuvant, cyclophosphamide, and polyICLC (Mel63). *J Immunother Cancer*, 9(1). https://doi.org/10.1136/jitc-2020-000934
- Smyth, M. S., & Martin, J. H. (2002). Picornavirus uncoating. *Mol Pathol*, *55*(4), 214-219. https://doi.org/10.1136/mp.55.4.214
- Stone, V., Shaw, J., Brown, D. M., Macnee, W., Faux, S. P., & Donaldson, K. (1998). The role of oxidative stress in the prolonged inhibitory effect of ultrafine carbon black on epithelial

- cell function. *Toxicol In Vitro*, *12*(6), 649-659. https://doi.org/10.1016/s0887-2333(98)00050-2
- Swain, S. K., Panda, S., Sahu, B. P., & Sarangi, R. (2022). Activation of Host Cellular Signaling and Mechanism of Enterovirus 71 Viral Proteins Associated with Hand, Foot and Mouth Disease. *Viruses*, *14*(10). https://doi.org/10.3390/v14102190
- Tamkovich, S. N., Cherepanova, A. V., Kolesnikova, E. V., Rykova, E. Y., Pyshnyi, D. V., Vlassov, V. V., & Laktionov, P. P. (2006). Circulating DNA and DNase activity in human blood. *Ann N Y Acad Sci*, 1075, 191-196. https://doi.org/10.1196/annals.1368.026
- Tan, C. W., Poh, C. L., Sam, I. C., & Chan, Y. F. (2013). Enterovirus 71 uses cell surface heparan sulfate glycosaminoglycan as an attachment receptor. *J Virol*, 87(1), 611-620. https://doi.org/10.1128/jvi.02226-12
- Tan, M. L., Choong, P. F., & Dass, C. R. (2009). Cancer, chitosan nanoparticles and catalytic nucleic acids. *J Pharm Pharmacol*, *61*(1), 3-12. https://doi.org/10.1211/jpp/61.01.0002
- Tan, S. H., Ong, K. C., Perera, D., & Wong, K. T. (2016). A monoclonal antibody to ameliorate central nervous system infection and improve survival in a murine model of human Enterovirus-A71 encephalomyelitis. *Antiviral Res*, 132, 196-203. https://doi.org/10.1016/j.antiviral.2016.04.015
- Tanghe, A., Denis, O., Lambrecht, B., Motte, V., van den Berg, T., & Huygen, K. (2000). Tuberculosis DNA vaccine encoding Ag85A is immunogenic and protective when administered by intramuscular needle injection but not by epidermal gene gun bombardment. *Infect Immun*, *68*(7), 3854-3860. https://doi.org/10.1128/iai.68.7.3854-3860.2000
- Tay, C., Kanellakis, P., Hosseini, H., Cao, A., Toh, B. H., Bobik, A., & Kyaw, T. (2019). B Cell and CD4 T Cell Interactions Promote Development of Atherosclerosis. *Front Immunol*, *10*, 3046. https://doi.org/10.3389/fimmu.2019.03046
- Tian, X., Su, X., Li, X., Li, H., Li, T., Zhou, Z., . . . Zhou, R. (2012). Protection against enterovirus 71 with neutralizing epitope incorporation within adenovirus type 3 hexon. *PLoS One*, 7(7), e41381. https://doi.org/10.1371/journal.pone.0041381
- TM, M. W., Lau, W. M., & Khutoryanskiy, V. V. (2018). Chitosan and Its Derivatives for Application in Mucoadhesive Drug Delivery Systems. *Polymers (Basel)*, 10(3). https://doi.org/10.3390/polym10030267
- Torresi, J., & Kollaritsch, H. (2019). 12 Recommended/Required Travel Vaccines. In J. S. Keystone, P. E. Kozarsky, B. A. Connor, H. D. Nothdurft, M. Mendelson, & K. Leder (Eds.), *Travel Medicine (Fourth Edition)* (pp. 101-124). Elsevier. https://doi.org/https://doi.org/10.1016/B978-0-323-54696-6.00012-4
- Tu, Y. X., Li, X. P., Kadir, Z., & Zhang, F. C. (2013). Molecular adjuvant interleukin-33 enhances the antifertility effect of Lagurus lagurus zona pellucida 3 DNA vaccine administered by the mucosal route. *Braz J Med Biol Res*, 46(12), 1064-1073. https://doi.org/10.1590/1414-431x20133126
- Tung, W. S., Bakar, S. A., Sekawi, Z., & Rosli, R. (2007). DNA vaccine constructs against enterovirus 71 elicit immune response in mice. *Genet Vaccines Ther*, *5*, 6. https://doi.org/10.1186/1479-0556-5-6
- Valente, J. F. A., Pereira, P., Sousa, A., Queiroz, J. A., & Sousa, F. (2021). Effect of Plasmid DNA Size on Chitosan or Polyethyleneimine Polyplexes Formulation. *Polymers (Basel)*, *13*(5). https://doi.org/10.3390/polym13050793
- Van Boeckel, T. P., Takahashi, S., Liao, Q., Xing, W., Lai, S., Hsiao, V., . . . Grenfell, B. T. (2016). Hand, Foot, and Mouth Disease in China: Critical Community Size and Spatial Vaccination Strategies. *Sci Rep*, *6*, 25248. https://doi.org/10.1038/srep25248
- van der Lubben, I. M., Verhoef, J. C., Borchard, G., & Junginger, H. E. (2001). Chitosan for mucosal vaccination. *Adv Drug Deliv Rev*, 52(2), 139-144. https://doi.org/10.1016/s0169-409x(01)00197-1
- Wang, J., Kong, M., Zhou, Z., Yan, D., Yu, X., Cheng, X., . . . Chen, X. (2017). Mechanism of surface charge triggered intestinal epithelial tight junction opening upon chitosan nanoparticles

- for insulin oral delivery. *Carbohydr Polym*, 157, 596-602. https://doi.org/10.1016/j.carbpol.2016.10.021
- Wang, J., Teng, Z., Chu, W., Fang, F., Cui, X., Guo, X., . . . Zhu, Y. (2018). The emergence and spread of one Coxsackievirus A16 Genogroup D novel recombinant strain that caused a clustering HFMD outbreak in Shanghai, China, 2016. *Emerg Microbes Infect*, 7(1), 131. https://doi.org/10.1038/s41426-018-0134-x
- Wang, L., Zhu, M., Fang, Y., Rong, H., Gao, L., Liao, Q., . . . Dong, C. (2021). Bioinformatics-based prediction of conformational epitopes for Enterovirus A71 and Coxsackievirus A16. *Sci Rep*, 11(1), 5701. https://doi.org/10.1038/s41598-021-84891-6
- Wang, W., Duo, J., Liu, J., Ma, C., Zhang, L., Wei, Q., & Qin, C. (2011). A mouse muscle-adapted enterovirus 71 strain with increased virulence in mice. *Microbes Infect*, *13*(10), 862-870. https://doi.org/10.1016/j.micinf.2011.04.004
- Wang, X., An, Z., Huo, D., Jia, L., Li, J., Yang, Y., . . . Wang, H. (2019). Enterovirus A71 vaccine effectiveness in preventing enterovirus A71 infection among medically-attended hand, foot, and mouth disease cases, Beijing, China. *Hum Vaccin Immunother*, *15*(5), 1183-1190. https://doi.org/10.1080/21645515.2019.1581539
- Wang, Y., Iyer, M., Annala, A. J., Chappell, S., Mauro, V., & Gambhir, S. S. (2005). Noninvasive monitoring of target gene expression by imaging reporter gene expression in living animals using improved bicistronic vectors. *J Nucl Med*, 46(4), 667-674.
- Wang, Y. F., Chou, C. T., Lei, H. Y., Liu, C. C., Wang, S. M., Yan, J. J., . . . Yu, C. K. (2004). A mouse-adapted enterovirus 71 strain causes neurological disease in mice after oral infection. *J Virol*, 78(15), 7916-7924. https://doi.org/10.1128/jvi.78.15.7916-7924.2004
- Watts, P., Smith, A., & Hinchcliffe, M. (2014). ChiSys® as a Chitosan-Based Delivery Platform for Nasal Vaccination. In (pp. 499-516). https://doi.org/10.1007/978-1-4614-9524-6 23
- Wieczorek, M., Abualrous, E. T., Sticht, J., Álvaro-Benito, M., Stolzenberg, S., Noé, F., & Freund, C. (2017). Major Histocompatibility Complex (MHC) Class I and MHC Class II Proteins: Conformational Plasticity in Antigen Presentation. Front Immunol, 8, 292. https://doi.org/10.3389/fimmu.2017.00292
- Wilson, M. R., Lightbody, J. H., Donaldson, K., Sales, J., & Stone, V. (2002). Interactions between ultrafine particles and transition metals in vivo and in vitro. *Toxicol Appl Pharmacol*, 184(3), 172-179. https://doi.org/10.1006/taap.2002.9501
- Wolff, J. A., Malone, R. W., Williams, P., Chong, W., Acsadi, G., Jani, A., & Felgner, P. L. (1990). Direct gene transfer into mouse muscle in vivo. *Science*, *247*(4949 Pt 1), 1465-1468. https://doi.org/10.1126/science.1690918
- Wong, S. S., Yip, C. C., Lau, S. K., & Yuen, K. Y. (2010). Human enterovirus 71 and hand, foot and mouth disease. *Epidemiol Infect*, 138(8), 1071-1089. https://doi.org/10.1017/s0950268809991555
- World Health Organization. Regional Office for the Western, P. (2018). *Hand, Foot and Mouth Disease Situation Update 2018*. http://iris.wpro.who.int/handle/10665.1/14191
- Wu, C. N., Lin, Y. C., Fann, C., Liao, N. S., Shih, S. R., & Ho, M. S. (2001). Protection against lethal enterovirus 71 infection in newborn mice by passive immunization with subunit VP1 vaccines and inactivated virus. *Vaccine*, 20(5-6), 895-904. https://doi.org/10.1016/s0264-410x(01)00385-1
- Xie, J., Yang, X. H., Hu, S. Q., Zhan, W. L., Zhang, C. B., Liu, H., . . . Luo, M. Y. (2020). Co-circulation of coxsackieviruses A-6, A-10, and A-16 causes hand, foot, and mouth disease in Guangzhou city, China. *BMC Infect Dis*, 20(1), 271. https://doi.org/10.1186/s12879-020-04992-x
- Xing, W., Liao, Q., Viboud, C., Zhang, J., Sun, J., Wu, J. T., ... Yu, H. (2014). Hand, foot, and mouth disease in China, 2008-12: an epidemiological study. *Lancet Infect Dis*, *14*(4), 308-318. https://doi.org/10.1016/s1473-3099(13)70342-6
- Xu, L., He, D., Li, Z., Zheng, J., Yang, L., Yu, M., . . . Xia, N. (2014). Protection against lethal enterovirus 71 challenge in mice by a recombinant vaccine candidate containing a

- broadly cross-neutralizing epitope within the VP2 EF loop. *Theranostics*, *4*(5), 498-513. https://doi.org/10.7150/thno.7457
- Xu, Y., Ma, S., Zhu, L., Huang, Z., Chen, L., Xu, Y., . . . Wang, Y. (2017). Clinically isolated enterovirus A71 subgenogroup C4 strain with lethal pathogenicity in 14-day-old mice and the application as an EV-A71 mouse infection model. *Antiviral Res*, 137, 67-75. https://doi.org/10.1016/j.antiviral.2016.11.008
- Yamayoshi, S., Ohka, S., Fujii, K., & Koike, S. (2013). Functional comparison of SCARB2 and PSGL1 as receptors for enterovirus 71. *J Virol*, 87(6), 3335-3347. https://doi.org/10.1128/jvi.02070-12
- Yang, Q., & Sarnow, P. (1997). Location of the internal ribosome entry site in the 5' non-coding region of the immunoglobulin heavy-chain binding protein (BiP) mRNA: evidence for specific RNA-protein interactions. *Nucleic Acids Res*, 25(14), 2800-2807. https://doi.org/10.1093/nar/25.14.2800
- Yang, S. (2015). Attenuated characteristics and bioprocess assessment of CA16 vaccine candidates [master's degree] Beijing: Chinese Academy of Medical Sciences &
- Peking Union Medical College].
- Yang, T., Xie, T., Li, H., Song, X., Yue, L., Wang, X., . . . Li, Q. (2020). Immune responses of a CV-A16 live attenuated candidate strain and its protective effects in rhesus monkeys. *Emerg Microbes Infect*, *9*(1), 2136-2146. https://doi.org/10.1080/22221751.2020.1823889
- Ye, Y., Xu, Y., Liang, W., Leung, G. P., Cheung, K. H., Zheng, C., . . . Lam, J. K. (2013). DNA-loaded chitosan oligosaccharide nanoparticles with enhanced permeability across Calu-3 cells. *J Drug Target*, 21(5), 474-486. https://doi.org/10.3109/1061186x.2013.766885
- Yee, P. T., Tan, K. O., Othman, I., & Poh, C. L. (2016). Identification of molecular determinants of cell culture growth characteristics of Enterovirus 71. *Virol J*, 13(1), 194. https://doi.org/10.1186/s12985-016-0645-9
- Yee, P. T. I., Tan, S. H., Ong, K. C., Tan, K. O., Wong, K. T., Hassan, S. S., & Poh, C. L. (2019). Development of live attenuated Enterovirus 71 vaccine strains that confer protection against lethal challenge in mice. *Sci Rep*, *9*(1), 4805. https://doi.org/10.1038/s41598-019-41285-z
- Yi, E. J., Shin, Y. J., Kim, J. H., Kim, T. G., & Chang, S. Y. (2017). Enterovirus 71 infection and vaccines. *Clin Exp Vaccine Res*, 6(1), 4-14. https://doi.org/10.7774/cevr.2017.6.1.4
- Yip, C. C., Lau, S. K., Woo, P. C., & Yuen, K. Y. (2013). Human enterovirus 71 epidemics: what's next? *Emerg Health Threats J*, *6*, 19780. https://doi.org/10.3402/ehtj.v6i0.19780
- Yoshida, K., Fujimoto, T., Muramatsu, M., & Shimizu, H. (2022). Prediction of hand, foot, and mouth disease epidemics in Japan using a long short-term memory approach. *PLoS One*, 17(7), e0271820. https://doi.org/10.1371/journal.pone.0271820
- Zaini, Z., & McMinn, P. (2012). A single mutation in capsid protein VP1 (Q145E) of a genogroup C4 strain of human enterovirus 71 generates a mouse-virulent phenotype. *J Gen Virol*, 93(Pt 9), 1935-1940. https://doi.org/10.1099/vir.0.043893-0
- Zaini, Z., Phuektes, P., & McMinn, P. (2012). A reverse genetic study of the adaptation of human enterovirus 71 to growth in Chinese hamster ovary cell cultures. *Virus Res*, 165(2), 151-156. https://doi.org/10.1016/j.virusres.2012.02.009
- Zarbock, A., Müller, H., Kuwano, Y., & Ley, K. (2009). PSGL-1-dependent myeloid leukocyte activation. *J Leukoc Biol*, 86(5), 1119-1124. https://doi.org/10.1189/jlb.0209117
- Zhang, K., Fang, H., Chen, Z., Taylor, J.-S. A., & Wooley, K. L. J. B. c. (2008). Shape effects of nanoparticles conjugated with cell-penetrating peptides (HIV Tat PTD) on CHO cell uptake. 19(9), 1880-1887.
- Zhang, N., & Bevan, M. J. (2011). CD8(+) T cells: foot soldiers of the immune system. *Immunity*, 35(2), 161-168. https://doi.org/10.1016/j.immuni.2011.07.010
- Zhang, S. Y., Xu, M. Y., Xu, H. M., Li, X. J., Ding, S. J., Wang, X. J., . . . Lu, Q. B. (2015). Immunologic Characterization of Cytokine Responses to Enterovirus 71 and Coxsackievirus A16 Infection in Children. *Medicine (Baltimore)*, 94(27), e1137. https://doi.org/10.1097/md.0000000000001137

- Zhang, W., Dai, W., Zhang, C., Zhou, Y., Xiong, P., Wang, S., . . . Huang, Z. (2018). A virus-like particle-based tetravalent vaccine for hand, foot, and mouth disease elicits broad and balanced protective immunity. *Emerg Microbes Infect*, 7(1), 94. https://doi.org/10.1038/s41426-018-0094-1
- Zhang, Y., Tan, X., Cui, A., Mao, N., Xu, S., Zhu, Z., . . . Xu, W. (2013). Complete genome analysis of the C4 subgenotype strains of enterovirus 71: predominant recombination C4 viruses persistently circulating in China for 14 years. *PLoS One*, 8(2), e56341. https://doi.org/10.1371/journal.pone.0056341
- Zhang, Y., Zhu, Z., Yang, W., Ren, J., Tan, X., Wang, Y., . . . Xu, W. (2010). An emerging recombinant human enterovirus 71 responsible for the 2008 outbreak of hand foot and mouth disease in Fuyang city of China. *Virol J*, 7, 94. https://doi.org/10.1186/1743-422x-7-94
- Zhao, K., Zhang, Y., Zhang, X., Li, W., Shi, C., Guo, C., . . . Wang, Y. (2014). Preparation and efficacy of Newcastle disease virus DNA vaccine encapsulated in chitosan nanoparticles. *Int J Nanomedicine*, *9*, 389-402. https://doi.org/10.2147/ijn.S54226
- Zhao, X., Yu, S. B., Wu, F. L., Mao, Z. B., & Yu, C. L. (2006). Transfection of primary chondrocytes using chitosan-pEGFP nanoparticles. *J Control Release*, 112(2), 223-228. https://doi.org/10.1016/j.jconrel.2006.01.016
- Zhu, F., Xu, W., Xia, J., Liang, Z., Liu, Y., Zhang, X., . . . Wang, N. (2014). Efficacy, safety, and immunogenicity of an enterovirus 71 vaccine in China. *N Engl J Med*, *370*(9), 818-828. https://doi.org/10.1056/NEJMoa1304923
- Zhu, F. C., Meng, F. Y., Li, J. X., Li, X. L., Mao, Q. Y., Tao, H., . . . Shen, X. L. (2013). Efficacy, safety, and immunology of an inactivated alum-adjuvant enterovirus 71 vaccine in children in China: a multicentre, randomised, double-blind, placebo-controlled, phase 3 trial. *Lancet*, 381(9882), 2024-2032. https://doi.org/10.1016/s0140-6736(13)61049-1

APPENDICES

APPENDIX I – Publication

Review article

Heng, W. T., Yew, J. S., & Poh, C. L. (2022).

Nanovaccines against Viral Infectious Diseases. Pharmaceutics, 14(12).

https://doi.org/10.3390/pharmaceutics14122554 (published Nov 2022)